

# Development of a Two-Wheel Inverted Pendulum and a Cable Climbing Robot

Mikail S. Arani

A Thesis

In The Department of

Mechanical, Industrial and Aerospace Engineering

Presented in Partial Fulfillment of the Requirements

For the Degree of Master of Applied Science at Concordia University

Montreal, Quebec, Canada

October 2019

©Mikail S. Arani, 2019

# CONCORDIA UNIVERSITY

## SCHOOL OF GRADUATE STUDIES

This is to certify that the thesis prepared,

By: **Mikail S. Arani**

**Entitled:** Development of a two-wheel inverted pendulum and a cable climbing robot

and submitted in partial fulfillment of the requirements for the degree of

### **Master of Applied Science**

Complies with the regulations of the University and meets the accepted standards with respect to originality and quality.

Signed by the final examining committee:

Dr. Chevy Chen	Chair
Dr. Ashutosh Bagchi	External Examiner
Dr. Youmin Zhang	Examiner
Dr. Wen Fang Xie	Thesis Supervisor

Approved by **Dr. Waizuddin Ahmed**  
Chair of Department of Graduate Program Director

2019-11-19  
Date **Dr. Amir Asif**  
Dean, Gina Cody School of Engineering and Computer Science



# ABSTRACT

## Development of a Two-Wheel Inverted Pendulum and a Cable Climbing Robot

Mikail S. Arani

The research work in this thesis constitutes two parts: one is the development and control of a Two-wheel inverted pendulum (TWIP) robot and the other is the design and manufacturing of a cable climbing robot (CCR) for suspension bridge inspection. The first part of this research investigates a sliding mode controller for self-balancing and stabilizing a two-wheel inverted pendulum (TWIP) robot. The TWIP robot is constructed by using two DC gear motors with a high-resolution encoder and zero backlashes, but with friction. It is a highly nonlinear and unstable system, which poses challenges for controller design. In this study, a dynamic mathematical model is built using the Lagrangian function method. And a sliding mode controller (SMC) is proposed for auto-balancing and yaw rotation. A gyro and an accelerometer are adopted to measure the pitch angle and pitch rate. The effect on the sensor's installation location is analyzed and compensated, and the precision of the pose estimation is improved accordingly. A comparison of the proposed SMC controller with a proportional-integral-derivative (PID) controller and state feedback controller (SFC) with linear quadratic regulation (LQR) has been conducted. The simulation and experimental test results demonstrate the SMC controller outperforms the PID controller and SFC in terms of transient performance and disturbance rejection ability.

In the second part of the research, a wheel-based cable climbing robotic system which can climb up and down the cylindrical cables for the inspection of the suspension bridges is designed and manufactured. Firstly, a rubber track climbing mechanism is designed to generate enough adhesion force for the robot to stick to the surface of a cable and the driving force for the robot to climb up and down the cable, while not too big to damage the cable. The climbing system includes chains and sprockets driven by the DC motors and adhesion system. The unique design of the adhesion mechanism lies in that it can maintain the adhesion force even when the power is lost while the system works as a suspension mechanism. Finally, a safe-landing mechanism is developed to guarantee the safety of the robot during inspection operations on cables. The robot has been fully tested in the inspection of Xili bridge, Guangzhou, P.R. China.

## **DEDICATION**

*To my beloved parents, my love Nargess, friends and everyone who digs science*

## ACKNOWLEDGEMENTS

First and foremost, I would like to express my deepest gratitude and respect to my supervisor Professor Dr. Wen Fang Xie who supported me throughout my research and study at Concordia University. She has devoted her time to support me in the entire research. Also, I am thankful to my co-supervisor Dr. Henry Hong. I would like to appreciate the financial support from Mr. Chaoyang Yu, who trusted and invested in my knowledge and gave me the opportunity to vast my creativity in building an industrial robot for his company, Guangdong Chengxin highway. Thanks to these amazing people, this project was such an amazing and successful adventure, which I hope this robot can make a big change in the automated inspection industry and help to keep Canada's bridges safe and reliable. I would like to thank Mr. Gilles Huard from Concordia Robotic lab. Thank you for your support, your knowledge and answering all my questions.

This project would have not been possible without all the wonderful and proficient people involved in it. My sincere thanks to Dr. Amir Ali Farough Nasiraie, who is not only my business partner in Canada Technology Plus Company but also the greatest friend I could ever ask for. Brainstorming with Amir and his support enlighten me to make this project a success. My special thanks to my lifetime friend Elyas for sharing his smart ideas with me. I would also like to thank my colleague, Hamid whom I learned a lot from throughout publishing an article and a book chapter with.

Many thanks to my friends, Ibrahim and Hossein, at Concordia and my amazing lifetime friends, Parsa, Saman, Ali, Hossein, Fardad, Saeed and Amir. Thank you again for all your support from the first day of projects. I would like to thank my beautiful love Nargess; I deeply appreciate your presence, love, care, and support in each step of this project.

Last but not least, I would like to thank my parents and my dear brother, Amirhossein. My father, a true role model representing a responsible and resourceful engineer who though me a lot, and my mother, who is a great teacher, an amazing mentor, a wonderful listener, and the kindest person I know. Thank you for your support in any possible way. Thank you for trusting in me and supporting the path I chose as a teenager. Thank you for believing in me in each and every single decision I have ever made. I am so grateful that you are my precious family.

# TABLE OF CONTENTS

CHAPTER 1 INTRODUCTION.....	1
1.1 Two-wheel inverted pendulum robot development.....	1
1.2 Cable inspection and cable climbing robot (CCR) development .....	2
1.3 Contribution.....	4
1.4 Organization of the thesis .....	5
CHAPTER 2 LITERATURE REVIEW .....	6
2.1 Control of two-wheel inverted pendulum.....	6
2.2 Cable climbing robot .....	7
2.2.1 GCH cable climbing robot background .....	7
2.2.2 CCR platforms review.....	8
2.3 Summary.....	16
CHAPTER 3 DEVELOPMENT OF A TWIP.....	17
3.1 Dynamics modeling of a two-wheel inverted pendulum.....	17
3.2 Two-wheel inverted pendulum robot controller design .....	21
3.2.1 Two-wheel inverted pendulum robot PID controller design.....	21
3.2.2 SFC designed by LQR .....	22
3.2.3 SMC .....	24
3.3 Summary.....	25
CHAPTER 4 DEVELOPMENT OF A CCR .....	26
4.1 Development strategy.....	26
4.2 Aims and objectives.....	26
4.2.1 New modular robotic architecture.....	27
4.3 High-level specification.....	27
4.4 Chassis of CCR.....	31
4.4.1 Chassis development strategy .....	31
4.4.2 Specification.....	31
4.4.3 Benchmarking .....	33
4.4.4 Development and justification of design.....	35
4.4.4.1 Size .....	35
4.4.4.2 Shape .....	37

4.4.5	Materials selection .....	39
4.4.6	Mounting systems .....	40
4.4.7	Final design .....	42
4.4.8	Manufacturing and assembly .....	44
4.5	Drivetrain.....	45
4.5.1	Drivetrain development strategy .....	45
4.5.2	Drivetrain specification.....	46
4.5.3	Benchmarking .....	47
4.5.4	Design, calculations, and decisions.....	47
4.5.4.1	Tracks vs. wheels.....	47
4.5.4.2	Design options .....	50
4.5.4.3	Dimensions .....	54
4.5.4.4	Adhesion mechanism.....	55
4.5.4.5	Chain and sprockets.....	56
4.5.4.6	Suspension .....	58
4.5.4.7	Motor requirements .....	58
4.5.5	Final design .....	61
4.5.6	Manufacture .....	63
4.6	CCR control and electronics.....	63
4.6.1	Specification.....	64
4.6.2	Electronic architecture design .....	66
4.6.3	Controllers design .....	67
4.6.4	Electronics and software .....	69
4.6.5	Control electronics .....	69
4.6.5.1	Communication .....	70
4.6.5.2	Microprocessor .....	73
4.6.5.3	Motor controllers .....	74
4.6.5.4	Sensors.....	74
4.6.6	Power electronics .....	76
4.6.6.1	Powerboard requirements .....	76
4.6.6.2	Trace widths .....	77
4.6.6.3	Cables sizing and fuse protection .....	78

4.6.7	Final designs.....	78
4.6.8	Manufacture .....	79
4.6.9	Safety system .....	80
4.6.9.1	Powerboard.....	80
4.6.10	Software design.....	81
4.7	Summary.....	82
CHAPTER 5 SIMULATION AND EXPERIMENT TESTS OF TWIP .....		83
5.1	Simulation results .....	83
5.2	Experimental results .....	85
5.3	Summary.....	88
CHAPTER 6 EXPERIMENTS AND RESULTS CCR .....		89
6.1	Chassis CCR.....	89
6.1.1	Adhesion mechanism FEA.....	89
6.1.2	Motor mounting FEA pillow mounting shaft.....	91
6.1.3	Chassis CCR performance validation .....	93
6.1.4	Drivetrain -testing of cable climbing robot.....	97
6.1.4.1	Virtual testing .....	97
6.1.4.2	Physical testing.....	100
6.1.5	Performance validation of drivetrain .....	101
6.1.6	Performance validation of control, electronics, and software.....	102
CHAPTER 7 CONCLUSION AND FUTURE WORKS ON TWIP AND CCR .....		105
7.1	Conclusion.....	105
7.2	Future works.....	106
REFERENCE .....		107



# TABLE OF FIGURES

FIGURE 1-1 THREE TYPES OF CABLES: A) REGULAR CABLE <sup>1</sup> , B) CABLE WOUND WITH A SPIRAL WIRE <sup>2</sup> , AND C) DIMPLED CABLE <sup>3</sup> .....	4
FIGURE 2-1 FIRST GENERATION OF TELE-OPERATED ROBOT .....	7
FIGURE 2-2 BRIDGE CABLE INSPECTION ROBOT- RESEARCH PROJECT .....	9
FIGURE 2-3 CATERPILLAR-BASED CABLE CLIMBING ROBOT .....	10
FIGURE 2-4 VERSATRAX MICROCLIMBER – COMMERCIAL (INUKTUN CO.) .....	12
FIGURE 2-5 MRC2IN-II.....	13
FIGURE 2-6 CCROBOT .....	15
FIGURE 3-1 SCHEMATIC DIAGRAM OF THE TWIP ROBOT .....	18
FIGURE 3-2 TWIP CLOSED-LOOP BLOCK DIAGRAM HAVING PID CONTROLLER ....	22
FIGURE 3-3 TWIP CLOSED-LOOP BLOCK DIAGRAM WITH SFCS .....	24
FIGURE 3-4 SMC BLOCK DIAGRAM FOR TWIP .....	25
FIGURE 4-1 DEVELOPMENT PROCESS WORKFLOW .....	26
FIGURE 4-2 CHASSIS DEVELOPMENT STRATEGY .....	31
FIGURE 4-3 SIMPLE CCR.....	33
FIGURE 4-4 CCR WITH EIGHT FLAT RUBBER WHEELS .....	33
FIGURE 4-5 CCR WITH FOUR CURVE RUBBER WHEELS.....	33
FIGURE 4-6 CCR WITH THREE ADHESION MECHANISM.....	34
FIGURE 4-7 CCR WITH THREE ADHESION MECHANISM CHAIN AND SPROCKET ....	34
FIGURE 4-8 CCR WITH THREE ADHESION MECHANISM URETHANE WHEELS.....	34
FIGURE 4-9 ROBOT HEIGHT AND WIDTH DIMENSIONS (LEFT), MAXIMUM LENGTH BETWEEN CABLES (RIGHT).....	35
FIGURE 4-10 FINAL CHASSIS DIMENSIONS .....	37
FIGURE 4-11 ROBOT HEXAGON FRAMES .....	38
FIGURE 4-12 ELECTRONIC BOX AND ALUMINUM FRAME.....	38
FIGURE 4-13 3D CAD FRAME OF ELECTRONIC BOX UP-SIDE .....	38
FIGURE 4-14 3D CAD FRAME OF ELECTRONIC BOX DOWN-SIDE.....	38
FIGURE 4-15 MISUMI PROFILE FIGURE .....	39
FIGURE 4-16 MISUMI ANGLE BRACKET.....	39

FIGURE 4-17 SCOPE FOR ADAPTING ALUMINUM EXTRUSIONS CHASSIS PLATFORM INTO LARGER SIZES .....	40
FIGURE 4-18 CHASSIS MOUNTING POINTS .....	41
FIGURE 4-19 MISUMI BRACKETS .....	41
FIGURE 4-20 3D PRINTED BATTERY HOUSING - CAD IMAGE.....	42
FIGURE 4-21 FINAL CHASSIS DESIGN- RENDERED CAD IMAGE.....	43
FIGURE 4-22 FINAL CHASSIS DESIGN WITH INTERNAL COMPONENTS - RENDERED CAD IMAGE.....	43
FIGURE 4-23 DRIVETRAIN DEVELOPMENT STRATEGY .....	45
FIGURE 4-24 EXISTING CABLE CLIMBING ROBOT DRIVETRAIN FEATURES .....	47
FIGURE 4-25 OPTION 1 – SIMPLEST DRIVETRAIN DESIGN .....	50
FIGURE 4-26 OPTION 2 – SECOND SIMPLEST DRIVETRAIN DESIGN .....	50
FIGURE 4-27 OPTION 3 – MIDDLE DRIVETRAIN DESIGN .....	51
FIGURE 4-28 OPTION 4 – SECOND MIDDLE DRIVETRAIN DESIGN .....	51
FIGURE 4-29 OPTION 5 – SECOND MIDDLE DRIVETRAIN DESIGN .....	52
FIGURE 4-30 OPTION 6 – SECOND MIDDLE DRIVETRAIN DESIGN .....	52
FIGURE 4-31 OPTION 7 – SECOND MIDDLE DRIVETRAIN DESIGN .....	53
FIGURE 4-32 DRIVETRAIN COST & COMPLEXITY VS. MOBILITY GRAPH .....	53
FIGURE 4-33 RESTRICTING DIMENSIONS IN THE DRIVETRAIN DESIGN .....	54
FIGURE 4-34 GENERAL INSTANCE OF SCISSOR MECHANISM .....	56
FIGURE 4-35 SCISSOR MECHANISM .....	56
FIGURE 4-36 CHAIN AND SPROCKET .....	57
FIGURE 4-37 SUSPENSION AND SHOCK ABSORBER MECHANISM.....	58
FIGURE 4-38 SAFE LOCKING MECHANISM.....	59
FIGURE 4-39 CCR DURING CLIMBING AT AN ANGLE 60 DEGREES LEFT AND 90 DEGREES RIGHT .....	59
FIGURE 4-40 FAULHABER DC MOTOR.....	61
FIGURE 4-41 FINAL FRAME DESIGN .....	62
FIGURE 4-42 FINAL ADHESION SYSTEM DESIG .....	62
FIGURE 4-43 DRIVETRAIN FINAL DESIGN.....	62
FIGURE 4-44 MANUFACTURED AND ASSEMBLED UNITS .....	63
FIGURE 4-45 ELECTRONICS AND SOFTWARE DEVELOPMENT STRATEGY .....	64

FIGURE 4-46 ROBOT MODULAR ELECTRONIC ARCHITECTURE.....	66
FIGURE 4-47 DC MOTORS CLOSED-LOOP BLOCK DIAGRAM HAVING PID CONTROLLER.....	68
FIGURE 4-48 LINEAR ACTUATORS CLOSED-LOOP BLOCK DIAGRAM HAVING PID CONTROLLER.....	68
FIGURE 4-49 THE PCB BEFORE COMPONENT SOLDERING .....	70
FIGURE 4-50 THE PCB AFTER COMPONENT SOLDERING .....	70
FIGURE 4-51 ELECTRONIC BOX DESIGN.....	71
FIGURE 4-52 XBEE RECEIVERS.....	72
FIGURE 4-53 RADIO CONTROLLER TRANSMITTER.....	72
FIGURE 4-54 ARDUINO DUE 32BIT ARM MICROCONTROLLER.....	74
FIGURE 4-55 CYTRON MOTOR CONTROLLER .....	74
FIGURE 4-56 ULTRASONIC SRF 08 .....	75
FIGURE 4-57 DUAL BUZZER ALARM.....	75
FIGURE 4-58 MPU6050 .....	75
FIGURE 4-59 HEDS5500A 12 .....	75
FIGURE 4-60 LAYOUT OF POWER BOARD AND MAINBOARD.....	79
FIGURE 4-61 3D REPRESENTATION OF THE BOARD .....	79
FIGURE 4-62 THE PCBs BEFORE COMPONENT SOLDERING .....	80
FIGURE 4-63 THE PCB AND COMPONENTS.....	81
FIGURE 4-64 CCR DISTANCE VIEWER SOFTWARE.....	81
FIGURE 5-1 TWIP ROBOT WITH DIFFERENT PITCH ANGLE .....	83
FIGURE 5-2 THE PITCH ANGLE AND ITS RATE OF PID CONTROLLER IN SIMULATION .....	84
FIGURE 5-3 THE PITCH ANGLE AND ITS RATE OF SFC IN SIMULATION .....	84
FIGURE 5-4 THE PITCH ANGLE AND ITS RATE OF SMC IN SIMULATION.....	85
FIGURE 5-5 THE EXPERIMENT RESULTS OF PITCH ANGLE AND ITS RATE OF PID CONTROLLER.....	86
FIGURE 5-6 THE EXPERIMENT RESULTS OF PITCH ANGLE AND ITS RATE OF SFC.	86
FIGURE 5-7 THE EXPERIMENT RESULTS OF PITCH ANGLE AND ITS RATE OF SMC	86
FIGURE 6-1 SAFETY FACTOR FOR ADHESION UNIT MOUNTING WITH 24 NM MOMENT .....	90

FIGURE 6-2 VON MISES STRESS FOR ADHESION UNIT MOUNTING WITH 24 NM MOMENT .....	90
FIGURE 6-3 SAFTY FACTOR OF MOTOR MOUNTING WITH 622 N FORCE.....	92
FIGURE 6-4 DISPLACEMENT OF MOTOR MOUNTING WITH 622 N FORCE.....	92
FIGURE 6-5 VON MISES STRESS OF MOTOR MOUNTING WITH 622 N FORCE .....	93
FIGURE 6-6 FINAL CHASSIS ASSEMBLY CLOSED HEXAGON.....	94
FIGURE 6-7 FINAL CHASSIS ASSEMBLY OPEN HEXAGON.....	94
FIGURE 6-8 FINAL CHASSIS ASSEMBLY AT THE CONCORDIA ROBOTIC CONTROL LAB .....	95
FIGURE 6-9 OPTIMUM ADHESION SYSTEM CHASSIS SHAPE .....	97
FIGURE 6-10 SAFTY FACTOR FEA MODELLING OF THE DRIVETRAIN UNIT .....	99
FIGURE 6-11 DISPLACEMENT FEA MODELLING OF THE DRIVETRAIN UNIT .....	99
FIGURE 6-12 DOUBLE U-SHAPED ALUMINUM CHANNELS .....	100
FIGURE 6-13 TEST IN XILI BRIDGE, GUANGZHOU, P.R. CHINA, MARCH 2019 .....	104

## LIST OF ABBREVIATION

AC	Alternating current
BC	British Columbia
CCR	Cable climbing robot
CoM	Center of mass
CNC	Computer numerical control
DoF	Degree of freedom
DC	Direct current
FEA	Finite element analysis
GCH	Guangdong Chengxin highway
Kg	Kilogram
MPa	Mega pascal
LQR	Linear quadratic regulator
Li-Po	Lithium polymer
MLTM	Ministry of Land, Transportation Maritime Affairs
mm	Millimeter
M/S	Meter/Second
M/S <sup>2</sup>	Meter per second squared
Min	Minute
Nm	Newton meter
PID	Proportional–integral–derivative
R&D	Research and development
RPM	Revolution per minute
SFC	State feedback control
SMC	Slide mode control
TWIP	Two-wheeled inverted pendulum

# CHAPTER 1 INTRODUCTION

## 1.1 Two-wheel inverted pendulum robot development

In recent years, self-balancing robots have attracted increasing attention in both industry and academia, since the design and implementation of control algorithms become more achievable with the rapid development of microcontrollers. Two-wheeled inverted pendulum (TWIP) robots have become more and more popular due to its lightweight, small footprint, rapid rotation, and high maneuverability. One of the applications of using these robots can be a service robot platform like Segway. However, the inherent instability and nonlinearity of the TWIP require a sophisticated control scheme.

PID is a commonly used non-model-based control method for a self-balancing robot, as there is no need to build the mathematics model. The three parameters can be tuned by trial and error or by experience. Although PID owns some robustness to disturbance and uncertainties to a certain extent, it cannot handle the sudden, large disturbance and modeling error [1]. Moreover, it is not a trivial task to obtain the optimized gains of a PID controller. To improve the performance of the controller, some advanced model-based controllers are needed to deal with the large disturbance and uncertainties.

Controlling the TWIP robot has recently been eased by introducing fuzzy logic and neural networks as the soft computing techniques [2, 3]. To illustrate, two fuzzy controllers have been designed for an inverted pendulum subjected to disturbance, as well as an artificial neural network-based real-time switching dynamic controller, which has been designed to solve the balancing problem on various loose surfaces such as sand, pebble, and soil [4]. The software has been developed by C++ as a visual robot interface to allow the required changes in parameters.

This TWIP's model-based control was proposed to address nonlinearity and disturbance. This approach in practical systems is the state feedback controller with optimized control gains. A linear SFC was designed based on a linear model that requires very accurate dynamic robot models. This

optimized SFC can, therefore, work within a certain range of operations and cannot manage system uncertainty. When changing the operating point, the control gains must be re-tuned to stabilize the robot, which is not very practical in operation. Due to the non-linearity of the system, linear controllers such as PID and state feedback controllers do not react efficiently, it has been focused on designing non-linear controllers such as robust feedback, backstepping, feedback linearization and sliding mode controllers (SMC) to provide an effective reaction to uncertainties and disturbance.

SMC is considered to have good robustness in modeling uncertainties and disturbance among these nonlinear controllers. It can manage the nonlinear unstable system with simple implementation, parameter variation insensitivity, and rapid response independence of external disturbance. Due to the facts mentioned above, in the current study, the SMC controller has been designed based on the TWIP linear dynamic model with 2-degree-of-freedom (DoF) and has been tested in the real robot.

An SMC controller is designed and implemented on a TWIP robot in this research. Firstly, using the Lagrangian function method, a 3-DoF dynamic model of a customer-built TWIP robot is derived. The robot consists of two gear DC motors that drive two wheels, one structure one battery, sensors, and one controller. It is a system that is highly nonlinear and unstable.

Then an SMC with easy implementation is designed to balance and stabilize the robot based on the built nonlinear model. Simulation tests are conducted to compare the proposed SMC with a PID controller and an LQR (linear quadratic regulator) tuned state feedback controller (SFC).

## **1.2 Cable inspection and cable climbing robot (CCR) development**

In the past decade, researchers have endeavored to make fully autonomous and intelligent cable climbing robots equipped with necessary sensors for inspection, aiming at making a cable climbing mechanism with obstacle avoidance capability to pass the rope equipment and bumps [5]. Also, researches have been done to devise a durable power supply method for the long cable inspection robots to make them sufficiently durable to perform inspection over long distances of vertical and horizontal without interruptions [18]. Inspection data quality enhancement has been another challenging issue in this field due to the fact that swinging of the inspection robot in windy climates

and even sometimes makes the captured images of the cable blurry during the navigation. The blurred images serve as the main inspection data for cable status evaluation [19]. These undesirable vibrations also make some problems in the robot's navigation, which mainly relies on a vision system, in most of the proposed designs. The robot's mechanical mechanism, as a main part of the robot design, may significantly affect other issues in the whole design process, such as energy consumption and inspection data quality [20]. Hence, this chapter aims to review some of the main efforts made over the past ten years in cable-climbing mechanism design for bridge cables inspection to provide a basis for future designs and developments in this field [21].

Over the last decade, climbing robots have become more and more important in many applications and posed a challenge to the robotics community. Starting with simple systems equipped with adhesion mechanisms like electromagnets, suction cups, or slide-rails, the difficulty of designing these robots has grown with their ability to handle different surfaces and in performing faster or more accurate navigation [22]. At the very beginning of climbing robot research, these systems have been designed to fit exactly one application or objective like a bridge steel cable or a PE cable. This limitation has decreased due to new locomotion types and adhesion mechanisms during the last years. At this point, climbing robots are considered to support inspection, maintenance, and construction tasks. In fact, they are helpful if they are able to perform the designated tasks more effectively and more accurate than the existing approaches. Especially for those tasks, which are dangerous for human beings, this safety aspect is of importance [23]. The common applications for such systems that are dangerous for humans are inspections of nuclear power stations (e.g., leakage detection, measurement of wall thickness or analysis of welding seams) and inspections of tanks and pipelines in the chemical industry. Furthermore, climbing robots are used to paint, coat, or clean the facades of buildings, or to perform welding tasks in the shipping industry, or to clean and inspect airplane wings and wind turbines. The climbing robots can be found in Figure 1-1 to depict some of the mentioned areas.





FIGURE 1-1 THREE TYPES OF CABLES: A) REGULAR CABLE<sup>1</sup>, B) CABLE WOUND WITH A SPIRAL WIRE<sup>2</sup>, AND C) DIMPLED CABLE<sup>3</sup>

The major difficulty of the climbing robots lies in generating driving force against gravity. Some robots use well-known and reliable adhesion techniques like magnets or grips to generate the force. For instance, such robots can be found in applications such as the ship industry or the inspections of planes, petrochemical tanks, or other steel surfaces. The exceptions are those systems whose adhesion principle (e.g., thermal glue) is still the focus of research. Although there exists a wide range of different systems, only a few climbing robots have been brought to commercial applications [24]. In this project, the research objective is to design and manufacture a wheel-based cable climbing robotic system which can climb up and down the cylindrical cables for the inspection of the suspension bridges.

### 1.3 Contribution

In this thesis, two robots are built and controlled: a Two-Wheel Inverted Pendulum (TWIP) robot and a Cable Climbing Robot (CCR).

The TWIP robot is developed and controlled by three controllers SMC, PID controller, and SFC. These controllers are compared according to their performance in regards to balancing and steering the movement of the TWIP system. The dynamic model of the TWIP is established by using the physic principles. A model-based SMC controller has been designed to have a better transient performance in stabilizing the TWIP robot than PID controller and SFC controller. A book chapter in *Springer Book, 2019* [25] and a paper in *The Canadian Society for Mechanical Engineering International Congress, 2019* [26] are published based on this research.

Supported by Guangdong Chengxin Highway (GCH), a cable climbing robot (CCR) has been designed and manufactured with an extremely stable structure that is capable of carrying over 10 kg of inspection and repairing equipment. PID controllers have been developed for the DC motors

to drive the robot. The robot features the wheel-driven mechanism, adjustable clamping, and novel adhesion design. To the best of author's knowledge, it is the first CCR capable of inspecting all regular bridge cables between 100 mm-300 mm diameters.

## **1.4 Organization of the thesis**

The thesis is organized as follows. Chapter 2 briefly reviews the control strategies of the TWIP robot, and the current cable climbing robots are given. In Chapter 3, a 3-DOF dynamic model of the TWIP robot has been built, and three controllers- PID, SFC, and SMC are designed. Chapter 4 presents the detailed design of the CCR. In Chapter 5, both simulation and experimental results on the controllers for TWIP are presented. Chapter 6 presents the experimental tests of the designed CCR. In Chapter 7, the conclusion and future works on both TWIP and CCR are given.

## CHAPTER 2 LITERATURE REVIEW

### 2.1 Control of two-wheel inverted pendulum

Recently, soft computing techniques such as fuzzy logic and neural networks have been used to control TWIP robot [2, 3]. Two fuzzy controllers based on Mamdani and Takagi-Sugeno are designed for an inverted pendulum subjected to disturbance. Moreover, an artificial neural network-based real-time switching dynamic controller is designed to solve the balancing problem on various loose surfaces such as sand, pebble, and soil [4]. A visual robot control interface is developed in C++ software development environment so that robot controller parameters can be changed as desired.

Newly, the model-based control of TWIP has been proposed to deal with the nonlinearity and disturbance. The State Feedback Controller (SFC) with optimized control gains is one of the most used methods in practical systems [5]. Gans and Hutchinson designed a linear SFC based on the linearized model, which needs very accurate dynamic models of the robots [6]. Hence, the optimized SFC can only work in a certain operating range and cannot deal with system uncertainty. When the operating point is changed, the control gains have to be re-tuned in order to stabilize the robot, which is not very practical in operation [7]. Due to the nonlinearity of the systems, the linear controllers such as PID and state feedback controllers do not react efficiently, therefore, some researchers concentrate on the design of nonlinear controllers such as robust feedback [8], backstepping [9], feedback linearization [10, 11] and sliding mode controllers (SMC) [12, 13] to provide effective reaction to the uncertainties and disturbance for TWIP robots. All these mentioned controllers are only validated through simulation, and no experimental tests of these controllers have been carried out on real TWIP robots [8]- [13].

Among these nonlinear controllers, SMC is known to have good robustness to model uncertainties and disturbance. It can deal with the nonlinear unstable system with easy implementation, insensitivity to parameters variation, and quick response independence of external disturbances. SMC has been successfully used for controlling the TWIP robot. In [14, 15, 16], the SMC controllers are designed based on two degrees [14] of freedom (DoF) linear dynamic model of TWIP and are tested in the real robots. In [3], the authors design a backstepping sliding mode controller for a TWIP robot and validate the trajectory tracking performance in a real TWIP.

However, the control design combines the backstepping and sliding mode controller and focuses on trajectory tracking. The combination increases the complexity of implementation on the real robots, and the robustness of the controller has not been demonstrated. The goal of the current study is to provide an effective SMC control design, which is easy for implementation on a real robot and has good robustness for dealing with uncertainties and sudden disturbance.

## 2.2 Cable climbing robot

### 2.2.1 GCH cable climbing robot background

In the past few years, GCH has been developing a series of CCRs ranging from inspector robots to manual controlled robots. The first generation of GCH CCR is shown in Figure 2-1. The robot weighs 70 kg and is powered by AC supply. The dimension of the robotics is too large to be fit through the smaller areas of the hunger space, which are becoming more common in the suspension bridge. The company is looking for a lighter and smaller CCR powered by battery, which is the main objective of this project.



FIGURE 2-1 FIRST GENERATION OF TELE-OPERATED ROBOT

### 2.2.2 CCR platforms review

This part of the thesis summarizes five commercially available cable climbing robots. A bridge cable inspection robot is a prototype of a portable cable climbing robots developed by Seoul University shown in Figure 2-2 [25]. This robot uses two powerful dc motors and a strong aluminum simple structure. The payload of the CCR is 10 kilograms. The second prototype is a caterpillar-based cable climbing robot shown in Figure 2-3 [26]. It is a robot for vertical hanger cables in suspension bridges that is powered by three dc motors and is designed with three pantograph mechanisms. This robot is made of aluminum alloy and has made more room for cameras and sensors. Also, the robot is equipped with a self-locking mechanism. The third robot is Versatrax MicroClimber shown in Figure 2-4. It is a commercial robot that is designed and sold to the inspection industries by the Inuktun company. This robot is a unique remotely operated robot designed to climb on almost any inclined or vertical cylindrical structure such as suspension and cable-stayed bridges. Another robot that has been studied is MRC2IN-II, shown in Figure 2-5 [27]. This robot is designed and made by the Korea Ministry of Land, Transportation Maritime Affairs (MLTM). The robot is powered by two dc motors and is designed with two pantograph mechanisms for climbing. Also, the robot can be equipped with four cameras for inspecting cables. The last robot that has been studied is the bio-inspired climbing robot developed by the Chinese University of Hong Kong as shown in Figure 2-6 [28]. Three linear actuators and six grippers have been designed and used in the robot. The robot is a prototype of climbing mechanisms study. Also, this robot is made just for Cable-stayed bridges. Versatrax MicroClimber entered in the market as a commercial robot since 2018, and Caterpillar-based Cable Climbing Robot came second.

The Seoul University cable climber robot was developed for cable-suspension bridges and cable-stayed bridges. The design of the robot and performance of the system with the cable are discussed in Table 2-1. This bridge cable inspection robot has been made as a research project.



FIGURE 2-2 BRIDGE CABLE INSPECTION ROBOT- RESEARCH PROJECT

TABLE 2-1 SPECIFICATIONS OF THE SEOUL UNIVERSITY CABLE CLIMBER ROBOT

Description	Unit	Parameters
Mass	kg	24~27
Operating time	min	60
Applicable cable diameters	mm	90~300
Climbing speed	m/s	0.05~8
Effective operating range	m	500
Applicable payload	Kg	5
Obstacle range possible to climb	mm	10
Max stall current	A	12
Operating voltage	V	12
Gear ratio	RPM	n=120:1
Inspection distance	m	200-600
Bridge type	Suspension and cable-stayed bridge	
Korea Ministry of land, infrastructure, and transport		

The Caterpillar is a cable climbing robot that has been made as a research project for a super long-span bridge by the Korea Ministry of land, transportation maritime affairs (MLTM) R&D center. This robot has been tested in real environments after sufficient experiments under an indoor environment composed of real hanger rope. The design of the robot and performance of the system with the cable are discussed in Table 2-2.

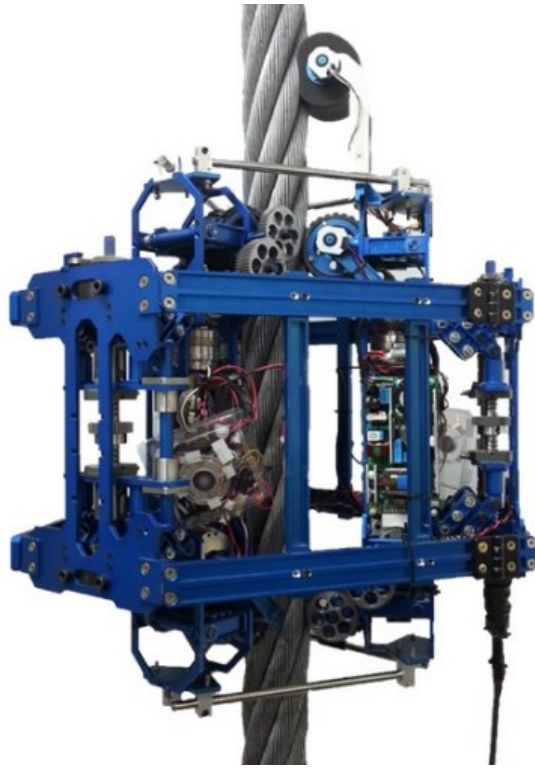


FIGURE 2-3 CATERPILLAR-BASED CABLE CLIMBING ROBOT

TABLE 2-2 SPECIFICATIONS OF CATERPILLAR-BASED CABLE CLIMBING ROBOT

<b>Description</b>	<b>Unit</b>	<b>Parameters</b>
Mass	kg	30
Operating time	min	60
Applicable cable diameters	mm	50~90
Climbing speed	m/s	0.035~0.08
Effective operating range	m	650
Applicable payload	Kg	5
Obstacle range possible to climb	mm	5
Max stall current	A	n/a
Operating voltage	V	n/a
Gear ratio	RPM	n/a
Inspection distance	m	100-800
Bridge type	Suspension and cable-stayed bridge	
Future robotics technology center supported by Korea Ministry of land, transportation maritime affairs (MLTM)		

Versatrax MicroClimber has been made as a commercial project by Inuktun Services Ltd. BC. Canada. The Versatrax MicroClimber robot is a unique remotely operated robot designed to climb on almost any inclined or vertical cylindrical structure. The vehicle is capable of crawling on cables, pipe, rope, or guy-wires while performing a variety of tasks. The design of the robot and performance of the system with the cable are discussed in Table 2-3.





FIGURE 2-4 VERSATRAX MICROCLIMBER – COMMERCIAL (INUKTUN CO.)

TABLE 2-3 SPECIFICATIONS OF THE VERSATRAX MICROCLIMBER ROBOT

Description	Unit	Parameters
Mass	kg	45
Operating time	min	n/a
Applicable cable diameters	mm	150~250
Climbing speed	m/s	2~4
Effective operating range	m	50-500
Applicable payload	Kg	n/a
Obstacle range possible to climb	mm	n/a
Max stall current	A	n/a
Operating voltage	V	n/a
Gear ratio	RPM	n/a
Inspection distance	m	100-400
Bridge type	Suspension and cable-stayed bridge	
Versatrax Micro climber Inuktun in command robotics LLC		

MRC2IN-II robot has been made and developed for a super long-span bridge by Korea ministry of land, transportation maritime affairs (MLTM) R&D center. This robot has been tested in real environments after sufficient experiments under an indoor environment composed of real hanger rope. The design of the robot and performance of the system with the cable are discussed in Table 2-4.



FIGURE 2-5 MRC2IN-II

TABLE 2-4 SPECIFICATIONS OF MRC2IN-II

<b>Description</b>	<b>Unit</b>	<b>Parameters</b>
Mass	kg	26.2~30
Operating time	min	60
Applicable cable diameters	mm	40~90
Climbing speed	m/s	0.06~0.08
Effective operating range	m	50
Applicable payload	Kg	n/a
Obstacle range possible to climb	mm	n/a
Max stall current	A	n/a
Operating voltage	V	12
Gear ratio	RPM	n/a
Inspection distance	m	50-300
Bridge type	Suspension and Cable-stayed bridge	
Korea Ministry of land, transportation maritime affairs		

CCR has been made as a research project and developed for a super long-span bridge by the Chinese University of Hong Kong, Shenzhen. Traveling along a cable with some obstacles or a small range of curvature requires at least three degrees of freedom. Thus, a mechanism with three degrees of freedom has been designed and developed for climbing a cable. The university used the results from kinematics and static mechanical analysis, and the detailed mechanical design has been obtained and worked efficiently. The design of the robot and performance of the system with the cable are discussed in Table 2-5.



FIGURE 2-6 CCROBOT

TABLE 2-5 SPECIFICATION OF CCROBOT

Description	Unit	Parameters
Mass	kg	15
Operating time	min	30
Applicable cable diameters	mm	40~90
Climbing speed	m/s	~0.05
Effective operating range	m	50
Applicable payload	Kg	15
Obstacle range possible to climb	mm	5
Max stall current	A	n/a
Operating voltage	V	n/a
Gear ratio	RPM	n/a
Inspection distance	m	50-300
Bridge type	Cable-stayed bridge	
The Chinese University of Hong Kong Shenzhen		

## 2.3 Summary

The GCH CCR has a simple and reliable platform, but it is not a portable CCR and it cannot climb up more than 40 meters. The Seoul University Bridge Cable Inspection Robot is another CCR that is not easy to be mounted on the cables and confronts swinging issue while climbing up. Caterpillar-based cable climbing robot cannot climb up smoothly and is not portable. Versatrax Micro Climber platform is a reliable CCR but its operating time is limited to 30 minutes. Also, its adjustability in regards to cable diameters is limited. MRC2IN-II is a reliable robot, however, it is not a portable CCR and has the swing problem while climbing up. CCROBOT is not a reliable CCR, unable to climb up smoothly and it not abale to adjust itself for vast size range of cables diameters.

The comparison among the 5 CCRs mentioned above shows that even though the robots have been designed and made for different types and sizes of cable, each of them has it own drawbacks. Also, these robots have been made with different mechanisms depending on the purpose of inspection. The market is still lacking an efficient climbing robot that can climb vertical or long slender cables (up to 1km) with high speed (8m/s). The robot is portable and is easy to be mounted on the cable.

## **CHAPTER 3 DEVELOPMENT OF A TWIP**

In this chapter, the modeling and control of a TWIP are specified.

### **3.1 Dynamics modeling of a two-wheel inverted pendulum**

The TWIP robot is built in our lab to serve as a test platform for various controllers. In order to control this type of unstable robot effectively, the first step is to model the robot's dynamic behavior in the yaw and pitch motions. The schematic diagram of the TWIP robot is shown in Figure 3-1, and the parameters' description is provided in

Table 3-1.

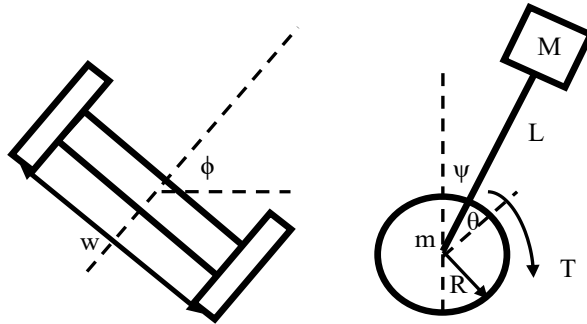


FIGURE 3-1 SCHEMATIC DIAGRAM OF THE TWIP ROBOT

The dynamic model of the robot is built based on the Lagrangian function method [29]. Equation 3-1 presents Lagrangian, where  $L_1$ ,  $L_2$ , and  $B$  are translation kinematic energy, rotational kinematic energy, and potential energy, respectively.

$$L_A = L_1 + L_2 + B \quad (3-1)$$

TABLE 3-1 PARAMETERS OF TWO WHEELED INVERTED PENDULUM

Parameters	Unit	Description	Parameters	Unit	Description
W=0.242	m	Body Width	$J_{\psi} = \frac{ML^2}{2}$	kgm <sup>2</sup>	Body pitch inertia moment
M=1.047	kg	Body Mass	$J_{\phi} = \frac{M(W^2 + D^2)}{12}$	kgm <sup>2</sup>	Body yaw inertia moment
m=0.118	kg	Wheels mass	R <sub>m</sub> =1.900	Ω	DC motor resistance
R=0.060	m	Diameter of wheel	K <sub>t</sub> =13.400	mNm/A	DC motor torque constant
g=9.810	m/s <sup>2</sup>	Gravity acceleration	K <sub>b</sub> =1.400	mv/rpm	DC motor back E.M.F constant
L=0.030	m	Distance between the center of the mass and the Wheel axle	f <sub>m</sub> = 0.0022		The friction coefficient between body and DC motor
D=0.050	m	Body Depth	θ, ψ, φ	rad	Rotary angle of the wheel, pitch angle and yaw angle of the robot
n=64:1	-	Gear ratio	l, r, b	-	Subscripts indicating left or right wheels and the robot body, respectively
$J_w = \frac{mR^2}{2}$	kgm <sup>2</sup>	Wheel inertia moment			

It is assumed that the robot has 3 degrees of freedom (DoFs). The generalized variables of the robot are the angle of the wheel (θ), pitch angle (φ), and yaw angle (ψ) [29]. According to the robot dynamics, the translational and rotational kinetic energies are described as follows (Equations 3-2):

$$L_1 = \frac{1}{2}m(\dot{x}_l^2 + \dot{y}_l^2) + \frac{1}{2}m(\dot{x}_r^2 + \dot{y}_r^2) + \frac{1}{2}M(\dot{x}_b^2 + \dot{y}_b^2 + \dot{z}_b^2) \quad (3-2)$$

$$L_2 = \frac{1}{2}J_w\dot{\theta}_l^2 + \frac{1}{2}J_w\dot{\theta}_r^2 + \frac{1}{2}J_{\psi}\dot{\psi}^2 + \frac{1}{2}J_{\phi}\dot{\phi}^2 + \frac{1}{2}n^2J_m(\dot{\theta}_l - \dot{\psi})^2 + \frac{1}{2}n^2J_m(\dot{\theta}_r - \dot{\psi})^2 \quad (3-3)$$

$$L_2 \neq L_1 \quad (3-4)$$



$$B = Mgz_b \quad (3-5)$$

The Lagrangian equations (3-6, 3-8) are:

$$\frac{d}{dl} \left( \frac{\partial L_a}{\partial \dot{\theta}} \right) - \frac{\partial L_a}{\partial \theta} = F_l + F_r \quad (3-6)$$

$$\frac{d}{dl} \left( \frac{\partial L_a}{\partial \dot{\psi}} \right) - \frac{\partial L_a}{\partial \psi} = -F_l - F_r \quad (3-7)$$

$$\frac{d}{dl} \left( \frac{\partial L_a}{\partial \dot{\phi}} \right) - \frac{\partial L_a}{\partial \phi} = \frac{W}{2R} (F_r - F_l) \quad (3-8)$$

where,  $F_l$  and  $F_r$  are the torques on the left and right wheels, respectively. Moreover, they could be defined as (3-9) and (3-10):

$$F_l = nK_t i_l \quad (3-9)$$

$$F_r = nK_t i_r \quad (3-10)$$

By substituting the kinetic and potential energies in the Lagrangian equations, the equations of motion are as follows:

$$\left( (2m + M)R^2 + 2J_w + 2n^2J_m \right) \ddot{\theta} + (MRL\cos\psi - 2n^2J_m)\ddot{\psi} - MLR\psi^2 \sin\psi = F_\theta \quad (3-11)$$

$$(MRL\cos\psi - 2n^2J_m)\ddot{\theta} + (ML^2 + J_\psi + 2n^2J_m)\ddot{\psi} - MgL\sin\psi - ML^2\dot{\phi}^2 \sin\psi \cos\psi = F_\psi \quad (3-12)$$

$$\left( \frac{1}{2}mW^2 + J_\phi + \frac{W^2}{2R^2} (J_w + n^2J_m) + ML^2 \sin^2 \psi \right) \ddot{\phi} + 2ML^2\dot{\psi}\dot{\phi} \sin\psi \cos\psi = F_\phi \quad (3-13)$$

The external forces can be presented as equations 3-14, 3-16:

$$F_\theta = \frac{nK_t}{R_m} (v_l + v_r) + 2 \left( \frac{n^2K_tK_b}{R_m} \right) \dot{\psi} - 2 \left( \frac{n^2K_tK_b}{R_m} \right) \dot{\theta} \quad (3-14)$$

$$F_\psi = -\frac{nK_t}{R_m} (v_l + v_r) - 2 \left( \frac{n^2K_tK_b}{R_m} \right) \dot{\psi} + 2 \left( \frac{n^2K_tK_b}{R_m} \right) \dot{\theta} \quad (3-15)$$

$$F_\phi = \frac{nK_tW}{2RR_m} (v_r - v_l) - \frac{W^2}{2R^2} \left( \frac{n^2K_tK_b}{2R_m} \right) \dot{\phi} \quad (3-16)$$

The equations mentioned above can be transformed into a nonlinear state-space equation, by defining (3-17):

$$[\theta, \dot{\theta}, \psi, \dot{\psi}, \phi, \dot{\phi}] \quad (3-17)$$

as the state variables (3-18):

$$X = [x_1, x_2, x_3, x_4, x_5, x_6] = [\theta, \dot{\theta}, \psi, \dot{\psi}, \phi, \dot{\phi}] \quad (3-18)$$

Hence, the general form of the state space is given as equations 3-19, 3-22:

$$M(x)\dot{x} = f(x) + u \quad (3-19)$$

where:

$$M(x) = \begin{bmatrix} 1 & 0 & 0 & 0 & 0 & 0 \\ M_{21} & M_{22} & -M_{24} & M_{24} & 0 & 0 \\ 0 & 0 & 1 & 0 & 0 & 0 \\ -M_{21} & M_{24} & M_{21} & M_{44} & 0 & 0 \\ 0 & 0 & 0 & 0 & 1 & 0 \\ 0 & 0 & 0 & 0 & M_{65} & M_{66} \end{bmatrix} \quad (3-20)$$

$$f(x) = \begin{bmatrix} f_1 \\ f_2 \\ f_3 \\ f_4 \\ f_5 \\ f_6 \end{bmatrix} = \begin{bmatrix} x_2 \\ MLRx_4^2 \sin x_3 \\ x_4 \\ MgL \sin x_3 + ML^2 x_6^2 \sin x_3 \cos x_3 \\ x_6 \\ -2ML^2 x_4 x_6 \sin x_3 \cos x_3 \end{bmatrix} \quad (3-21)$$

$$u = \begin{bmatrix} 0 \\ u_2 \\ 0 \\ -u_2 \\ 0 \\ u_6 \end{bmatrix} = \begin{bmatrix} 0 & 0 \\ \frac{nK_t}{R_m} & \frac{nK_t}{R_m} \\ 0 & 0 \\ -\frac{nK_t}{R_m} & -\frac{nK_t}{R_m} \\ 0 & 0 \\ \frac{nK_t w}{2RR_m} & -\frac{nK_t w}{2RR_m} \end{bmatrix} \begin{bmatrix} v_r \\ v_l \end{bmatrix} \quad (3-22)$$

where  $u$  is the control input which is generated by the controllers in this study.

## 3.2 Two-wheel inverted pendulum robot controller design

This part of the research presents three control design methods for implementing planar turning motion of a two-wheeled inverted pendulum. The controls task requires that the inverted pendulum is kept stabilized during the whole turning motion process along a pre-settled track.

### 3.2.1 Two-wheel inverted pendulum robot PID controller design

To stabilize the two-wheel inverted pendulum, the proportional-integrator-derivative (PID) controllers are designed with the following transfer function:

$$G_c = K_p + K_D s + \frac{K_I}{s} \quad (3-23)$$

Two PID controllers in parallel are designed. The first PID controller aims at regulating the body pitch angle. The second PID controller aims at regulating the angular position of the wheels [49, 50].

There are two measurements of the angles from two different sources. The measurement from the accelerometer gets affected by sudden horizontal movements (it could be used to measure the  $\Psi$ ), and the measurement from the gyroscope gradually drifts away from the actual value (it could be used to measure  $\Theta$ ). In other words, the accelerometer reading gets affected by short-duration signals, and the gyroscope reading is affected by long-duration signals. To stabilize the robot, two PID controllers work simultaneously to control pitch and wheel angles, which are measured by accelerometer and gyroscope, respectively.

The PID controller is applied to the simulated model, which is presented in equation 3-23. Figure 3-2 is the block diagram of closed-loop position control for the TWIP. The parameters of the PID controllers are obtained by trial and error. The tuned parameters are given as in Table 3-2.

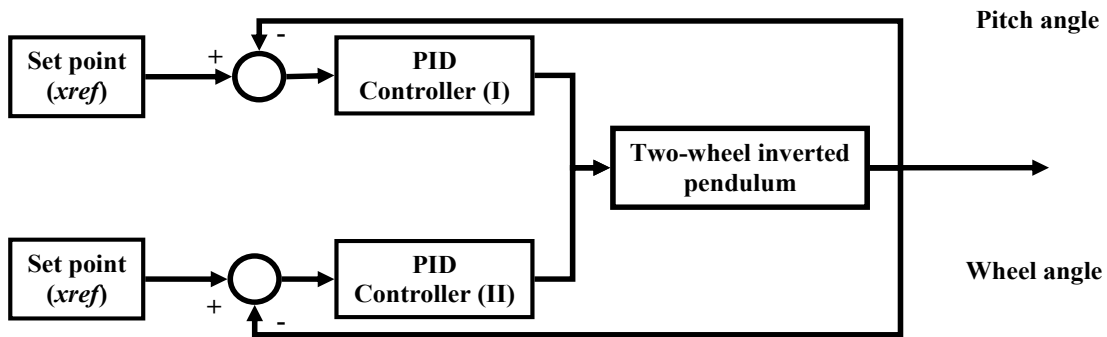


FIGURE 3-2 TWIP CLOSED-LOOP BLOCK DIAGRAM HAVING PID CONTROLLER

TABLE 3-2 PID CONTROLLER PARAMETERS

	$K_P$	$K_I$	$K_D$
$\Psi$	5.19	0.009	0.00045
$\Theta$	5.50	0.00078	0.00025

In Figure 3-2,  $xref$  represents the desired states, and we set  $xref=0$  rad to stabilize the TWIP.

### 3.2.2 SFC designed by LQR

To stabilize the two-wheel inverted pendulum, the optimal SFC is designed using LQR. Equation 3-24 is the linear quadratic regulator objective function:

$$J = \int_0^{\infty} x^T(t)Qx(t) + u^T(t)Ru(t)dt \quad (3-24)$$

The optimal control input which minimizes the above objective function (3-25) is presented in equation 3-22:

$$u(t) = -Kx(t) \text{ where } K = R^{-1}B^TP \quad (3-25)$$

Matrix  $P$  can be obtained by solving Riccati equation 3-26:

$$A^TP + PA - PBR^{-1}B^TP + C^TC = 0 \quad (3-26)$$

where  $A$ ,  $B$ , and  $C$  are state-space matrices. Two optimal LQRs are designed for left and right DC motors. There are two measurements of the angle from two different sources. The measurement from the accelerometer gets affected by sudden horizontal movements (it could be used to measure the  $\psi$ ), and the measurement from the gyroscope gradually drifts away from the actual value (it could be used to measure  $\theta$ ). In other words, the accelerometer reading gets affected by short-duration signals, and the gyroscope reading is affected by long-duration signals. To stabilize the robot, two-state feedback controllers work simultaneously to control the states of DC motors.

The state feedback controller is applied to the simulated model, which is presented in equation 3-22. Figure 3-3 is the block diagram of closed-loop state control for the TWIP. The gains details are given as in Table 3-3.

TABLE 3-3 SFC GAINS

	$[k_1, k_2, k_3, k_4, k_5, k_6]$
<b>Left motor</b>	$[-0.7071, -0.3078, -11.3966, -1.6791, 0.0000, 0.2111]$
<b>Right motor</b>	$[-0.7071, -0.3078, -11.3966, -1.6791, 0.0000, -0.2111]$

$xref$ : represents the desired states, in this case, to stabilize the TWIP, the  $xref=0$  rad (Figure 3-3).

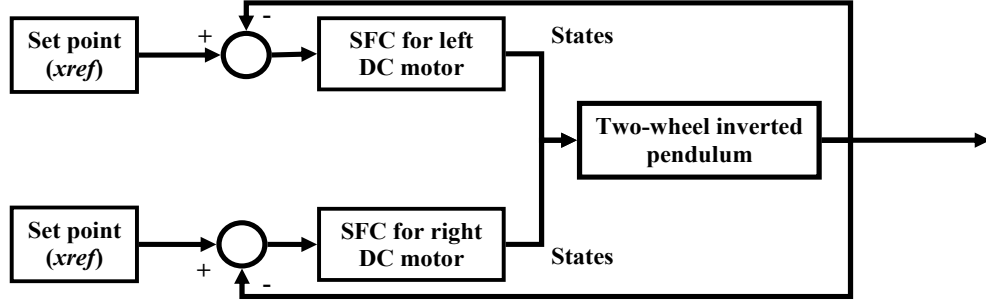


FIGURE 3-3 TWIP CLOSED-LOOP BLOCK DIAGRAM WITH SFCs

### 3.2.3 SMC

As the yaw motion and self-balancing of the robot need to be controlled properly, a sliding mode control is proposed and designed to achieve self-balancing and stabilizing. Due to the system's nonlinearity and uncertainty, SFC could not precisely balance the pendulum and reject the large disturbance within a short period. Hence, the sliding mode controller is designed to handle the nonlinearity of the system using the sliding surface approach.

The design of the wheel angle sliding mode controller is presented as follows:

$$s_1 = c_1\psi + c_2\dot{\psi} \quad (3-27)$$

$$\dot{s}_1 = -\varepsilon_1 \text{sign}(s_1) \quad (3-28)$$

$$u_2 = \frac{c_1(M_{24}^2 - M_{22}M_{44})\dot{\psi} + (M_{24}^2 + M_{22}M_{44})\varepsilon_1 \text{sign}(s_1)}{c_2(-M_{24} - M_{22})} + \frac{c_2M_{24}f_2 - c_2M_{22}f_4}{c_2(-M_{24} - M_{22})} + \frac{c_2M_{12}(-M_{24} + M_{22})\dot{\theta} - c_2M_{21}(M_{24} + M_{22})\dot{\psi}}{n} \quad (3-29)$$

The design of the yaw motion sliding mode controller is presented as (3-30):

$$s_2 = c_3\phi + c_4\dot{\phi} \quad (3-30)$$

By substituting the equations to the robot dynamic, the second input can be calculated as (3-31):

$$u_6 = \frac{M_{66}\varepsilon_2 \text{sign}(s_2)}{-c_4} - f_6 + \dot{\phi}(M_{65} - c_3M_{66}) \quad (3-31)$$

where:

$$f_2 = MLRx_4^2 \sin x_3 \quad (3-32)$$

$$f_4 = MgL \sin x_3 + ML^2 x_6^2 \sin x_3 \cos x_3 \quad (3-33)$$

$$f_6 = -2ML^2 x_4 x_6 \sin x_3 \cos x_3 \quad (3-34)$$

From equations 3-35 and 3-36, the inputs of left and right wheels are:

$$v_r = \frac{RR_m}{nK_{tw}} u_6 - \frac{R_m}{2nK_t} u_2 \quad (3-35)$$

$$v_l = -\frac{RR_m}{nK_{tw}} u_6 - \frac{R_m}{2nK_t} u_2 \quad (3-36)$$

Figure 3-4 depicts the block diagram of closed loop position control with a sliding mode controller for the TWIP.

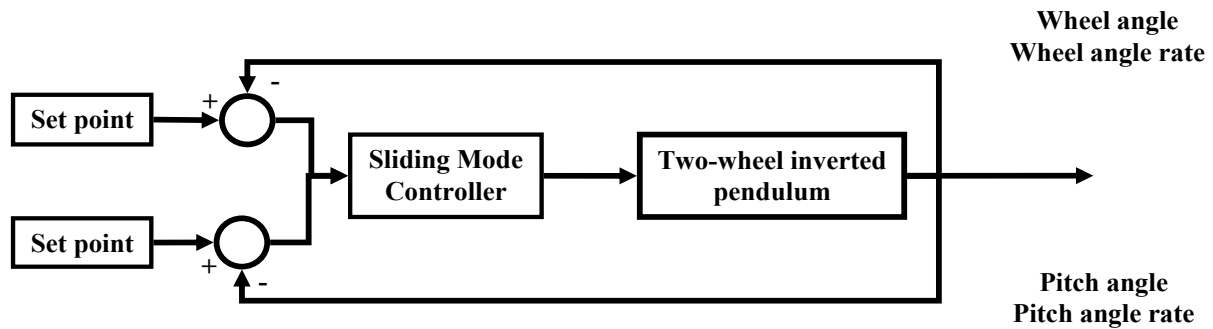


FIGURE 3-4 SMC BLOCK DIAGRAM FOR TWIP

### 3.3 Summary

In this chapter, the dynamic model of TWIP is built by using Lagrangian function method. Three controllers—PIC controller, SFC controller and SMC controllers have been designed based on the built model. The simulation and experimental tests on the developed controller will be carried out later.

## CHAPTER 4 DEVELOPMENT OF A CCR

The methodology of the cable climbing robot is detailed in the following sections. The development of the CCR in this research includes both mechanical and electrical systems design, analysis of design, robot controller design and robot programming and testing, etc.

### 4.1 Development strategy

To aid the development process, a workflow is shown in Figure 4-1.

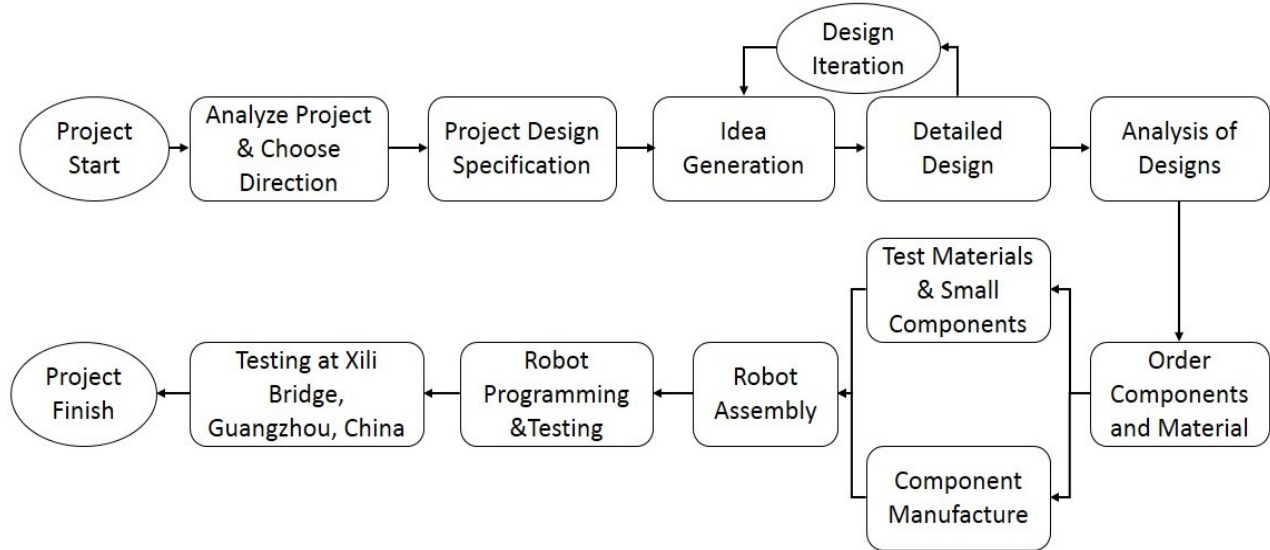


FIGURE 4-1 DEVELOPMENT PROCESS WORKFLOW

### 4.2 Aims and objectives

1. Design a new cable climbing robot:
  - a. Design a high-performance climbing mechanism and adhesion mechanism with suspension features;
  - b. Design the robot control system and train the operator.

2. Develop a small robot capable of inspecting for the difference between cable sizes 100 mm and 300 mm of hanger cables with the following core development aims:

- a. A modular architecture that allows the platform to be easily modified;
- b. Lightweight and deployable by one person;
- c. Reliable, and easily repairable;
- d. Own the defect determining and positioning system capability to aid the robot in becoming fully autonomous;
- e. Develop a high-speed adhesion scissor and lateral force support for smooth climbing with self-lock linear actuators;
- f. Long-term aim to allow future engineers to develop this robot into a commercial bridge cable climber robot.

#### **4.2.1 New modular robotic architecture**

A new modular robotic architecture is developed, describing the physical layout and connections between components. The main features with this modular approach were:

- Fixed critical dimensions of the platform where the highest cost would be incurred during the modification;
- Flexible structure allowing non-critical dimensions to be altered quickly;
- A standard set of interchangeable components reducing complexity;
- Future development time is reduced.

The scope of this cable climbing robot project is to develop the smallest possible version of the platform with strong capabilities.

#### **4.3 High-level specification**

G.C.H company requirements are served as a base specification for the Cable Climbing Robot. It is decided to design and build a swift, small, modular, and lightweight robot to fit through the difference between cable sizes 100 mm and 300 mm of hanger cables, the most challenging part.



Developing a reliable lightweight robot under 50 kg would allow it to be deployed by a single operator. The design is split into four subsystems (Table 4-1).

TABLE 4-1 SYSTEM DESIGN

1. Chassis	2. Drivetrain	3. Adhesion mechanism	4. Electronics & software
	a. Drivetrain mechanism	a. Scissor mechanism	a. Control electronics
	b. Climbing & self-landing	b. Self-locking & shock absorber	b. Power electronics c. Computer software

Table 4-2 details the high-level specification for the new design.

TABLE 4-2 SPECIFICATION FOR THE CABLE CLIMBING ROBOT (ND: NOT DIRECTLY)

ID	Objective	Description	Company requirements								
				Chassis	Drivetrain	Climbing & self-landing	Scissor mechanism	Self-Locking & shock Absorber	Control electronics	Power electronics	Computer software
1	Control speed	Control the climbing speed	Yes		X	X	X	X	X	X	X
2	Crash avoider	Using an ultrasonic sensor for avoiding a crash.	ND		X				X	X	X
3	Coreless DC motor	Customize a Faulhaber coreless DC motor with an encoder.	ND		X	X		X	X	X	
4	Planetary gearbox	Customize a Faulhaber high torque planetary gear.	ND		X	X		X	X		
5	Chain and sprocket system	Sprockets and chains are used for power transmission.	ND	X	X	X		X			
6	Scissors mechanism	A mechanism is used in devices such as lift tables and scissor lifts.	ND	X			X	X			

TABLE 4-3 SPECIFICATION FOR THE CABLE CLIMBING ROBOT (ND: NOT DIRECTLY- CONTINUED)

ID	Objective	Description	Company requirements	Chassis	Drivetrain mechanism	Climbing & self-landing	Scissor mechanism	Self-Locking & shock Absorber	Control electronics	Power electronics	Computer software
7	Pillow block bearings	A pillow block is a pedestal used to provide support for rotating shaft with the help of compatible bearings & various accessories.	ND	X	X	X					
8	Data transistor	The wireless data received by an XBee module is included in a received packet frame along with the remote transmitter and options for receipt.	ND						X	X	X
9	Suspension	Suspension springs cushion cable surface unevenness and ensure that the urethane wheels always maintain reliable contact with the surface.	ND	X	X	X					
10	Autonomous control	Climbing and information have auto-drive keys and cameras.	ND		X				X	X	X
11	Distance viewer software	Have a single panel on a monitor for observing the distance.	Yes						X	X	X
12	COM is close to the canter of cable	Centre of mass is close to the canter of cable to help with inclines.	ND	X							

TABLE 4-4 SPECIFICATION FOR THE CABLE CLIMBING ROBOT (ND: NOT DIRECTLY- CONTINUED)

ID	Objective	Description	Company requirements	Chassis	Drivetrain mechanism	Climbing & self-landing	Scissor mechanism	Self-Locking & shock Absorber	Control electronics	Power electronics	Computer software
13	Protected batteries	Must be housed, so potential damage is reduced.	Yes	X							
14	Easy access & replace	Must take <60 seconds to access & swap batteries.	ND	X						X	
15	Battery monitor	Must provide a cell voltage level to the operator.	Yes			X			X	X	
16	Powerboard	Provide all systems with correct voltage & power.	Yes			X				X X	X
17	Emergency stop	Have an E-Stop which cuts power to motors.	ND						X	X	X
18	Camera controller	There is enough power supply cable and space to add the online stream.	Yes						X	X	X
19	Urethane wheel	Urethane wheels are used for fast movement on stay cables.	ND		X						
20	Linear actuator	Use a linear actuator for each scissor mechanism.	ND						X	X	X
21	Hexagonal body	It must be small enough to fit through cables	ND	X							
22	Wireless range	Must have ~600 meters wireless range outdoors	Yes						X	X	X
23	65~70 Minutes power	Must endure 30 minutes inspection rounds	Yes						X	X	X

## 4.4 Chassis of CCR

The primary function of the chassis is to store and protect internal components and to provide a platform to mount and integrate the robot's subsystems.

### 4.4.1 Chassis development strategy

Figure 4-2 describes the development strategy of the chassis.

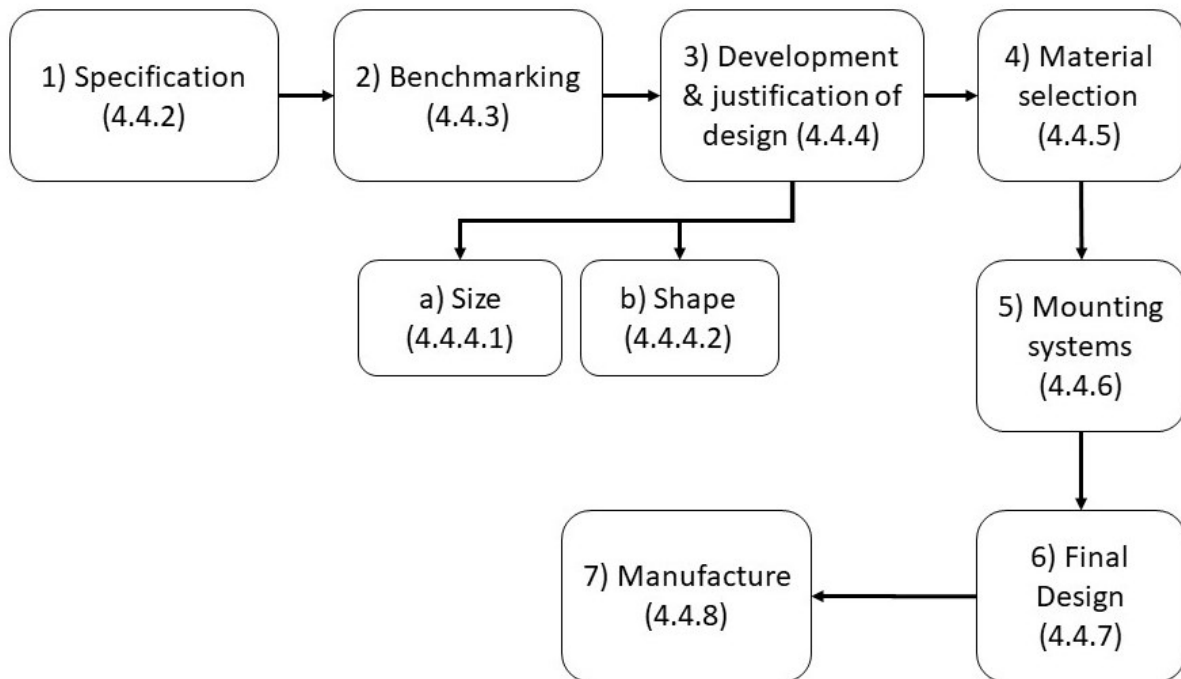


FIGURE 4-2 CHASSIS DEVELOPMENT STRATEGY

### 4.4.2 Specification

Table 4-5 details the chassis and shell specification developed from the aims and objectives, original high-level specification (section 4.3), and GCH Co. Ltd requirements.

TABLE 4-5 CHASSIS AND STRUCTURE SPECIFICATION

<b>ID</b>	<b>Constraint</b>	<b>Description</b>
<b>1</b>	Modular architecture	Develop a core modular architecture that will allow the robotic platform to be easily modified or upgraded by future engineer developers in the company.
<b>2</b>	Cost	Chassis components must be low cost.
<b>3</b>	Repair and maintenance	Easy to repair and maintain. The design should consider ease of assembly/ disassembly and ease of access.
<b>4</b>	Durability	Must be able to withstand the transfer of kinetic energy from collisions. Must prevent debris from getting in the chassis where possible. Must protect internal systems from damage.
<b>5</b>	Mass	The robot must be deployable by one person (37 kg max.). There must be an even distribution of mass within the chassis. Low CoG to improve mobility when climbing incline cables.
<b>6</b>	Size	Must fit all electronics, gearboxes, motors, etc. Combined with the adhesion and drivetrain, it must fit through small cable obstacles.
<b>7</b>	Systems integration	Must account for the fixed dimensions required for the drive train. Must integrate with the scissors module and allow space for adhesion mechanisms electronics. Must store and protect electronic components. Must safely store the battery and allow for easy access. Some components must be insulated from conductive materials.
<b>8</b>	Load resistance	Must be able to withstand a fall from 150 mm. Must take the load of mounting and unmounting. Must be resistant to loads generated within the drivetrain system.
<b>9</b>	Ease of manufacture and assembly	Taking account of the time constraints, chosen materials, and structures must be easily manufactured and assembled in the Concordia Robotic Lab.
<b>10</b>	Material availability	Materials must be readily available from local distributors.

### 4.4.3 Benchmarking

Table 4-6 shows the design progression of the CCR chassis' over time (Figure 4-3, Figure 4-8).

TABLE 4-6 PREVIOUS CABLE CLIMBING ROBOT CHASSIS STRUCTURES

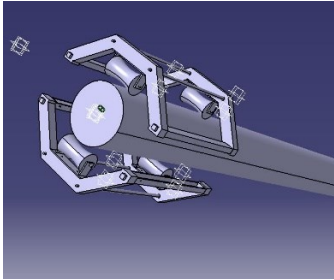
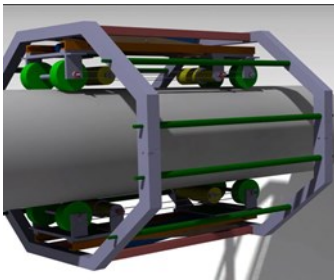
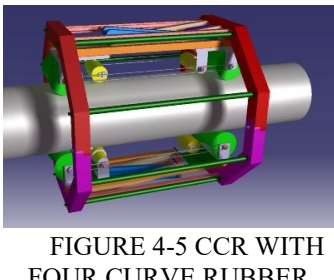
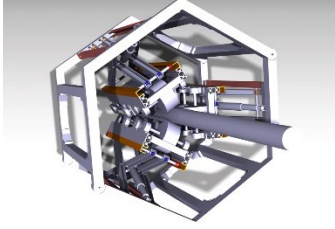
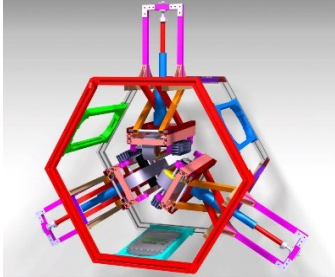
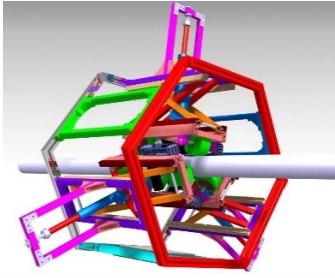
Year	Material	Photo	Construction	Cost	Comments
2016-17	14 mm Aluminum (Al)	 <p>FIGURE 4-3 SIMPLE CCR</p>	Plate construction (Used CNC milling and lathe)	N/A	Bolted together using CAP screws, pockets removed where strength is not required saving mass.
2017-17	10 mm Al	 <p>FIGURE 4-4 CCR WITH EIGHT FLAT RUBBER WHEELS</p>	Plate construction (Used CNC milling, lathe, and laser cut)	2,600 CAD	Adhesions could be easily replaced if damaged. Braces needed to be added to increase rigidity and reduce bending.
2017-17	15 mm Al	 <p>FIGURE 4-5 CCR WITH FOUR CURVE RUBBER WHEELS</p>	Plate construction (Used CNC milling, lathe, and laser cut)	3,900 CAD	N/A

TABLE 4-7 PREVIOUS CABLE CLIMBING ROBOT CHASSIS STRUCTURES (CONTINUED)

Year	Material	Photo	Construction	Cost	Comments
2017-18	3 mm Al	 <p data-bbox="418 783 662 863"><i>FIGURE 4-6 CCR WITH THREE ADHESION MECHANISM</i></p>	<p data-bbox="711 541 971 705">Plate construction (Used CNC milling, lathe, and laser cut)</p>	5,000 CAD	<p data-bbox="1107 470 1446 779">Side plate fitted across chassis to increase stiffness. Torsion bar had to be inserted after the robot landed on one of the front pulleys.</p>
2018-19	3 mm Al	 <p data-bbox="386 1274 662 1377"><i>FIGURE 4-7 CCR WITH THREE ADHESION MECHANISM CHAIN AND SPROCKET</i></p>	<p data-bbox="711 1035 971 1178">Plate construction (Used CNC milling, lathe, laser cut)</p>	5,500 CAD	<p data-bbox="1107 1010 1446 1203">Adhesions mechanism horizontally fitted to increase the force between the robot and the cable.</p>
Final	3 mm Al	 <p data-bbox="386 1787 662 1890"><i>FIGURE 4-8 CCR WITH THREE ADHESION MECHANISM URETHANE WHEELS</i></p>	<p data-bbox="711 1493 1011 1749">Structural space frame-plate construction (Used CNC milling, lathe, laser cut, water jet cut)</p>	10,300 CAD	<p data-bbox="1107 1545 1442 1717">Urethane wheels added for smooth climbing. A high-performance chain added as a power transmitter.</p>

CCR robots reviewed in section 2.2.2 and previous CCR designs (Table 4-6) indicate that the most common factors between designs are the materials used, predominantly aluminum, and the curved shape of the chassis, which aid mobility [30]. All previous designs are curved at the front and back to avoid catching and have control components outside of the shell. The cost is also increased over time. These factors are considered in the design process [31].

## 4.4.4 Development and justification of design

### 4.4.4.1 Size

The robot's maximum chassis dimensions are found through geometric relationships (Equations 4-1, 4-2, and 4-3) derived from two specification constraints Figure 4-9.

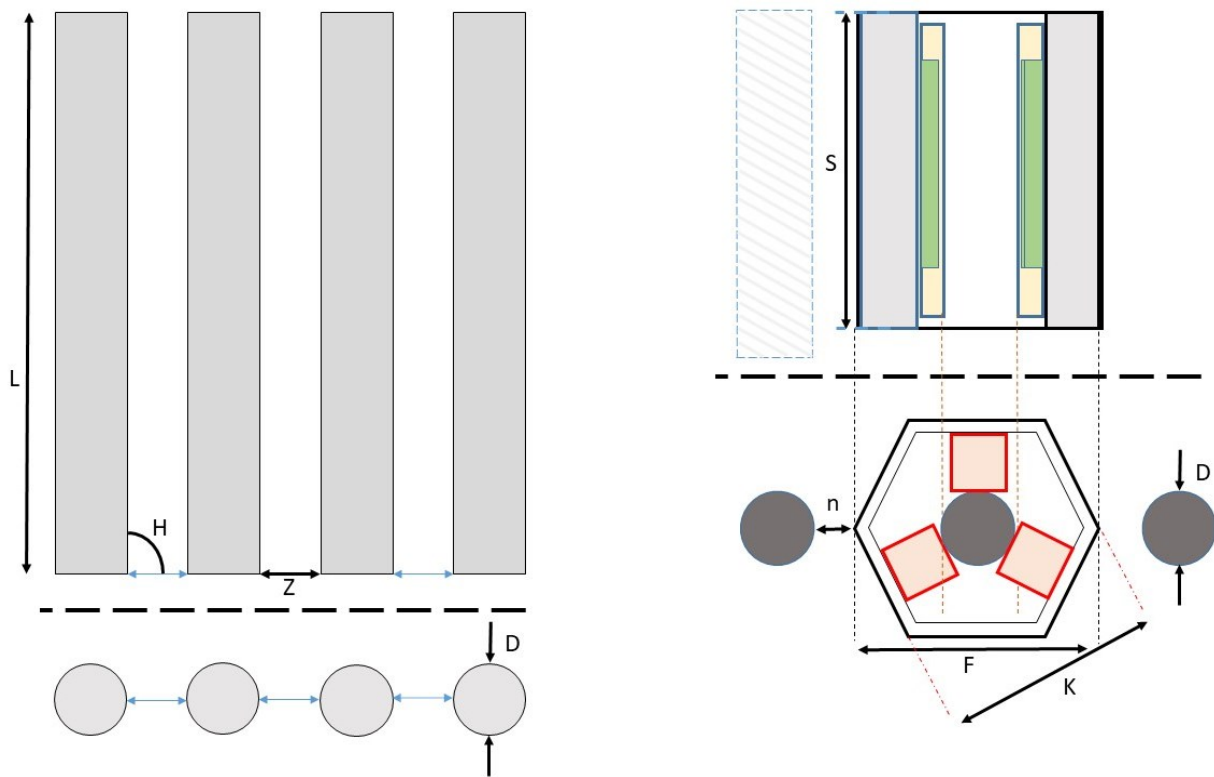


FIGURE 4-9 ROBOT HEIGHT AND WIDTH DIMENSIONS (LEFT), MAXIMUM LENGTH BETWEEN CABLES (RIGHT)



For known hexagon size (K) and chosen robot width (F), the maximum robot height is given by equation 4-1. Safety distance (n) is calculated from a chosen value of cable distance (Z), equation 4-2. The maximum robot length (S) is calculated using equation 4-3.

n= Safety distance      D= Cable diameter      C=Adhesion mechanism size

Z=Cable distance      H= Cable angel      t= Body thickness

$$K = D + 2t + 2C \quad (4-1)$$

$$n + \frac{F}{2} = Z + D \quad (4-2)$$

$$F < S < 2K \quad (4-3)$$

Table 4-8 details the maximum chassis dimensions calculated.

TABLE 4-8 THE MAXIMUM CHASSIS DIMENSIONS

ID	Parameter	Symbol	Dimension
1	Cable length	L	10-500 m
2	Cable angel	H	35-90 degree
3	Maximum robot width	F	65 cm
4	Maximum robot diagonal	K	80 cm
5	Cable diameter	D	100-300 mm
6	Best robot length	S	67-85 cm
7	The minimum distance between cables	Z	32.5 cm
8	Safety distance	n	10-30 cm

The final robot width and maximum length must take into account the tracks. The maximum height should account for the drivetrain system [32].

Table 4-9 details the maximum possible chassis dimensions and the chosen dimensions illustrated in Figure 4-10.

TABLE 4-9 THE MAXIMUM POSSIBLE CHASSIS DIMENSIONS AND THE CHOSEN DIMENSIONS

Parameter	Maximum (mm)	Chosen (mm)	Explanation
Width (w)	692.8	650	Minimized to reduce COG, 42.8 mm clearance was chosen to increase clearance while turning
Length (L)	900	720	180 mm for more stability between chassis and rubber tracks
Cable diameter (D)	300	330	30 mm clearance was chosen to install the robot easily

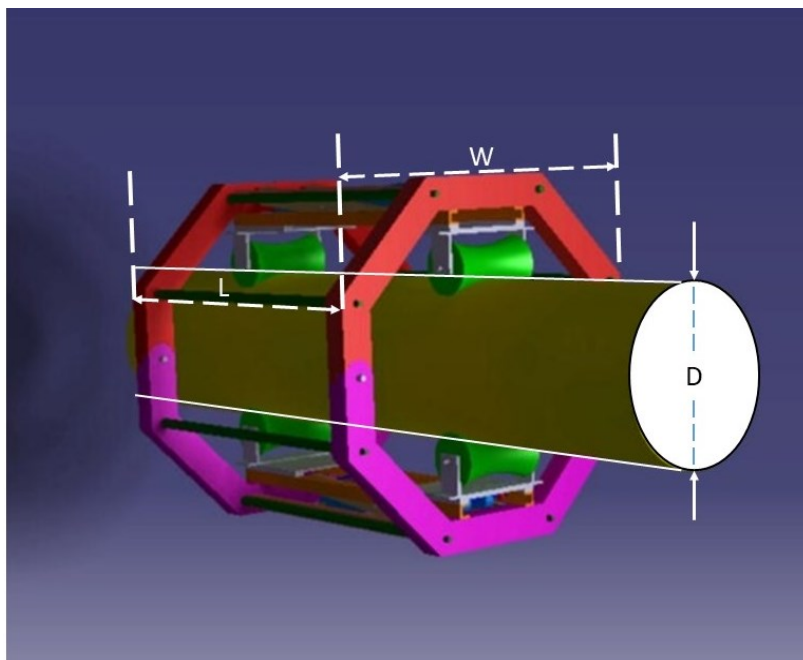


FIGURE 4-10 FINAL CHASSIS DIMENSIONS

#### 4.4.4.2 Shape

Two critical factors are used to determine the shape of the robot:

1. Shape, size, and location of internal components.
2. Collision avoidance and mobility.

Major internal components are approximated in Computer-Aided Design (CAD) software and assembled into an initial chassis design to assess whether the components would fit into the available package (Figure 4-11, Figure 4-12). Accurate components are then created in CAD (Figure 4-13, Figure 4-14).

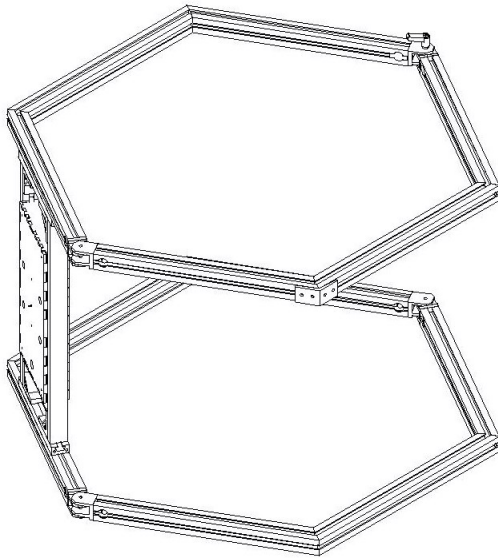


FIGURE 4-11 ROBOT HEXAGON FRAMES

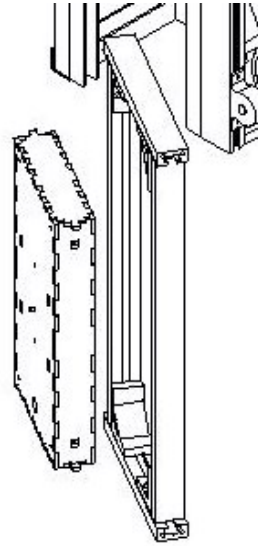


FIGURE 4-12 ELECTRONIC BOX AND ALUMINUM FRAME

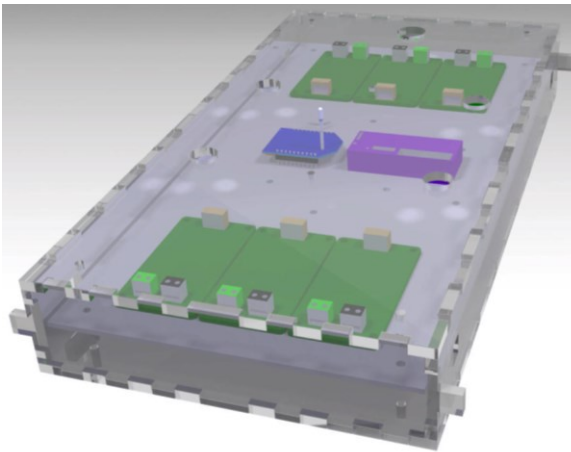


FIGURE 4-13 3D CAD FRAME OF ELECTRONIC BOX UP-SIDE

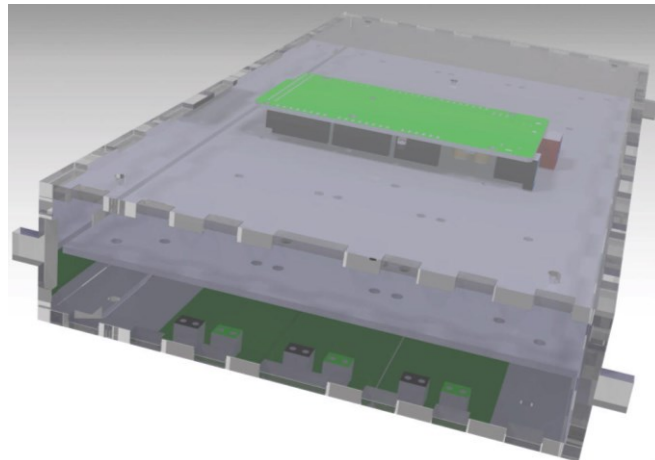


FIGURE 4-14 3D CAD FRAME OF ELECTRONIC BOX DOWN-SIDE

Although the robots listed in section 1.2 are curved front and backs to avoid collisions and improve mobility, this decreases the useable volume. This also increases manufacturing complexity and reduces the ease of modification. Due to these factors, a hexagon-shaped structure is selected [33].

#### 4.4.5 Materials selection

The specification led to the comparison of three aluminum variants and a lightweight, off-the-shelf aluminum beam being chosen Misumi with a high strength to weight ratio. Misumi has an integrated construction technique using brackets that bolt inside the T-slot of the beam (Figure 4-15, Figure 4-16). These rigid yet non-permanent fixings allow modification and provide easy assembly (Table 4-10).

TABLE 4-10 ANALYSIS OF POSSIBLE CHASSIS MATERIALS

Material	Ease of manufacture	Ease of assembly	Light-weight	Low cost	Modular	Rigid	Durable	Average
Sheet components	2	2	4	4	2	1	3	2.57
Aluminum	2	3	1	3	2	5	5	3.00
Misumi	4	4	4	4	5	4	4	4.14



FIGURE 4-15 MISUMI PROFILE FIGURE



FIGURE 4-16 MISUMI ANGLE BRACKET

Misumi's aluminum extrusions and accessories are larger and stronger, so it would allow a larger platform to be developed to meet different operational requirements. The objective is to build the smallest, highest capability model; however, Figure 4-17 shows how the size can be increased.

\*Misumi is the brand name for this range of extruded aluminum beam with T-Slots used for prototyping.

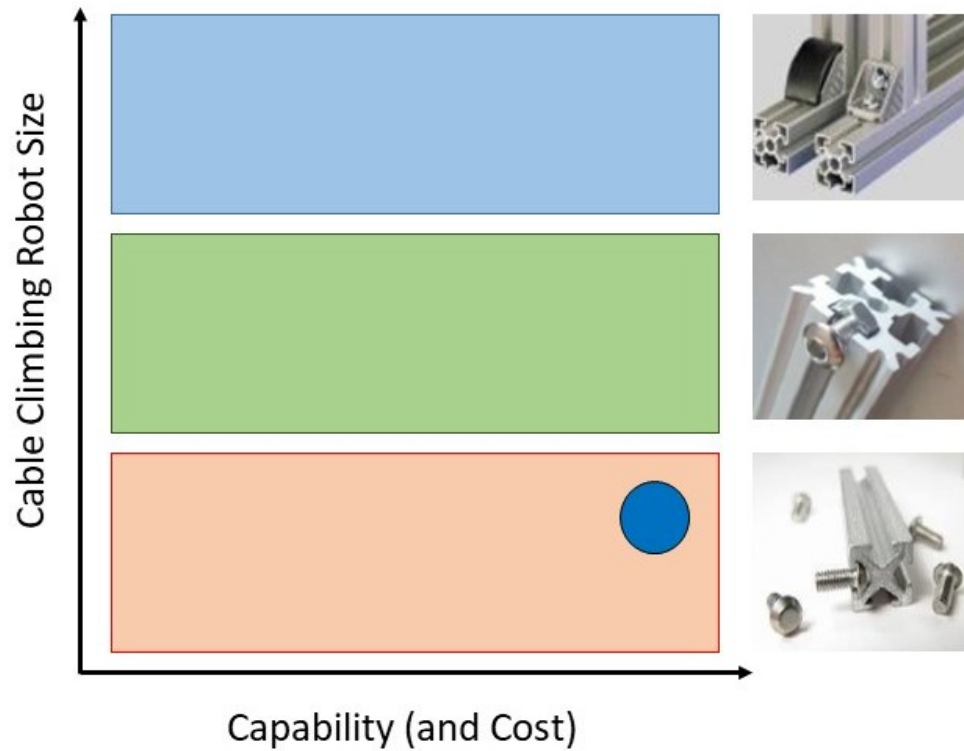


FIGURE 4-17 SCOPE FOR ADAPTING ALUMINUM EXTRUSIONS CHASSIS PLATFORM INTO LARGER SIZES

#### 4.4.6 Mounting systems

Six load transfer points are established:

12 x Pillow block bearing

3 x DC gearbox motors

3 x Linear actuators

3 x Adhesion mechanisms

Bespoke mounting plates are designed and manufactured for these (Figure 4-18).

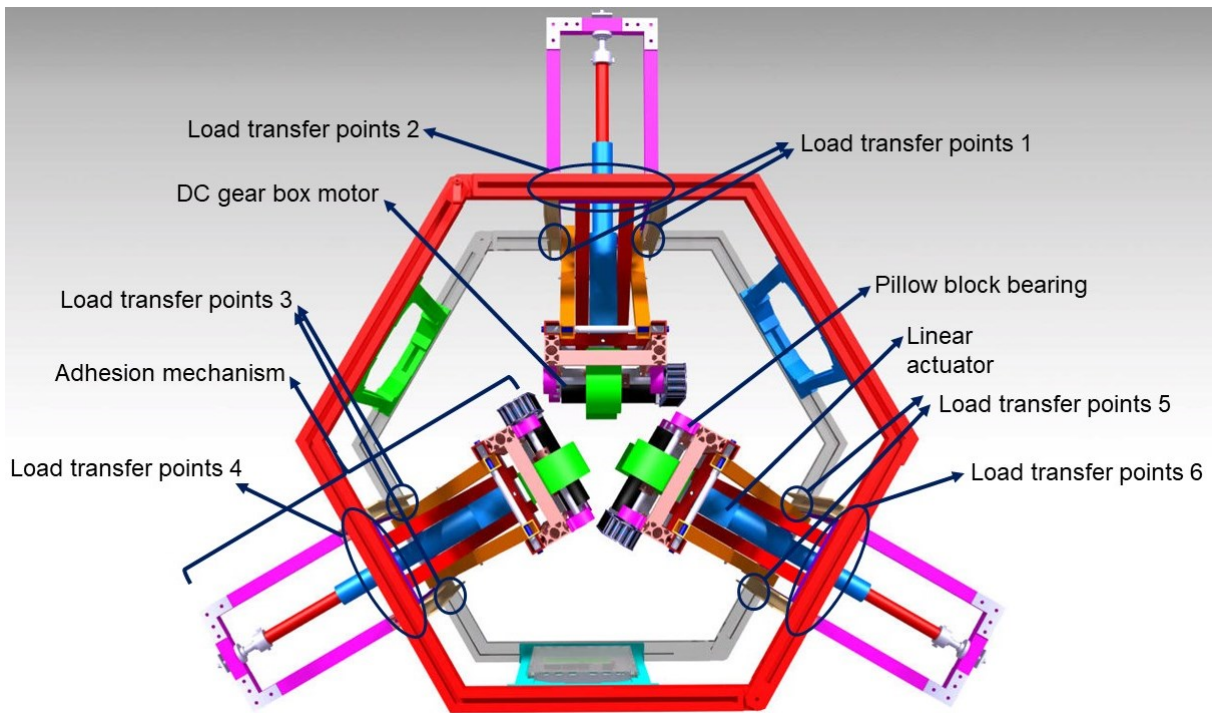


FIGURE 4-18 CHASSIS MOUNTING POINTS

To utilize off-the-shelf parts, standardize the fixings, and minimize cost, Misumi's aluminum extrusions brackets (Figure 4-19) are used and modified where required (82% standard vs. 18% modified) [34].



FIGURE 4-19 MISUMI BRACKETS

Most of the components are mounted directly onto Misumi's aluminum extrusions using the brackets, and the remaining components are mounted onto local brands.

The housing for the electronics stuff is laser cut from 5 mm thickness plexiglass (Figure 4-20). This allows the removal of the control electronics along with the emergency landing system if they are not required. This aligns with the modularity objectives [35].

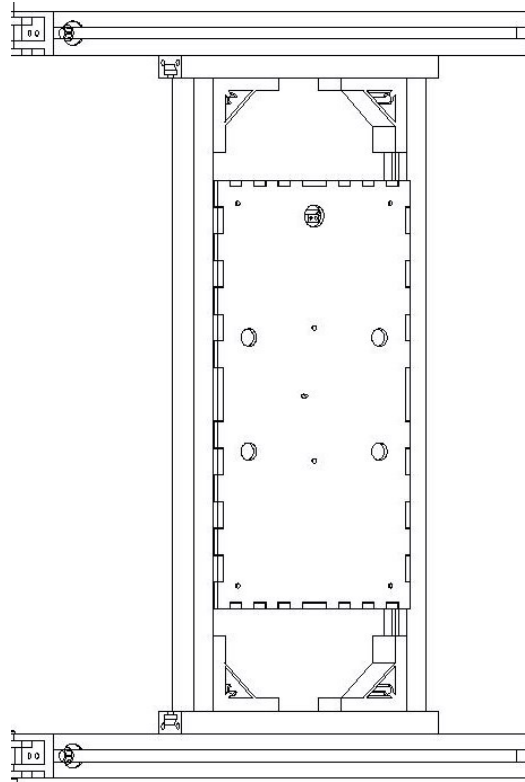


FIGURE 4-20 3D PRINTED BATTERY HOUSING - CAD IMAGE

#### 4.4.7 Final design

CAD images (Figure 4-21, Figure 4-22) show various stages of completion of the final design.

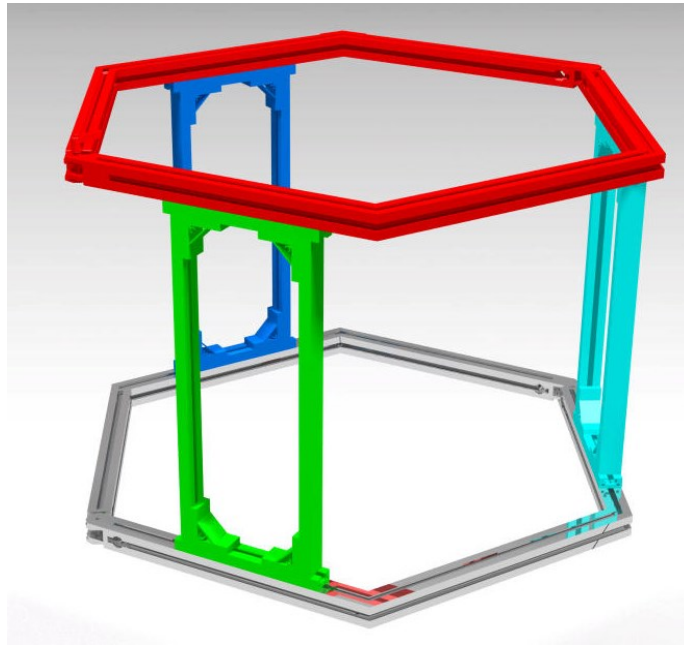


FIGURE 4-21 FINAL CHASSIS DESIGN- RENDERED CAD IMAGE

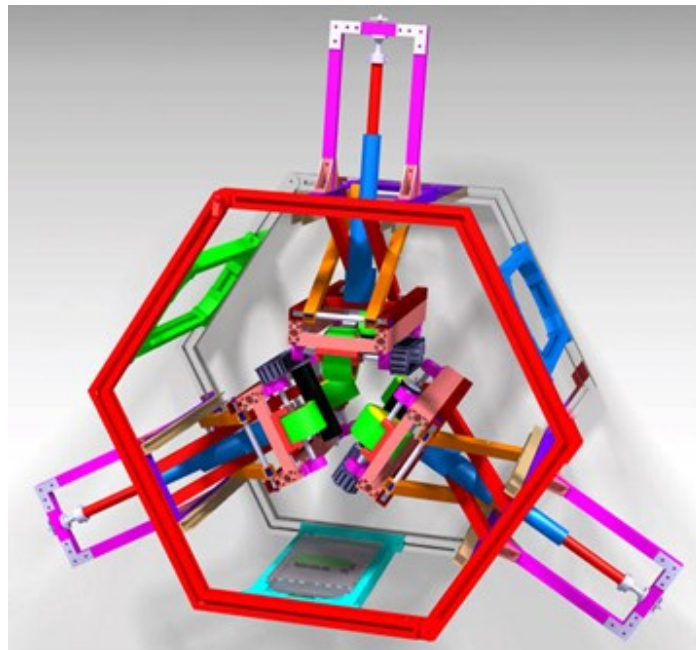


FIGURE 4-22 FINAL CHASSIS DESIGN WITH INTERNAL COMPONENTS - RENDERED CAD IMAGE



#### 4.4.8 Manufacturing and assembly

Table 4-11 details the manufacturing method of each part and justification.

TABLE 4-11 CONSTRUCTION METHODS AND JUSTIFICATIONS

Component	Qty.	Construction Method	Comments
Misumi brackets	12	Band saw and milling	Required perpendicular ends
U-Shaped channels	14	Band saw and folded	Save resources by using methods not requiring a technician
Suspension guider	8	CNC milled	The quickest method for the desired shape
Scissor mechanism pins	12	Saw and milling	Save resources by using methods not requiring a technician
Driveshafts	12	CNC milled	The quickest method for the desired shape
Aluminum profiles	14	Saw and folded	Save resources by using methods not requiring a technician
L-Shaped angles - mounting	6	Water jet cut	Outsourced to save in-house resources
Flat aluminum extrusions	6	Band saw and folded	Save resources by using methods not requiring a technician
Aluminum extrusions - rectangular tubes	12	Milled and drilled	Save resources by using methods not requiring a technician
Rotary shafts	10	Brand new	Outsourced to save in-house resources
Pillow type unit	12	Brand new	Outsourced to save in-house resources
Fit link chains	3	Brand new	A complex part outsourced to save in-house resources
Sprocket	8	Brand new	Outsourced to save in-house resources
Control box	1	Laser cut	Simplest manufacture method
Strong spring TF	3	Brand new	Outsourced to save in-house resources

## 4.5 Drivetrain

A drivetrain is essential for a CCR robot to traverse the target terrain common in bridge cables.

### 4.5.1 Drivetrain development strategy

Figure 4-23 describes the development strategy of the drivetrain.

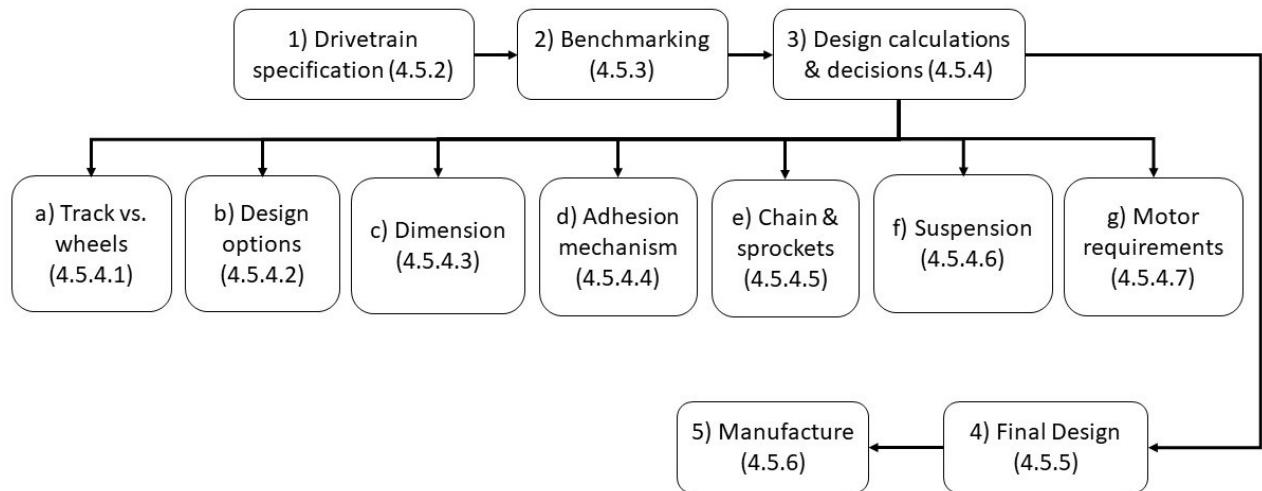


FIGURE 4-23 DRIVETRAIN DEVELOPMENT STRATEGY

## 4.5.2 Drivetrain specification

The significant constraints are presented in Table 4-12.

TABLE 4-12 DRIVETRAIN SPECIFICATION

<b>ID</b>	<b>Constraint</b>	<b>Description</b>
<b>1</b>	Cost	Components should be sourced/designed such to save cost
<b>2</b>	Mass	The robot is to be deployable by one person, limiting the mass to 35 kg
<b>3</b>	Modular	The drivetrain must employ a modular approach allowing different designs to be interchanged
<b>4</b>	Size	The drivetrain must be large enough to drive the robot but small enough to fit through confined spaces
<b>5</b>	Repair/ maintenance	Simple to manufacture parts for easy maintenance
<b>6</b>	Complexity	Parts need to be simple and few
<b>7</b>	Durability	Be impact resistant to the expected forces from its environment
<b>8</b>	Reliability	Disaster environments require high levels of reliability in uncertain terrain
<b>9</b>	Torque	High levels of torque will be required to climb 90-degree slopes
<b>10</b>	Traction	Traction with the ground is essential for slope climbing
<b>11</b>	Obstacle crossing	Needs to climb over 10 mm high, and cross 15 mm wide obstacles
<b>12</b>	Clearance	As high as possible
<b>13</b>	Mobility	Complex terrain requires a high level of mobility
<b>14</b>	Power source	Compatible with and completely powered by a 12 V battery
<b>15</b>	Control	Controlled remotely, requiring ease of use and information fed back to the driver
<b>16</b>	Wiring	Easily wired to the control system
<b>17</b>	Environment	To be suitable for dry indoor environments

### 4.5.3 Benchmarking

This cable climbing robot has a new adhesion mechanism, which is not common among other cable inspection robots (Figure 4-24). This adhesion mechanism provides a good platform to base the new drivetrain on, and it let to the robot to move along bridge cable systems, such as bridge cables, pipes, steel wires, and circular poles for inspection.

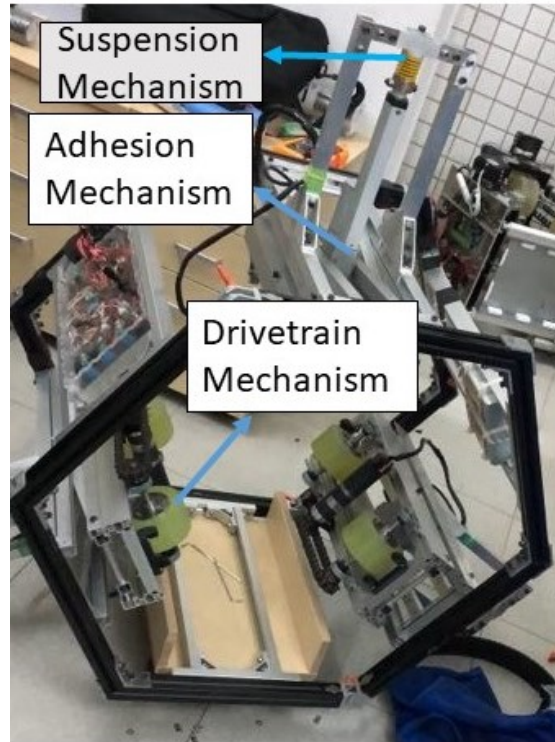


FIGURE 4-24 EXISTING CABLE CLIMBING ROBOT DRIVETRAIN FEATURES

### 4.5.4 Design, calculations, and decisions

#### 4.5.4.1 Tracks vs. wheels

Due to the cost and complexity, the form of transport is limited to tracks or wheels. Table 4-13 compares tracks and wheels against the specification 4.5.2).

TABLE 4-13 TRACKS AND WHEEL COMPARISON AGAINST SPECIFICATION

<b>ID</b>	<b>Constraint</b>	<b>Tracks</b>	<b>Wheels</b>	<b>Scale</b>	<b>Reason for choice</b>
<b>1</b>	Cost	0	1	4	Wheels are more common and involve fewer parts leading to being cheaper
<b>2</b>	Mass	0	1	4	Tracks have more components than wheels, leading to a greater mass
<b>3</b>	Modular	1	0	4	Tracks can have parts mounted inside them, leading to the possibility of a self-contained unit
<b>4</b>	Size	0	1	3	Tracks are more flexible in the shape/size of the design, but wheels are smaller.
<b>5</b>	Adaptability	0	1	3	Wheels only need the tread to be changed for different levels of grip or clearance. Tracks need to be completely replaced to change these aspects.
<b>6</b>	Repair/ maintenance	0	1	3	If the tread breaks, the whole wheel needs replacing and the track needs all tread elements replacing
<b>7</b>	Complexity	0	1	2	Wheels have fewer components so are less complex
<b>8</b>	Durability	0	1	2	Generally made from thick rubber, so more durable than lots of little treads
<b>9</b>	Reliability	0	1	3	Tracks have more components so more can break than in a wheel

TABLE 4-14 TRACKS AND WHEEL COMPARISON AGAINST SPECIFICATION (CONTINUED)

<b>ID</b>	<b>Constraint</b>	<b>Tracks</b>	<b>Wheels</b>	<b>Scale</b>	<b>Reason for choice</b>
<b>10</b>	Torque	1	0	3	Both have the same torque tracks can apply it more effectively
<b>11</b>	Traction	1	0	3	Wheels only contact the ground in a small area whereas tracks are much larger attaining better traction
<b>12</b>	Obstacle crossing	1	1	2	Tracks and wheels length allows them to traverse obstacles which wheels would otherwise get stuck in/on
<b>13</b>	Clearance	0	1	2	Without special consideration, tracks give less clearance than wheels
<b>14</b>	Mobility	1	0	3	Greater obstacle crossing capabilities give tracks better mobility
<b>15</b>	Power	-	-	-	As the power will be the same for both, so will not be compared
<b>16</b>	Control	-	-	-	Control methods will be the same for both
<b>17</b>	Wiring	-	-	-	Wiring to motors will not depend on wheels/tracks
<b>18</b>	Environment	1	0	4	Tracks have lower ground pressure and can, therefore, handle a wider range of environments, e.g., spiral wire/ gimped cable
<b>Total</b>		19	26		

The comparison determines that tracks are the most suitable form of a motion for the new CCR robot.

#### 4.5.4.2 Design options

Three considered concepts are reviewed in detail (Figure 4-25 - Figure 4-31). The cost and complexity increase with improved mobility (Figure 4-32).

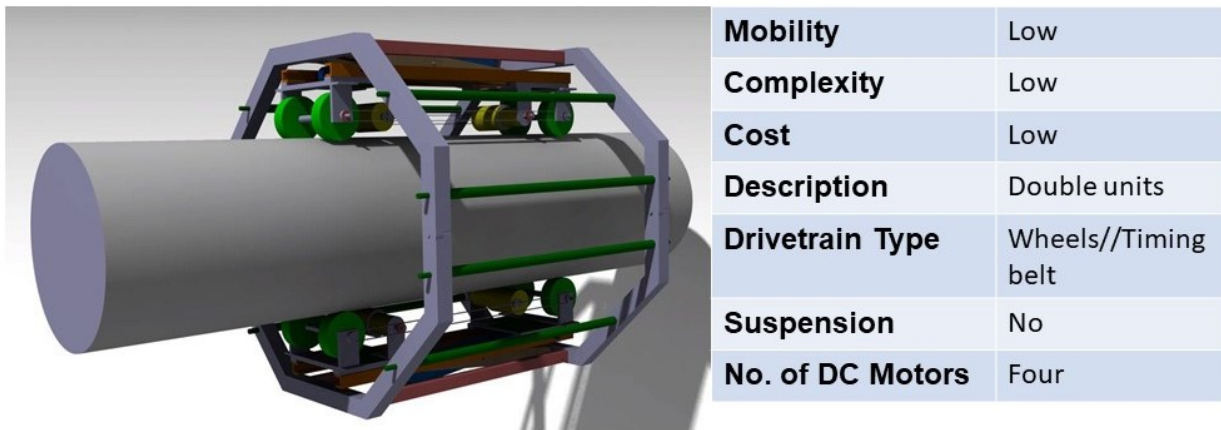


FIGURE 4-25 OPTION 1 – SIMPLEST DRIVETRAIN DESIGN

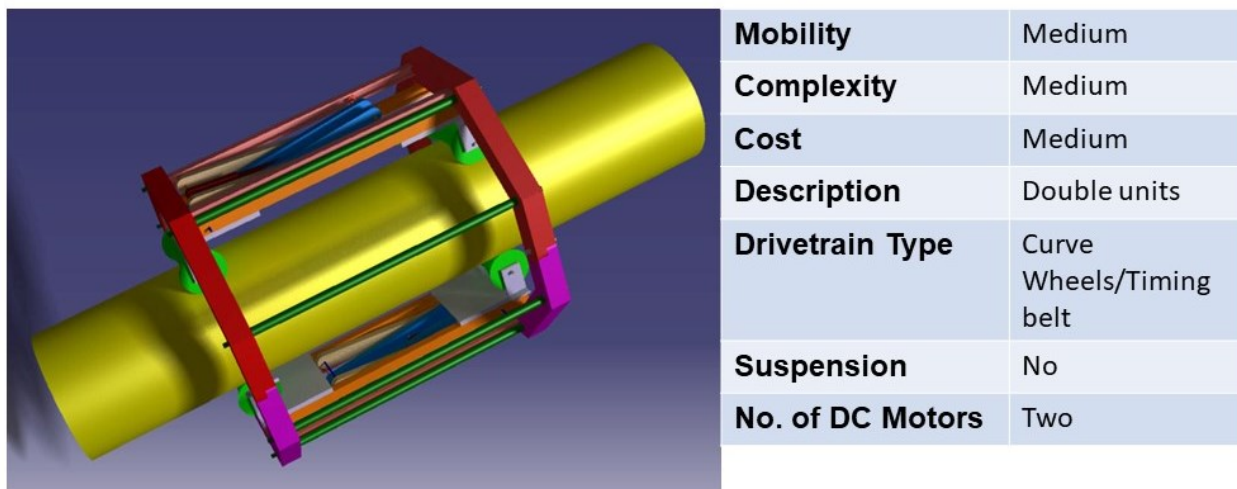
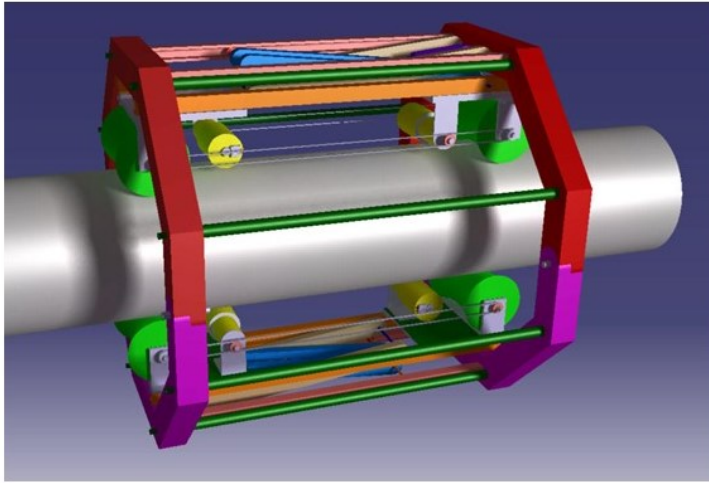
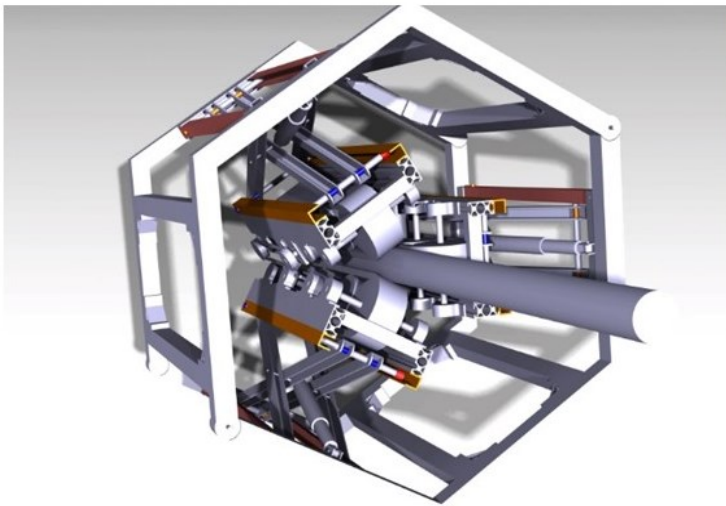


FIGURE 4-26 OPTION 2 – SECOND SIMPLEST DRIVETRAIN DESIGN



<b>Mobility</b>	Medium
<b>Complexity</b>	Medium
<b>Cost</b>	Low
<b>Description</b>	Double units
<b>Drivetrain Type</b>	Curve wheels
<b>Suspension</b>	No
<b>No. of DC Motors</b>	Two

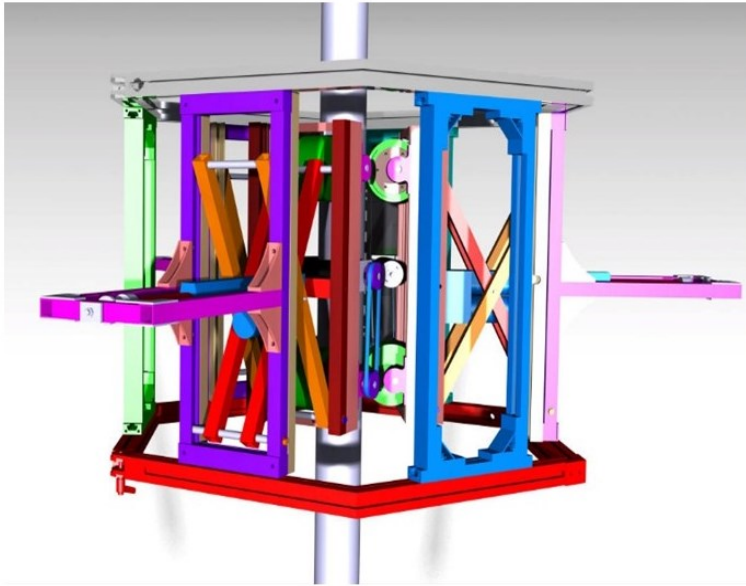
FIGURE 4-27 OPTION 3 – MIDDLE DRIVETRAIN DESIGN



<b>Mobility</b>	Medium
<b>Complexity</b>	High
<b>Cost</b>	High
<b>Description</b>	Triple units
<b>Drivetrain Type</b>	Rubber track
<b>Suspension</b>	No
<b>No. of DC Motors</b>	Three

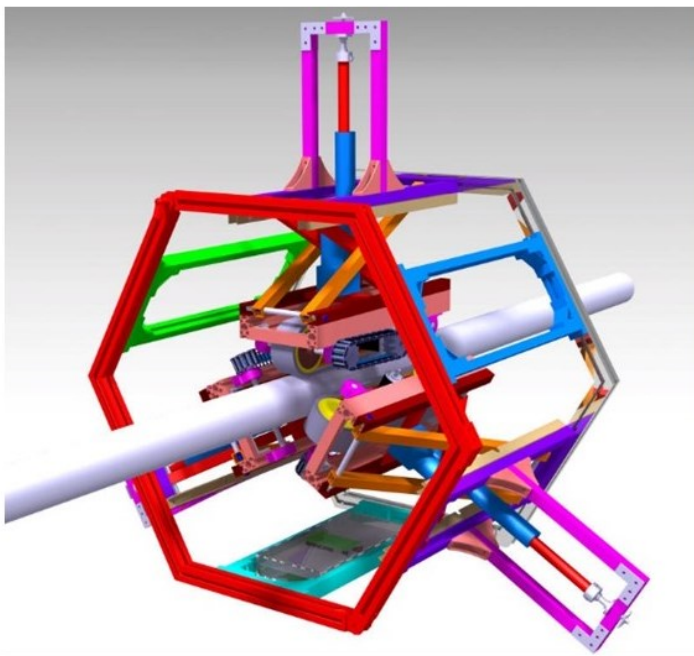
FIGURE 4-28 OPTION 4 – SECOND MIDDLE DRIVETRAIN DESIGN





<b>Mobility</b>	Medium
<b>Complexity</b>	High
<b>Cost</b>	High
<b>Description</b>	Triple units
<b>Drivetrain Type</b>	Rubber track/Timing belt
<b>Suspension</b>	Yes
<b>No. of DC Motors</b>	Three

FIGURE 4-29 OPTION 5 – SECOND MIDDLE DRIVETRAIN DESIGN



<b>Mobility</b>	Medium
<b>Complexity</b>	High
<b>Cost</b>	High
<b>Description</b>	Triple units
<b>Drivetrain Type</b>	Rubber track/Sprocket and chain
<b>Suspension</b>	Yes
<b>No. of DC Motors</b>	Three

FIGURE 4-30 OPTION 6 – SECOND MIDDLE DRIVETRAIN DESIGN

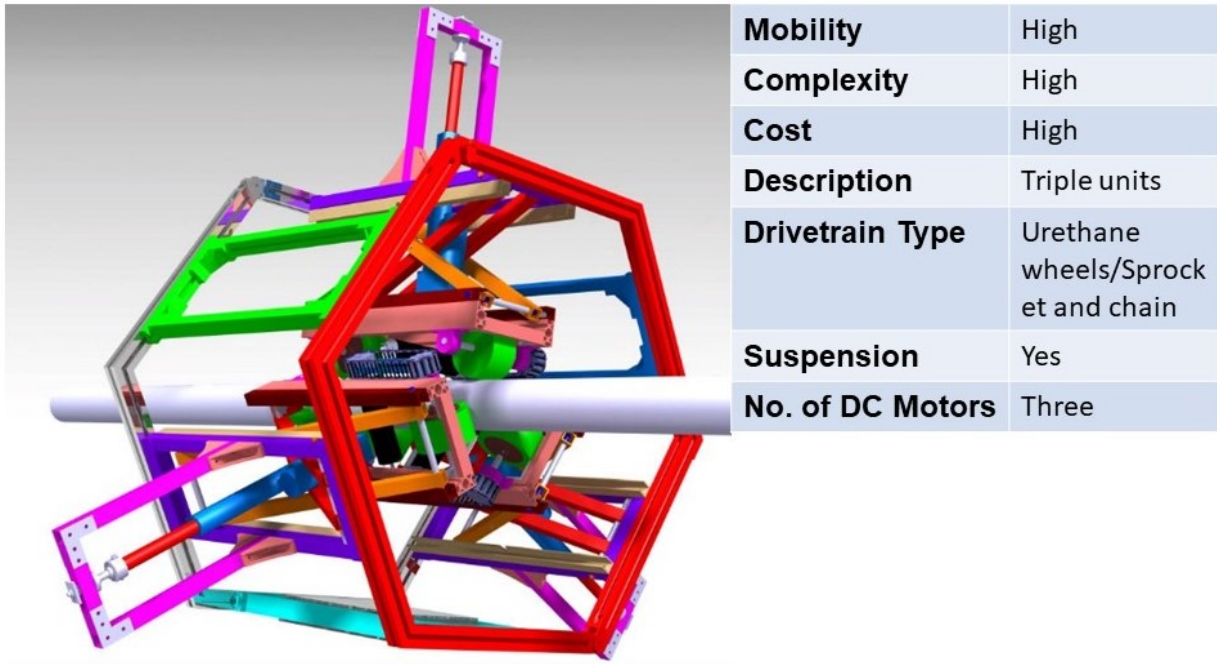


FIGURE 4-31 OPTION 7 – SECOND MIDDLE DRIVETRAIN DESIGN

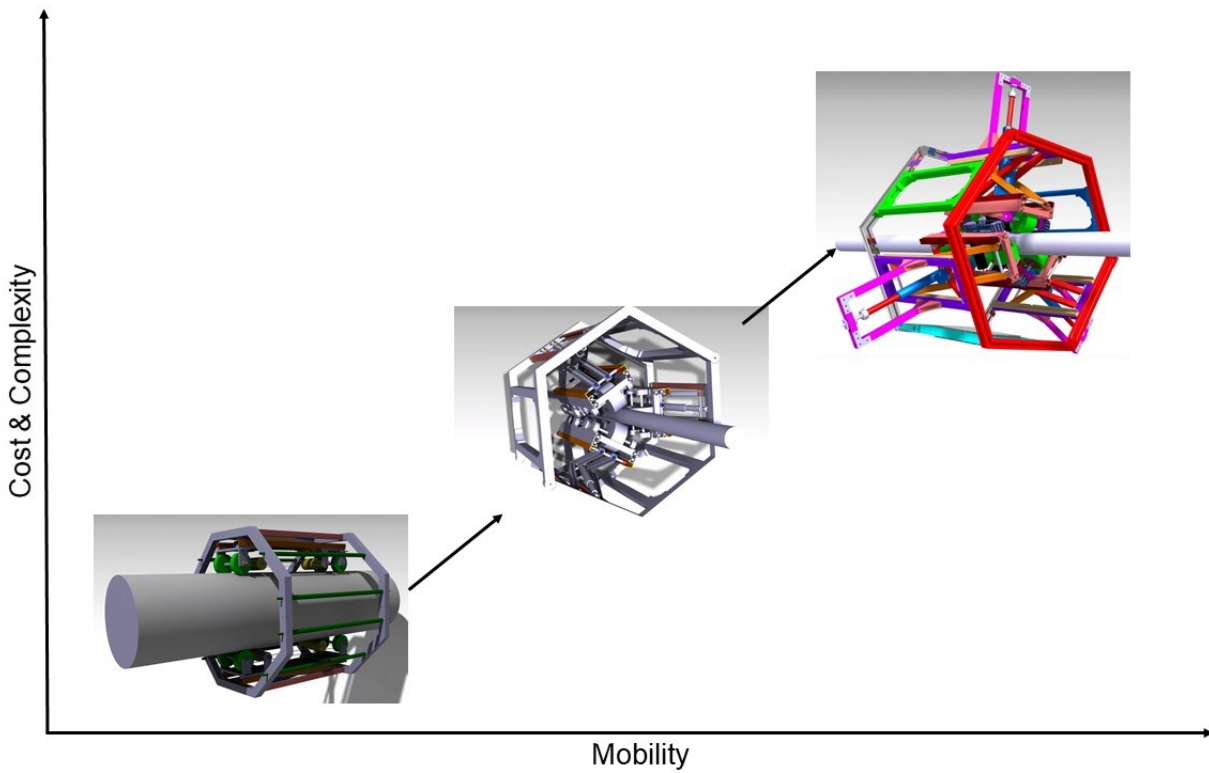


FIGURE 4-32 DRIVETRAIN COST & COMPLEXITY VS. MOBILITY GRAPH

While option 1 (Figure 4-25) and option 3 (Figure 4-27) would be the lowest cost and easiest to implement, the most cost-effective design, option 7 (Figure 4-31), is chosen as this best meets the specification. This option also has the greatest ability to climb different cables. Due to the modularity requirement, the design should still allow the track units to be removed and replaced with a single unit as in option 1 (Figure 4-25) to allow it to be adapted to suit its environment.

#### 4.5.4.3 Dimensions

The robot specification is such that it should fit through a 600mm triangle and have a turning circle of less than 600 mm (Table 4-15). This has a direct effect on the size of the track units. The restricting dimensions of the track units and their placement on the robot are illustrated in Figure 4-33.

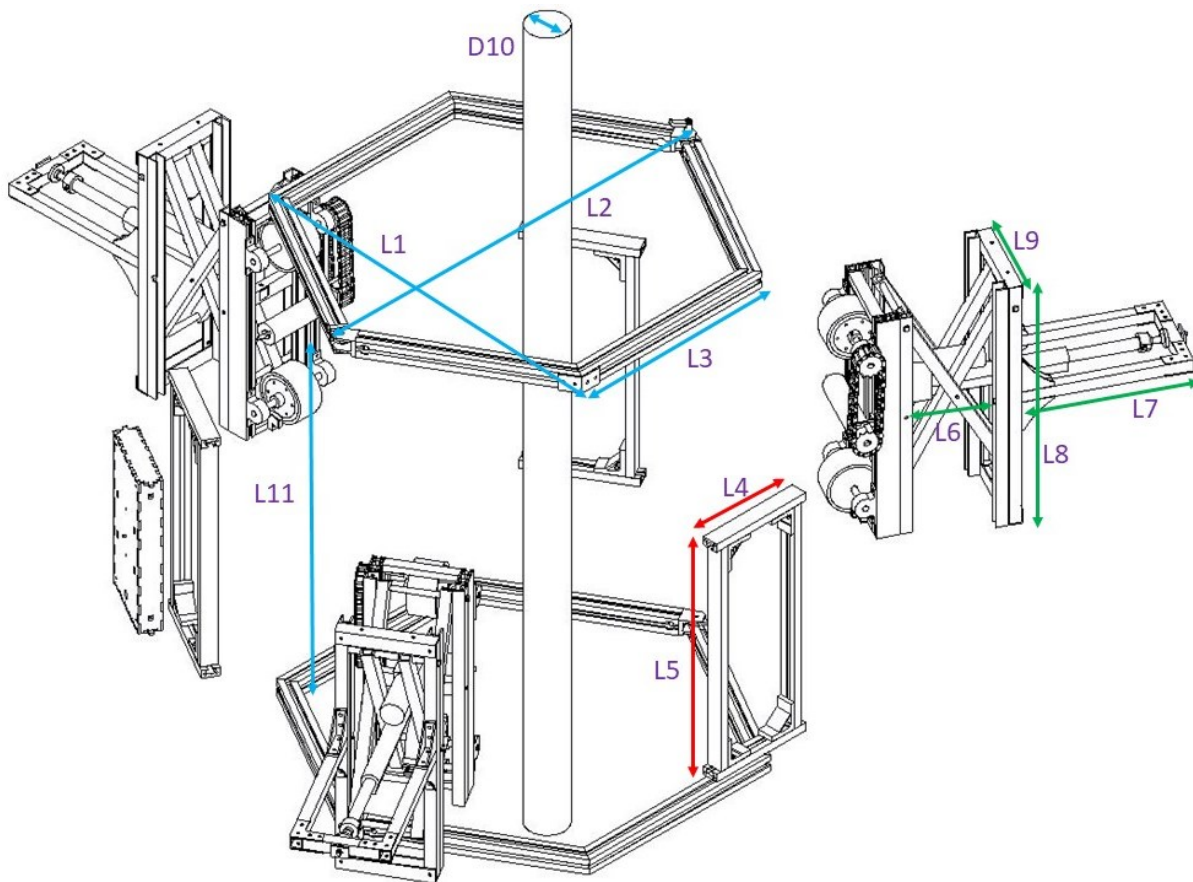


FIGURE 4-33 RESTRICTING DIMENSIONS IN THE DRIVETRAIN DESIGN

TABLE 4-15 DRIVETRAIN DIMENSION

Dimension	Reference	Value (mm)
Length	L11	519
Width	2.93(L7+L1/2)	2.93(286+350)
Height	L2	800
Length box	L5	429
Width box	L4	165
Distance between wheels	5*L4/2	325
Hexagon diameter	L1	700
Cable diameter	D10	100-300

#### 4.5.4.4 Adhesion mechanism

The adhesion force between the robot and the cable is an important factor of a climbing robot because it affects the robot operation and might damage the polyethylene cable. Hence, the cable climbing robots should be adapted to the changes in the cable diameter because the diameter of the suspension hanger varies in the range of 100 mm– 300 mm. Thus, the proposed robot is developed to be applied in a variety of cable diameters using a scissor mechanism [41].

According to the scissor mechanism, the output power is always transmitted perpendicularly so that it can reduce the loss of adhesion forces (Equation 4-4). As shown in Figure 4-34, the initial position of the slider is D, the length of the link is L, and the initial angle is  $\theta$ . Depending on the position of the slider, the height of the Scissor mechanism is calculated as follows [42].

$$F = n \left( L + \frac{B}{2} \right) \frac{\sqrt{C - 2(b-B) \cos \theta + D \cos^2 \theta}}{(b - B \tan \theta - D \sin \theta)} \quad (4-4)$$

The designed scissor mechanism of the cable climbing robot is shown in Figure 4-35.

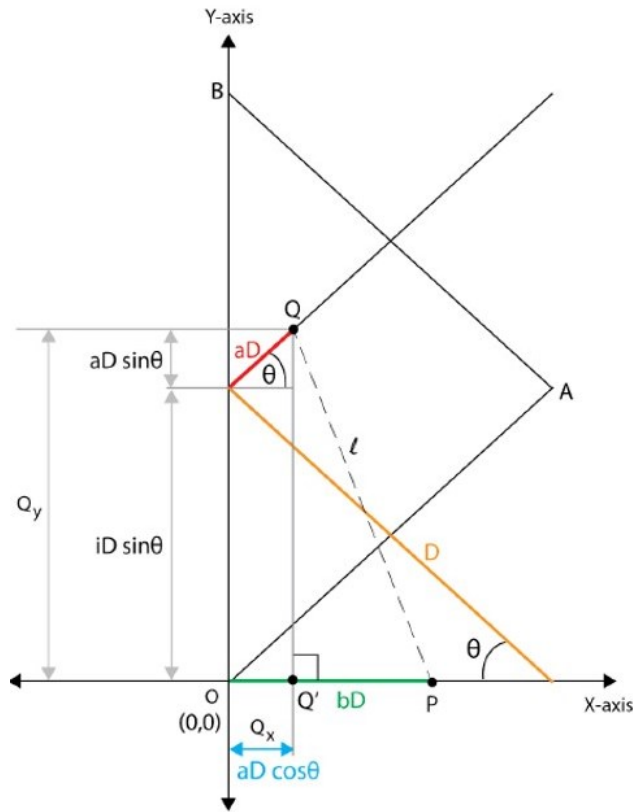


FIGURE 4-34 GENERAL INSTANCE OF SCISSOR MECHANISM

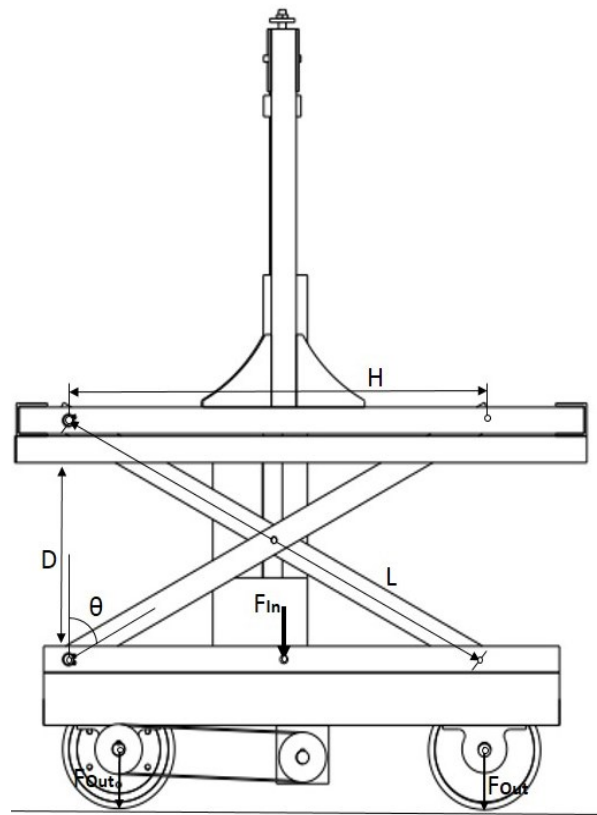


FIGURE 4-35 SCISSOR MECHANISM

#### 4.5.4.5 Chain and sprockets

Cable climbing robot systems should be equipped with some protection mechanism to prevent falling because suspension bridge cables are usually located at high vertical positions from the ground. Sprockets and chains are also used for power transmission from one shaft to another where slippage is not admissible, sprocket chains being used instead of belts or ropes and sprocket-wheels instead of pulleys (Figure 4-36).

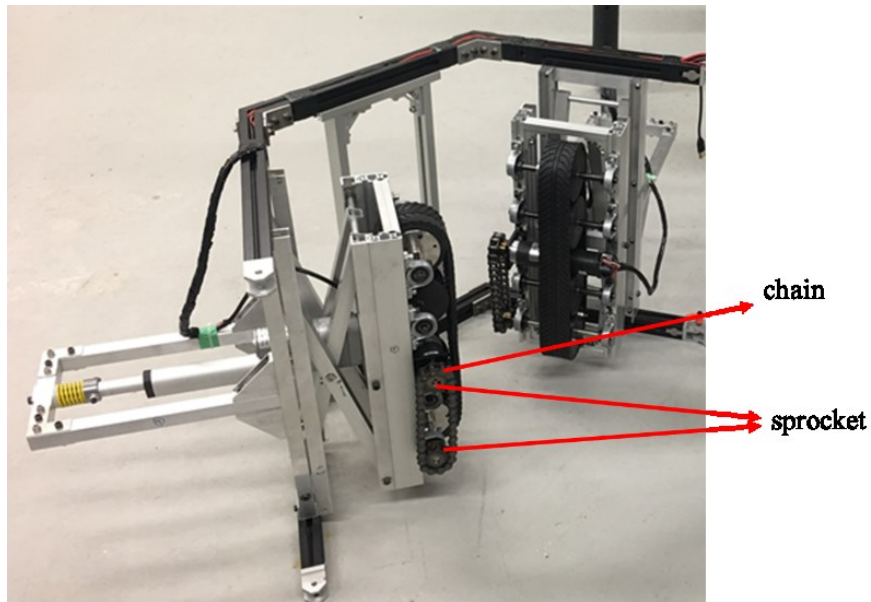


FIGURE 4-36 CHAIN AND SPROCKET

The chain and the sprocket used in the final design are detailed in Table 4-16.

TABLE 4-16 FINAL CHAIN AND SPROCKET CHOSEN

<b>Type</b>	Standard chains	<b>Composition instructions</b>	18.1	
<b>Pitch</b>	12.7	<b>Number of tracks</b>	1	
<b>Material</b>	Steel	<b>Max. allowed tension(kN)</b>	~99	
<b>Chain no.</b>	40	<b>Number of Links</b>	32	
<b>Pin format</b>	Rivet type			
<b>For chain no.</b>	40 B (1/2" pitch)	<b>Number of tracks</b>	Single row	
<b>Material</b>	[Steel] 1045 carbon steel	<b>Bore style</b>	With finished bore	
<b>Bore dia. D</b>	10K	<b>Keyway b2 * t2</b>	4*1.8	
<b>Number of teeth (T)</b>	10	<b>Chain type</b>	RS	

#### 4.5.4.6 Suspension

Suspension springs can cushion cable surface unevenness and ensure that the urethane wheels always maintain reliable contact with the surface (Figure 4-37).

Two types of robot systems are developed for inclined cables in cable-stayed bridges and vertical hanger ropes in suspension bridges. The hardware of the cable inspection robots has the following unique features.

(i) The range of cable diameters are from 100 mm to 300 mm, and the maximum payload is 47 kg for hanger ropes and stay cables, respectively.

(ii) The robot is controlled with and transmits sensor data to the control system through wireless communication.

(iii) The self-locking system is designed to prevent reverse force on the motor and dissipate the freefalling force for an unpredicted power outage to maintain reliable contact with the surface.

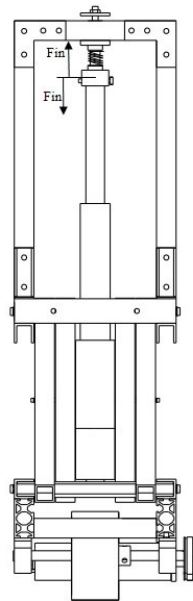


FIGURE 4-37 SUSPENSION AND SHOCK ABSORBER MECHANISM

#### 4.5.4.7 Motor requirements

Equations 4-5 and 4-6, Table 4-17 show what the required torque and rpm for the tracks drive motors are, for given inputs. An important design objective of the cable-suspension bridge robot

is that the robot should have enough climbing force to inspect vertical hanger cables, and, for an unpredictable power outage, the gravity force due to the robot dead weight should be effectively counteracted to avoid freefall. To accomplish these design objectives, electrical DC motors are used to actuate the robot system on hanger cables [43, 44]. The robot system employs a scissor mechanism for various cables gauges and a self-locking mechanism for a power outage (Figure 4-38). The self-locking system is designed to prevent reverse force on the motor and to reduce falling acceleration during a power outage. A simple gear system is used, which consists of differential gears, including worm and pinion gears and worm wheels attached to disk dampers [45, 46].

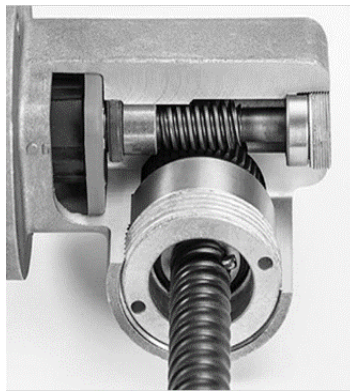


FIGURE 4-38 SAFE LOCKING MECHANISM

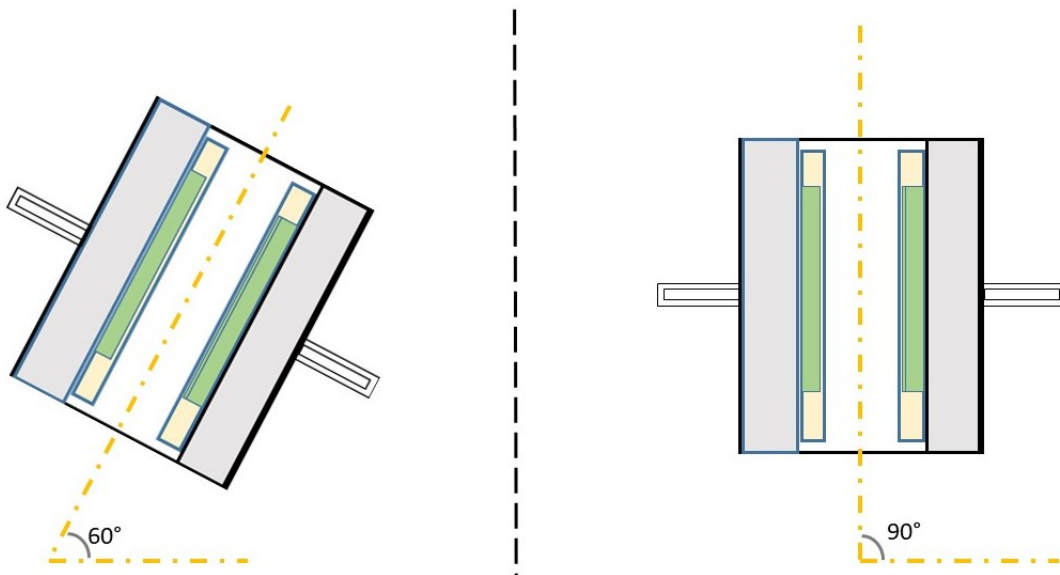


FIGURE 4-39 CCR DURING CLIMBING AT AN ANGLE 60 DEGREES LEFT AND 90 DEGREES RIGHT



TABLE 4-17 TRACK MOTOR REQUIREMENTS

<b>Input requirements</b>	<b>Value</b>	<b>Unit</b>
<b>Mass</b>	35	[kg]
<b>Number of drive motors</b>	6	n/a
<b>The radius of a drive wheel</b>	0.06	[m]
<b>Robot velocity</b>	1	[m/s]
<b>Maximum incline</b>	90	[deg]
<b>Desired acceleration</b>	1	[m/s <sup>2</sup> ]
<b>Total efficiency</b>	65	[%]
<b>Output requirements</b>		
<b>Torque</b>	4.579	[Nm]
<b>Angular velocity</b>	159.24	[rpm]

$$T = \left(\frac{100}{E}\right) \frac{(A+GSIN\theta)MR}{N} \quad (4-5)$$

where;

- τ is torque (N/m)
- e is the efficiency of motor/gears/wheels (%)
- a is acceleration (m/s<sup>2</sup>)
- g is acceleration due to gravity (m/s<sup>2</sup>)
- θ is the angle of incline (o)
- m is mass (kg)
- r is the radius of effective wheel (m)
- n is the number of motors

$$\Omega = 60 \frac{N}{2\pi R} \quad (4-6)$$

where;

- ω is the angular velocity (rpm)
- v is the velocity (m/s)
- r is the radius of effective wheel (m)

TABLE 4-18 FAULHABER DC MOTOR

<b>Input Voltage:</b>	12 V DC
<b>Gear ratio:</b>	120:1
<b>Gear output Torque:</b>	20 Nm
<b>Speed:</b>	46 rpm
<b>Operational Temperature:</b>	-30 C~+125 C
<b>Current (full load):</b>	4A
<b>Motor Type:</b>	coreless DC motor/ graphite commutation
<b>Motor and gear bearings</b>	ball bearing, preloaded
<b>Unit Weight:</b>	740 gr
<b>Motor max efficiency</b>	% 84
<b>Motor output torque:</b>	131 mNm
<b>Motor power:</b>	110 w



FIGURE 4-40 FAULHABER DC MOTOR

### 4.5.5 Final design

The track units and adhesion systems are designed and improved in a series of iterations until the final design shown in Figure 4-41, and Figure 4-42 is reached. Specifications for the motors and sprockets and chains used can be found in Table 4-19, including the required values calculated in section 4.5.4.4. It is clear by comparing what the motors can supply with what is required, that the motors are able to supply the required torque and rpm. The chosen motors have a very high safety factor. However, they are cheap and compact, so finding less powerful motors are deemed unnecessary. The large safety margin also allows for a wide range of possible modifications in the future.

TABLE 4-19 FINAL DRIVETRAIN MOTOR SPECIFICATIONS

<b>Section</b>	<b>Name of motor</b>	<b>The torque of the motor (mNm)</b>	<b>RPM of motor</b>	<b>Added gear ratio (X:1)</b>	<b>Torque after gears (Nm)</b>	<b>RPM after gears</b>
<b>Drive motors</b>	3863H012CR+38A	131	5600	120:1	20	46
	120;1+HEDS5500A 12+MG20+X0743					
<b>Required</b>					16	42
<b>Scissor mechanism</b>	Progressive	98	5100	560:1	203	9
	automation PA-14P					
<b>Required</b>					150	7

The possible smallest and simplest solutions are chosen for each design step, using easily sourced and replaceable parts where ever possible. The only complex parts are scissor mechanisms. They are designed to fit all required parts (pins, rotary shafts, ball bearings, metal collars, and drivetrain units), including wiring, and need a milling machine to make. They are, however, not expensive, so having a few spares is a very affordable possibility. All other drivetrain parts can be made on a lathe & pillar drill with a little spare material or ordered from Misumi. Each drive unit is identical and can be attached to any side and any cable that is in the applicable cable diameters range. Figure 4-43 shows the finished design in CAD.

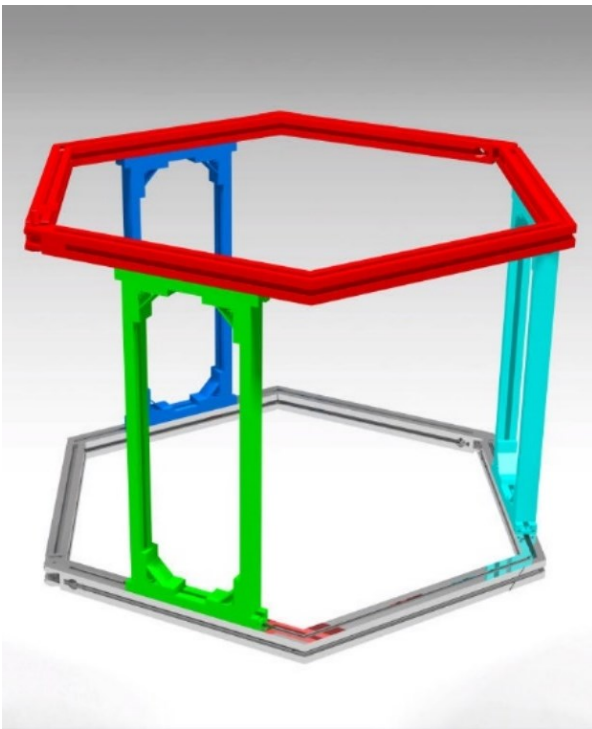


FIGURE 4-41 FINAL FRAME DESIGN

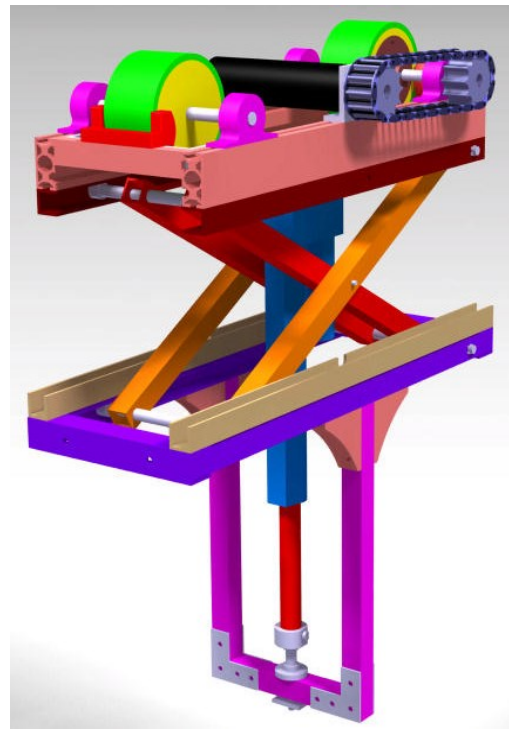


FIGURE 4-42 FINAL ADHESION SYSTEM DESIGN

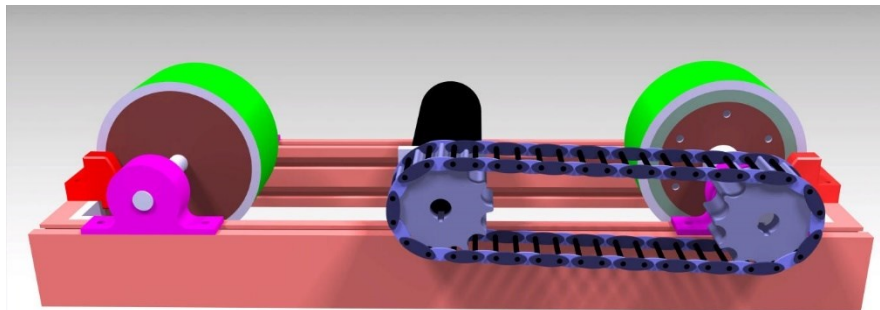


FIGURE 4-43 DRIVETRAIN FINAL DESIGN

### 4.5.6 Manufacture

All of the parts are machined at the Concordia University, except for some leather machining and milling machine. The components are then assembled into the track units (Figure 4-44).

Chain tensioning blocks are not added to the CAD model due to time constraints; however, they are designed and brought the total clearance of the robot to over 40mm. They also direct any impact force away from the sprockets and into the chain unit.

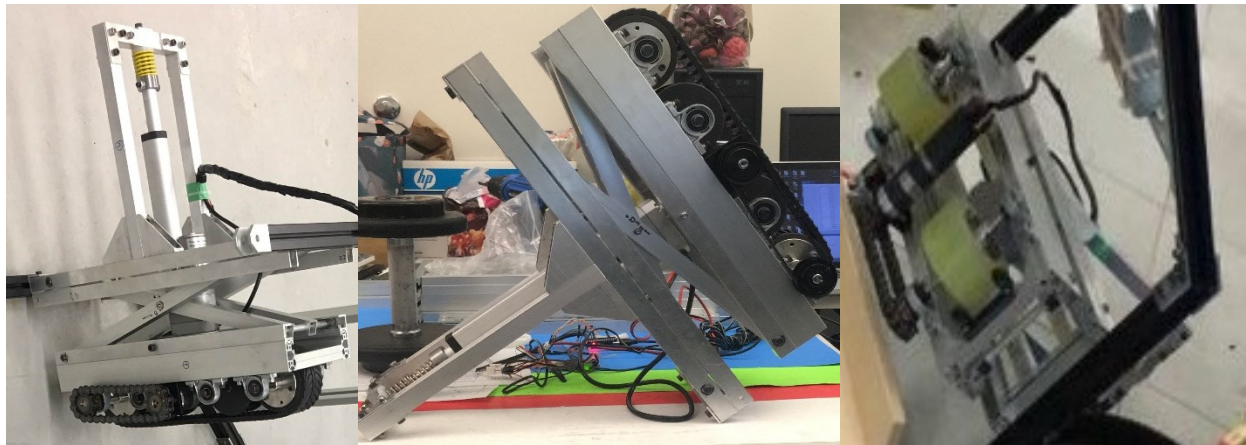


FIGURE 4-44 MANUFACTURED AND ASSEMBLED UNITS

### 4.6 CCR control and electronics

The key challenge for creating reliable robots that achieve their full potential is the development of controllable mechanisms and unites using materials that integrate sensors, actuators, and computation, and that together enable the structure to deliver the desired behavior.

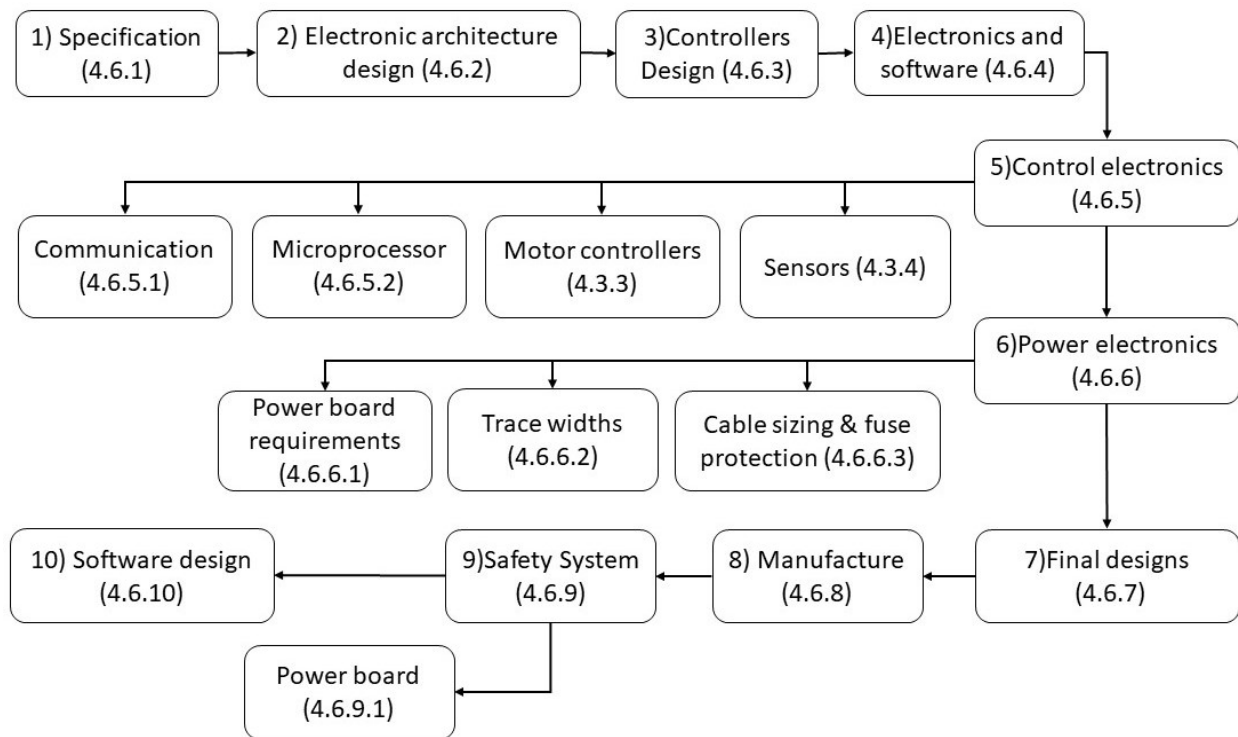


FIGURE 4-45 ELECTRONICS AND SOFTWARE DEVELOPMENT STRATEGY

### 4.6.1 Specification

The specification for the new electronics and software system in Table 4-20 is developed from the aims and objectives, original high-level specification (section 4.3), and company requests.

TABLE 4-20 ELECTRICAL SYSTEM SPECIFICATION 4.3

<b>ID</b>	<b>Constraint</b>	<b>Description</b>
<b>1</b>	Size	Components are chosen, and electronic designs should be as small as possible in volume but also not exceed dimensions specified by the chassis, drivetrain design parameters to ensure they can fit in the small package space.
<b>2</b>	Mass	Weight must be considered when choosing components and reduced where possible.
<b>3</b>	Modular	Chosen components must have plug and play modularity with connectors for simple removal. Removal of devices should not affect the robot's operation of other devices or its reliability.
<b>4</b>	Cost	Electronic components must be low cost.
<b>5</b>	Reliability	Low cost should not affect the reliability of the device.
<b>6</b>	Communication	Must be able to communicate wirelessly with an operator's computer.
<b>7</b>	Data	The electronics should be able to control the robot from data supplied by an operator remotely (wheels, adhesion mechanism)
<b>8</b>	Wiring	Simple, tidy, and easy to follow the wiring. Fixed terminal blocks for connections. Single point ground connection to prevent ground loops. Produce and accurate wiring diagram for the electrical network.
<b>9</b>	Emergency stop	An emergency stop system must be implemented, as good practice with all robotic systems, to remove all power electronics and communication systems active.
<b>10</b>	Fuse protection	Protect the battery and the robot using fuse protection.
<b>11</b>	Protect battery	Adequate protection from connecting in reverse polarity.
<b>12</b>	Monitor battery	Supply operator with battery charge levels remotely to estimate remaining drive time and prevent over-discharge.

## 4.6.2 Electronic architecture design

A modular electronic architecture is designed to allow a core system to function and provide basic robotic operations (Figure 4-46). This system could then be expanded to control additional systems, providing additional sensing, camera maneuverability, or manipulation capabilities [48].

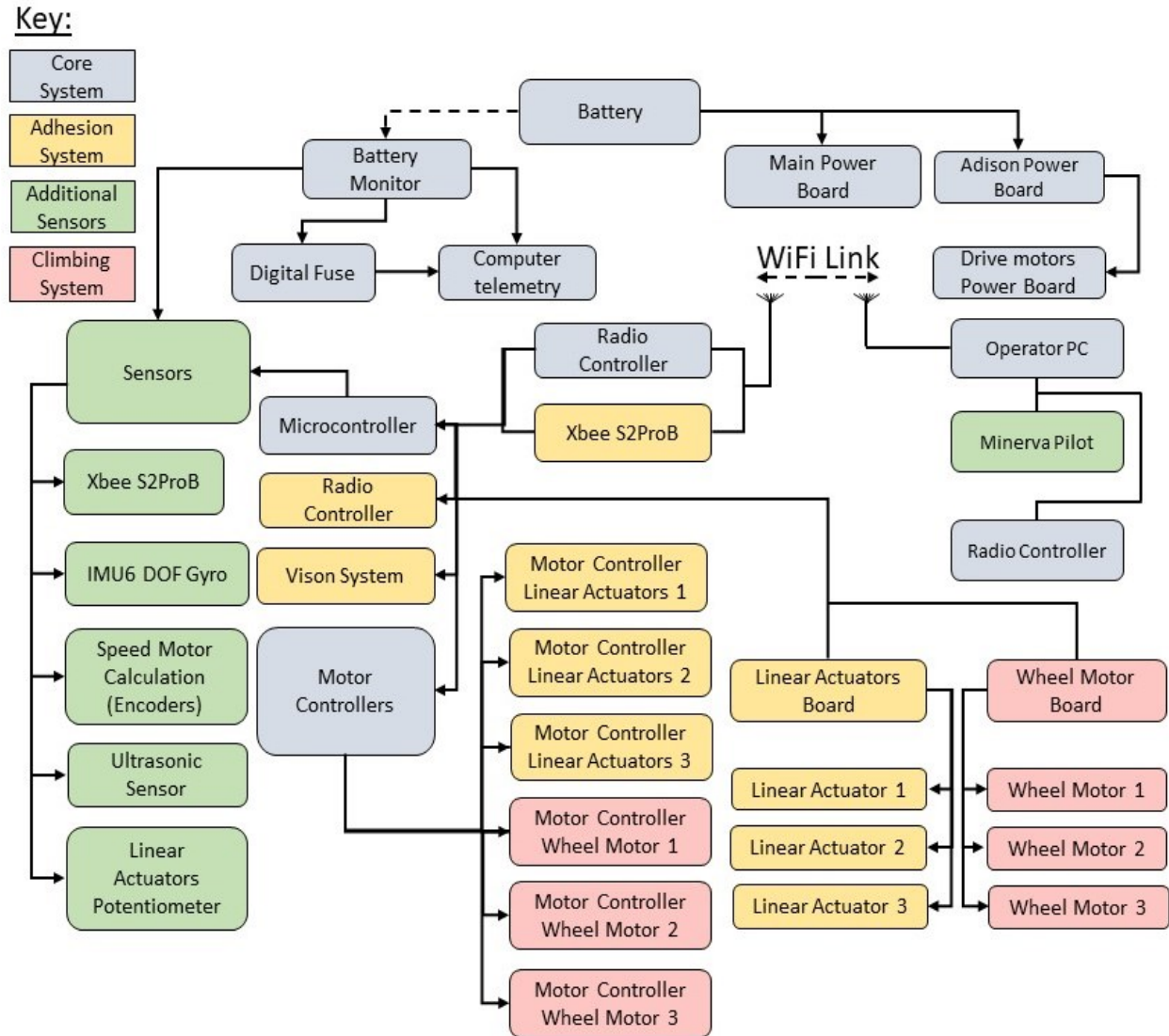


FIGURE 4-46 ROBOT MODULAR ELECTRONIC ARCHITECTURE

### 4.6.3 Controllers design

Cable climbing robot is designed with the integration of both hardware and software for various real-world applications. Working with the applications, the robot is to inspect the full length of the cable and apply different speeds to execute the user-defined tasks. The way the robot has to make a motion is pre-programmed by the user in applications with the integrated embedded system components present with the robot design. There are possibilities for the robot to deviate from the programmed trajectory due to the intervention of disturbances. Mostly, some errors are introduced in the trajectory of the robot. This creates the need for a robust controller to make the robot run in real-world applications. From the results, it is clear that the robot's velocity cannot be easily maintained due to uneven floor conditions, and due to some disturbances. The designed cable climbing robot is supposed to be continuously monitored with the help of encoder sensors and be controlled by the controller at every instant as its trajectory is being tracked. Proportional-Integrated-Derivative (PID) controller is one of the methods to synchronize and control the multiple motors. To control the cable climbing robot, the proportional-integrator-derivative (PID) controllers is designed with the following transfer function:

$$u(t) = K_p e(t) + K_i \int_0^t e(\tau) dt + K_d \frac{de}{dt} \quad (4-7)$$

where  $K_p$  is proportional gain,  $K_i$  is the integral gain, and  $K_d$  is the derivative gain. Those values are available in Table 4-21.

TABLE 4-21 PID VALUES TUNED

	<b>K<sub>P</sub></b>	<b>K<sub>I</sub></b>	<b>K<sub>D</sub></b>
<b>M1</b>	19.15	9	0.0005
<b>M2</b>	19.15	9	0.0005
<b>M3</b>	20	11	0.0005

Two PID controllers are designed. The first PID controller aims at synchronizing of three dc motor speed (Figure 4-47). The second PID controller aims at regulating the synchronizing position linear actuators (Figure 4-48). And the parameters' description is provided in Table 4-22.



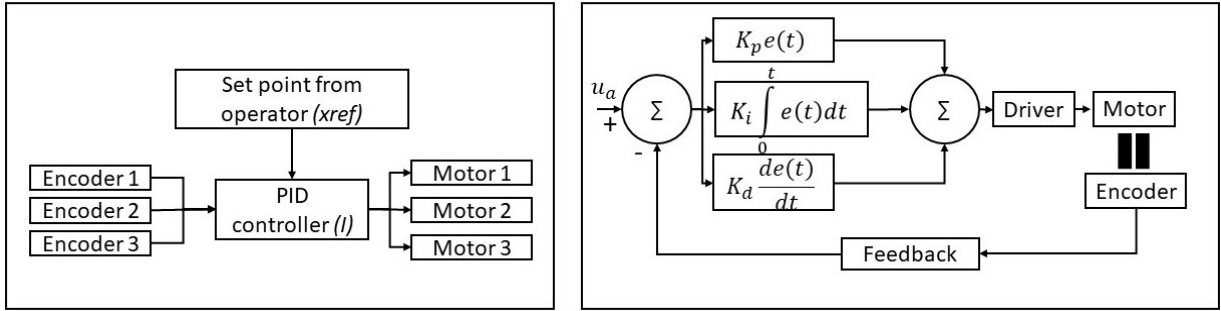


FIGURE 4-47 DC MOTORS CLOSED-LOOP BLOCK DIAGRAM HAVING PID CONTROLLER

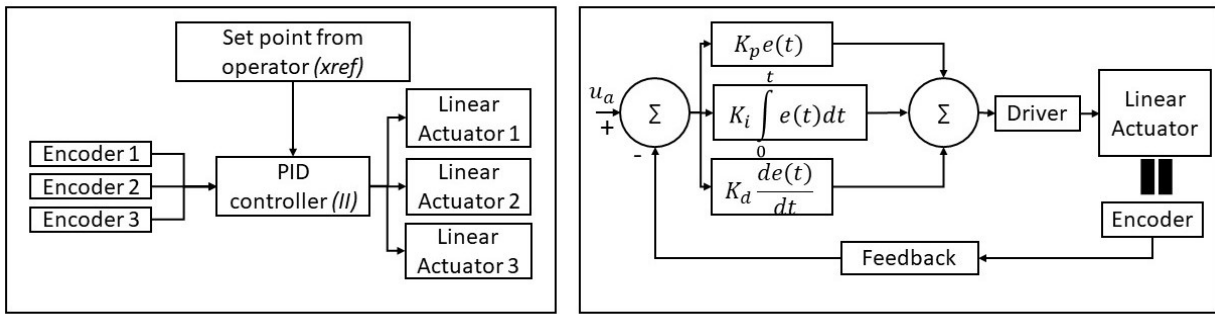


FIGURE 4-48 LINEAR ACTUATORS CLOSED-LOOP BLOCK DIAGRAM HAVING PID CONTROLLER

TABLE 4-22 PARAMETERS OF TWO PID CONTROLLERS

Parameters	Unit	Description	Parameters	Unit	Description
<b>m=0.818</b>	kg	Wheels mass	$R_m=0.16$	$\Omega$	DC motor resistance
<b>R=0.060</b>	m	Diameter of wheel	$K_t=19.9$	mNm/A	DC motor torque constant
<b>g=9.810</b>	m/s <sup>2</sup>	Gravity acceleration	$K_b=2.8$	mv/rpm	DC motor back E.M.F constant
<b>Efficiency, Max.</b>	$\eta_{max}$	%83	-	-	-

#### 4.6.4 Electronics and software

Electronics and robot software is required to power and control the cable climbing robot systems remotely while providing the operator with enough information to do this safely.

#### 4.6.5 Control electronics

Power distribution boards (PDBs) are used extensively throughout electronic systems as a means of dividing electrical power from the supply system to subsidiary systems (Figure 4-49, Figure 4-50). There are various methods by which one can regulate the voltage and thus distribute the required power throughout a system. Common methods of power distribution utilize voltage regulation. Voltage regulation is required to create a voltage reference from which the subsidiary circuit can operate at a stable voltage (Table 4-23) [51].

TABLE 4-23 PCB COMPONENTS LIST

1~6 dc	motor driver
A	XBee
B	radio controller
C	on/off key
D	microprocessor
E	encoder dc motor
F, G, H	driver dc motor ports
I	radio controller pins
J	encoder dc motor
K	XBee port
L	ultrasonic port
M	driver dc motor ports

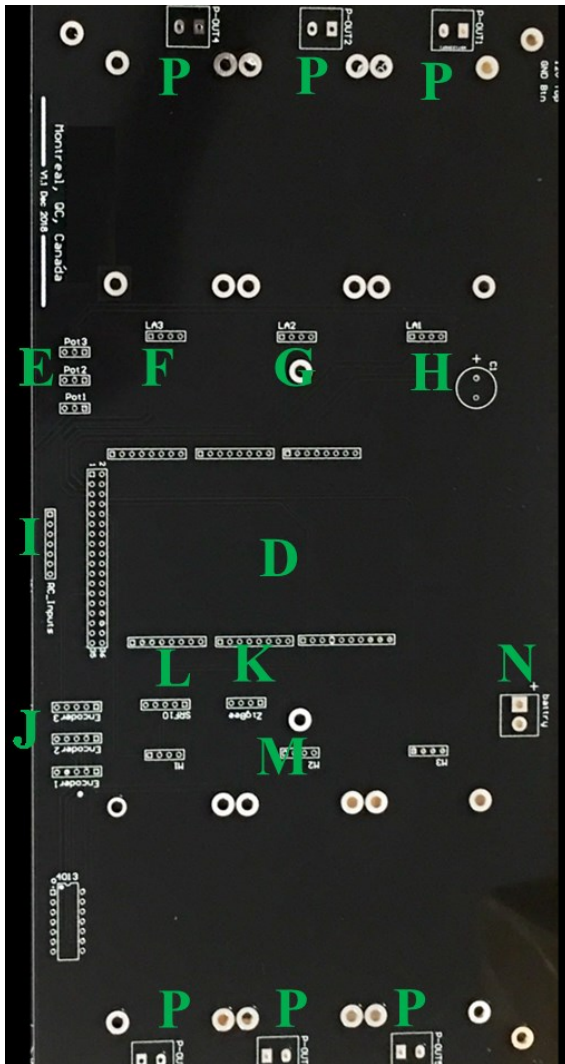


FIGURE 4-49 THE PCB BEFORE COMPONENT SOLDERING

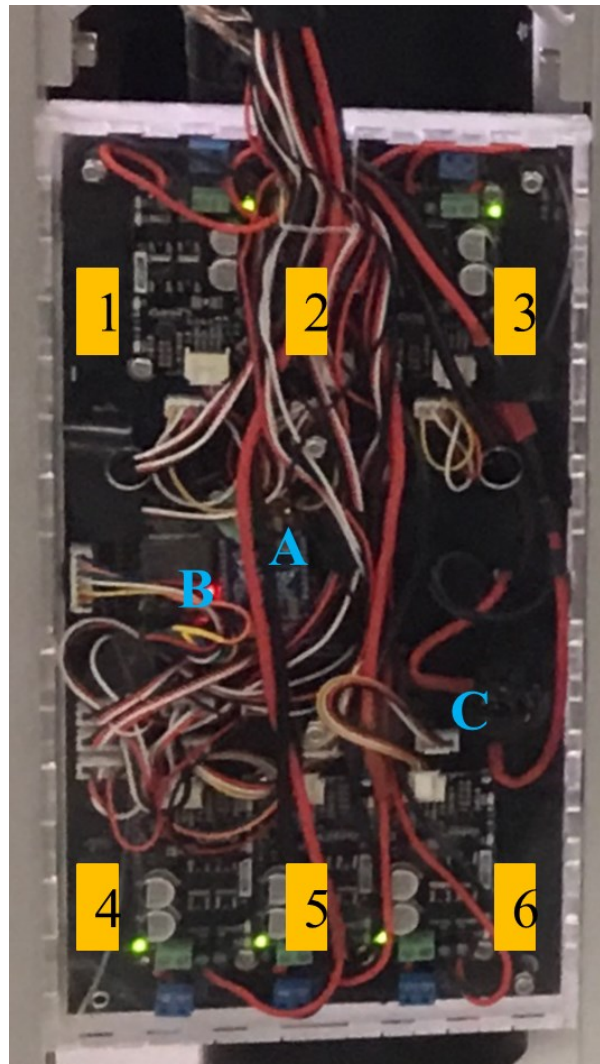


FIGURE 4-50 THE PCB AFTER COMPONENT SOLDERING

#### 4.6.5.1 Communication

To improve connectivity, the new electronic box design allows the router's antennas to extend out (Figure 4-51).

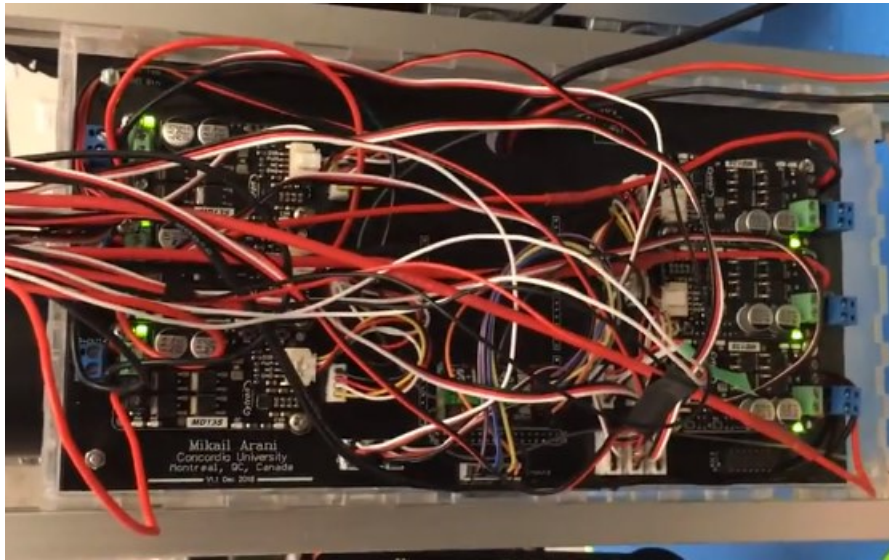
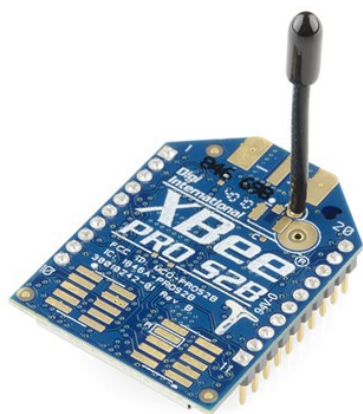


FIGURE 4-51 ELECTRONIC BOX DESIGN

A review of available routers is conducted, and dual-band (2.4 GHz and 5 GHz) router is chosen with a power output of 63 mW (XBee-pro s2b) (Table 4-24), two times greater than the existing router. The new series 2b (Figure 4-52) improves upon the power output and data protocol of the Pro Series2. Series 2b modules allow one to create complex mesh networks based on the ZigBee mesh firmware. These modules allow a very reliable and simple communication between microcontrollers, computers, systems, point to point, and multi-point networks are supported [52].

TABLE 4-24 SPECIFICATIONS OF THE XBEE-PRO (S2B)

<b>Performance</b>	<b>Indoor/ outdoor range</b>	<b>Up to 90 m/ up to 3200 m</b>
	Transmit power output	63 W (+18 dBm)
	RF data rate	250,000 b/s
	Data throughput	Up to 35000 b/s
	Serial interface data rate	1200 b/s - 1 Mb/s
	Receiver sensitivity	-102 dBm
<b>Power requirements</b>	Supply voltage	2.7 - 3.6 V
	Operating current (transmit, max output power)	132 - 220 mA @3.3 V
	Operating current (receive)	62 mA @3.3 V
	Idle current (receiver off)	15 mA



(a) Robot receiver



(b) Computer receiver

FIGURE 4-52 XBEE RECEIVERS

Also, each radio controller transmitter (Figure 4-53) has a unique ID. When binding with a receiver, the receiver saves that unique ID and can accept only data from the unique transmitter. This avoids picking another transmitter signal and dramatically increase interference immunity and safety (Table 4-25).

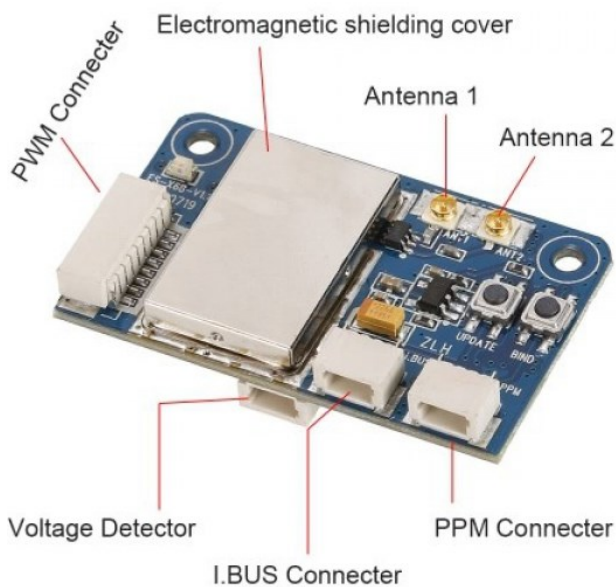


FIGURE 4-53 RADIO CONTROLLER TRANSMITTER

TABLE 4-25 RADIO CONTROLLER SPECIFICATION

<b>Description</b>	<b>Brand name: Flysky</b>
<b>Item</b>	X6B i-bus 2.4 GHz- 6 CH receiver
<b>Channels</b>	6 (PWM), 8 (PPM), 18 (i-bus)
<b>Model type</b>	Multi-Rotor
<b>RF range</b>	2.408- 2.475 GHz
<b>Bandwidth</b>	500 KHz
<b>Number of bands</b>	135
<b>RF Power</b>	No more than 20 dBm
<b>RX Sensitivity</b>	-95 dBm
<b>2.4GHz protocol</b>	AFHDS 2 A
<b>Modulation type</b>	GFSK
<b>Stick resolution</b>	1024
<b>Low voltage alarm</b>	Yes
<b>DSC port</b>	PPM/ PWM/ i-bus
<b>Antenna length</b>	93mm (dual antenna)
<b>Power input</b>	4.0 - 8.4 V
<b>Online update</b>	Yes (wireless)
<b>Range</b>	>300 m
<b>Weight</b>	4.5 g
<b>Size</b>	36*22*7.5 mm
<b>i-bus port</b>	Yes

#### 4.6.5.2 Microprocessor

The Arduino Due 32bit ARM microcontroller (Figure 4-54) is a microcontroller board based on the Atmel SAM3X8E ARM cortex-m3 CPU. It is the first Arduino board based on a 32-bit ARM core microcontroller. It has 54 digital input and output pins of which 12 can be used as PWM outputs, 12 analog inputs, four UARTs (hardware serial ports), an 84 MHz clock, an USB OTG capable connection, two digitals to analog, a power jack, a reset button and an erase button.



FIGURE 4-54 ARDUINO DUE 32BIT ARM MICROCONTROLLER

### 4.6.5.3 Motor controllers

The chosen controller (Figure 4-55) is the only DC motor controller found which supplies the correct power (voltage and current) (Table 4-26) to the drive motors and fits inside the electronic box.

TABLE 4-26 MOTOR CONTROLLER SPECIFICATION



<b>Currents</b>	<b>13 A DC motor driver - grove compatible</b>	<p>The image shows a black PCB for a Cytron MD13S DC motor controller. It features two large electrolytic capacitors labeled '330 50V RVT'. There are several pins and connectors, including a 5-pin header on the left and a 5-pin header on the right. The board is populated with various electronic components like transistors, diodes, and integrated circuits. The brand name 'Cytron' and model 'MD13S' are clearly visible.</p>
<b>Maximum current</b>	Up to 13 A continuous and 30 A peak (10 seconds)	
<b>Logic level input</b>	3.3 - 5 V	
<b>Support motor voltage ranges</b>	6 - 30 V	
<b>Bi-directional control for one brushed DC motor</b>		

FIGURE 4-55 CYTRON MOTOR CONTROLLER

### 4.6.5.4 Sensors

Sensors are required to allow teleoperated control of the robot and obtain the maximum number of points at the inspection site. Table 4-27 summarizes the sensors required, their purpose, and the chosen sensor.

TABLE 4-27 CHOSEN SENSORS

Sensor and purpose	Picture	Description
<p>Range finder sensor: crash avoider</p>	 <p>FIGURE 4-56 ULTRASONIC SRF 08</p>	<p>Communication with the SRF 08 ultrasonic rangefinder is via the I2C bus. This is available on popular controllers such as the OOPic and Stamp BS2p, as well as a wide variety of micro-controllers. To the programmer, the SRF08 behaves in the same way as the ubiquitous 24xx series EEPROM's, except that the I2C address is different.</p>
<p>Battery monitor: avoid losing robot control</p>	 <p>FIGURE 4-57 DUAL BUZZER ALARM</p>	<p>Battery voltage checker and low voltage buzzer. Three test mode test range 11.1 to 12.6 volts, which is possible to test the battery pack without balance connectors, and loudly buzzer can be heard from a distance.</p>
<p>6 DoF gyro, accelerometer IMU: increase robot efficiency and safety</p>	 <p>FIGURE 4-58 MPU6050</p>	<p>Tri-Axis accelerometer with a full-scale programmable range and the working voltage is between 3 to 5 volts. This module combines a 3-axis gyroscope and a 3-axis accelerometer. I2C Digital-output of 6 or 9-axis Motion Fusion data in the rotation matrix is important for accurate control.</p>
<p>Encoder: synchronous motors and control of climbing speed</p>	 <p>FIGURE 4-59 HEDS5500A 12</p>	<p>Optical encoder with digital outputs, three channels, and 500 lines per revolution for line driver.</p>



## 4.6.6 Power electronics

Analyzing the evolution of CCR power distributions systems allow the designer to recognize drawbacks from real-world circuits and how these are overcome. Identifying these characteristics and using the plethora of past information allow the designer to improve continuously.

### 4.6.6.1 Powerboard requirements

Individual output power requirements for the main power board and the dc motors power board are dictated by the control electronics chosen in Section 5.4, resulting in the output requirements in Table 4-28 and Table 4-29.

TABLE 4-28 REQUIRED OUTPUTS FOR THE MAIN POWER BOARD

Name	Voltage (V)	Current (A)	Power (W)	Fuse (A)	Note
<b>XBee</b>	12	1.1	13.2	2	Usually 0.9 A but additional 0.2 A due to newer antenna
<b>Ultrasonic</b>	5	0.5	2.5	1	-
<b>Battery monitor</b>	12	0.3	3.6	1	-
<b>Gyro</b>	5	0.2	1	1	-
<b>Radio controller transmitter</b>	5	0.2	1	1	-
<b>Total of 5 volts power</b>			<b>8.1</b>	-	-
<b>Total of 12 volts power</b>			<b>13.2</b>	-	-

TABLE 4-29 REQUIRED OUTPUTS FROM ACTUATORS AND DC-MOTORS

Name	Voltage (V)	Current (A)	Power (W)	Fuse (A)	Note
<b>Linear actuators</b>	12	9.8	117.6	12	Usually 9 A but additional 0.8 A due to lock position
<b>DC great motors</b>	12	11	132	13	-
<b>Total of 12 volts power</b>			249.6	-	-

The total power requirement of the control electronics is 265 W (This includes all actuators and dc-motors running at full load). This equates to a maximum current draw of 22.08 A from the battery, calculated by equation 4-8 [53]:

$$I = \frac{265}{12} = 22.08 \text{ A} \quad (4-8)$$

Where:

I is the current (A);

P is the power (W);

V is the voltage (V);

This is composed of 2.61 A and 3.6 A from the main power board and actuators and DC motors, respectively. As the actuators and dc-motors are used infrequently a running time of the robot is calculated to be 1 hour 19 minutes (Equation 4-9):

$$Time = \frac{Battery\ Capacity\ (Ah)}{Current\ Draw} = 16.5 \text{ Ah} \left( \frac{150W}{12V} \right) = 1.32 \text{ hours} \quad (4-9)$$

#### 4.6.6.2 Trace widths

The PCBs copper traces are designed to handle the appropriate operational current. The trace widths are calculated using the IPC 2221 PCB technical design requirements (Equation 4-10) [54].

Imperial units of measurement are used for the design of the PCB trace widths "...as a general rule, use imperial for tracks, pads, spacings, and grids. Only use mm for mechanical and

manufacturing type requirements like hole sizes and board dimensions” [55]. The thickness of the copper trace is fixed at 35  $\mu\text{m}$  (1.38 mils) due to the manufacturing process.

$$I = k \times \Delta T^{0.44} \times A^{0.725} \quad (4-10)$$

where:

I is current (A)

A is the cross-sectional area ( $\text{mils}^2$ )

$\Delta T$  is the temperature rise ( $^{\circ}\text{C}$ )

K is a constant = 0.048 for outer layers and 0.024 for inner layers.

Rearranging equation 4-11, 4-12 gives the area in  $\text{mils}^2$  for the required current.

$$\text{Area (mils}^2\text{)} = \left( \frac{I}{k \times \Delta T} \right)^{0.44 \left( \frac{1}{0.725} \right)} \quad (4-11)$$

$$\text{Width(mils)} = \frac{A}{\text{Thickness} \times 1.378} \quad (4-12)$$

#### 4.6.6.3 Cables sizing and fuse protection

Cable sizing is based on the 17th Edition IEEE wiring regulations [56]. Easy to replace fuses ‘Little fuse’ is chosen to ensure protection for safety-critical circuits. A minimum fuse value of 135% larger than the load current is chosen as recommended in the Optifuse fuse selection guide [57].

#### 4.6.7 Final designs

The circuits are designed using Altium Designer (Figure 4-60, Figure 4-61) and then transferred to PCB manufacturer. The PCB is a two-layer board with power and ground routed on the bottom and signals on the top. The ‘IPC 2221 - A guides to better design the layout of the board’ [54] are followed. To save space inside the chassis, the driver boards are also designed to allow direct mechanical and electrical connection to the microprocessor.

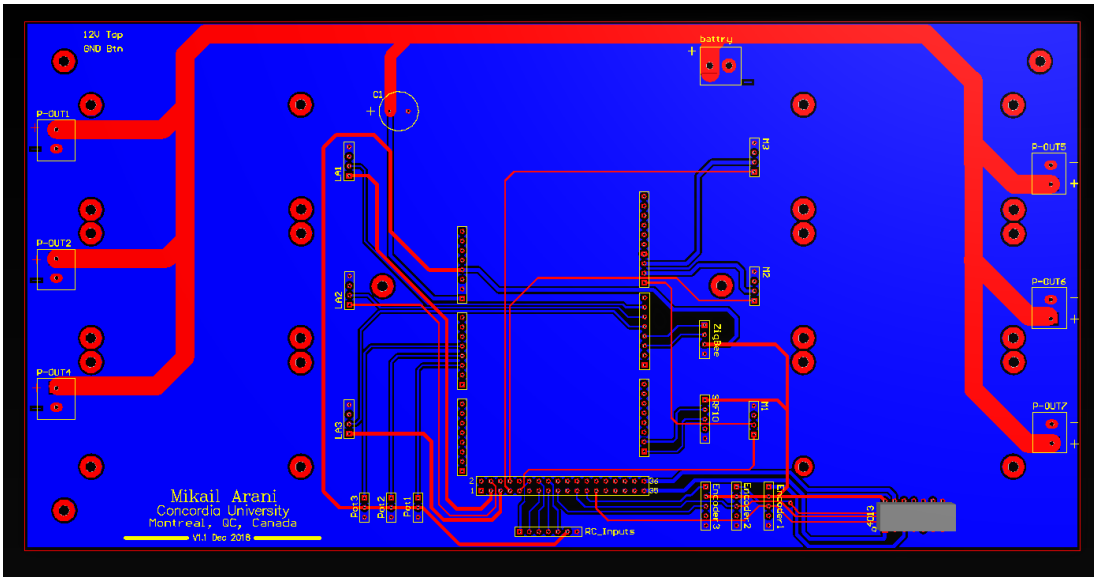


FIGURE 4-60 LAYOUT OF POWER BOARD AND MAINBOARD

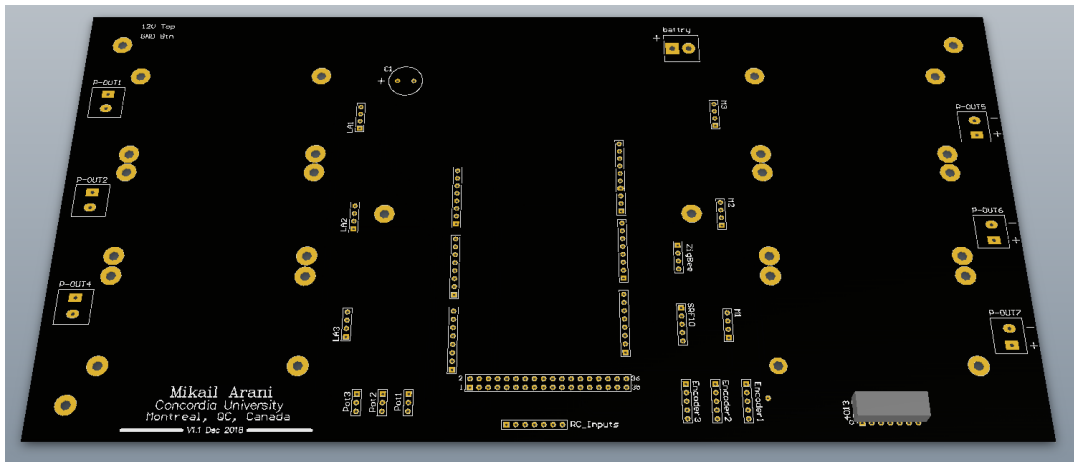


FIGURE 4-61 3D REPRESENTATION OF THE BOARD

#### 4.6.8 Manufacture

The PCBs are manufactured by the PCB Way (Figure 4-62) using a computer-controlled router. Through-hole and surface-mount components are soldered by hand. Spacers are machined using a lathe to give structural strength to the breakout boards and the microprocessor.

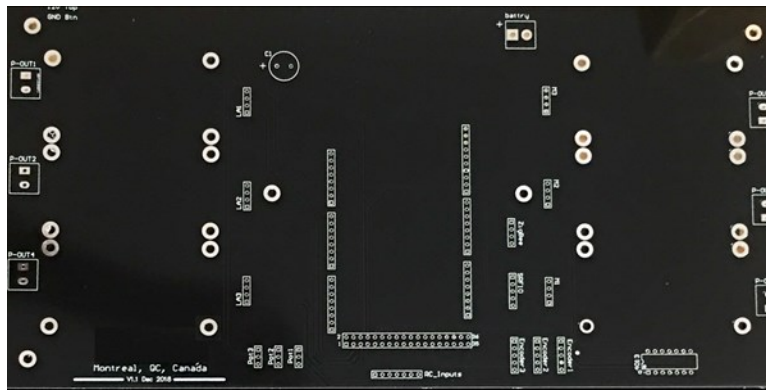


FIGURE 4-62 THE PCBs BEFORE COMPONENT SOLDERING

## 4.6.9 Safety system

The robot requires an emergency stop button to halt the drivetrain and adhesion units' linear actuators when presses but maintain power to all other control components. The maximum current the six motor control boards for the drivetrain can draw is 30 amperes. However, the maximum efficiency current of the motors is 13 amperes and should stay within 50% of this under normal loading conditions. This equates to a maximum current draw of 117 amperes from the battery under normal conditions (Equation 4-13).

$$(\text{max efficient current} * \text{variation} * \text{No. motors}) = (13 * 1.5 * 6) = 117 A \quad (4-13)$$

A safety factor of 15% is added, making the required relay's current rating of 135 amperes. A 140 amperes fuse is included, designed to blow if the current exceeded these normal operating conditions, protecting the circuitry and relay [58]. The linear actuator motors operate on 12 volts dc, with the ability to draw 3 amperes. A separate relay is needed to operate at a different voltage of 12 volts. The emergency stop circuit is first simulated using Multisim to ensure the correct operation and measure current flow through the circuit.

### 4.6.9.1 Powerboard

The testing procedure, including continuity testing for the PCBs, described in Figure 4-63, demonstrates the voltage measurements made with a multi-meter for the main power board. Once the test completes, the boards are mounted in the chassis. The DC motors control electronics are shown connected in Figure 4-63.

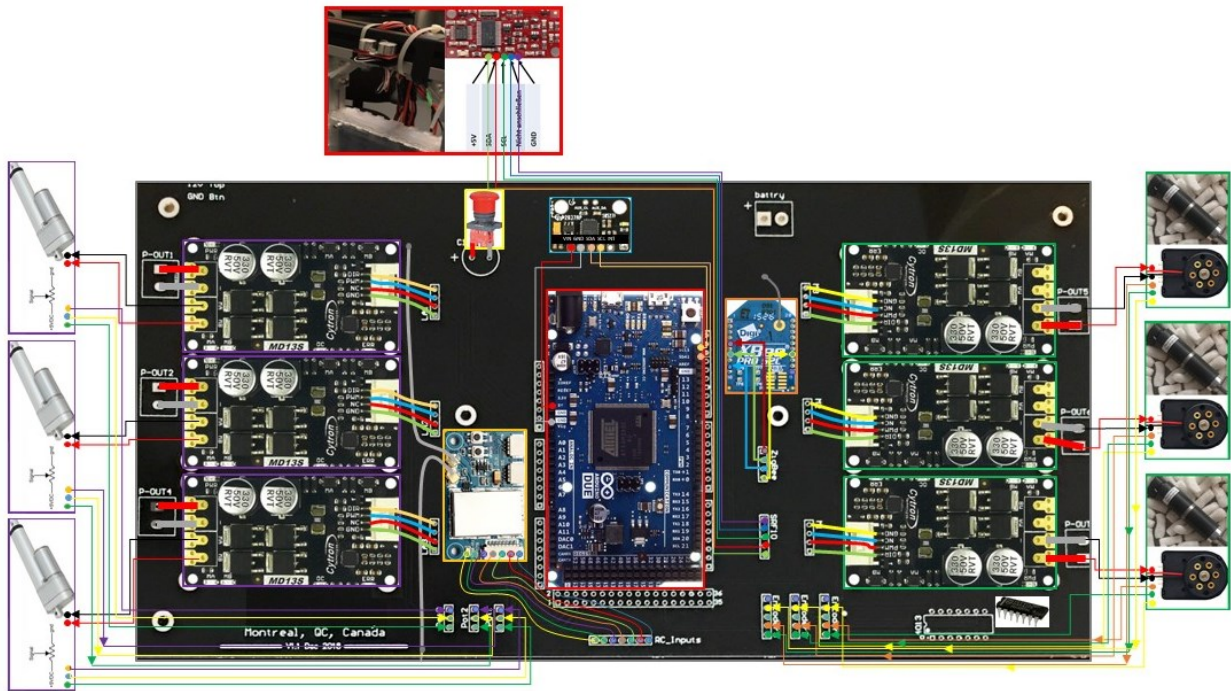


Figure 4-63 The PCB and components

#### 4.6.10 Software design

C++ is chosen for the new robot. C++ is a flexible framework for writing robot software and allows the software to be run as nodes across different devices to allow distributed computing (Figure 4-64). This allows the modularity and plug and plays functionality required. C++ also provides access to a lot of open-source libraries, available to use and modify freely, decreasing development time and increasing functionality. This allows future teams to develop in their strongest language [59, 60].

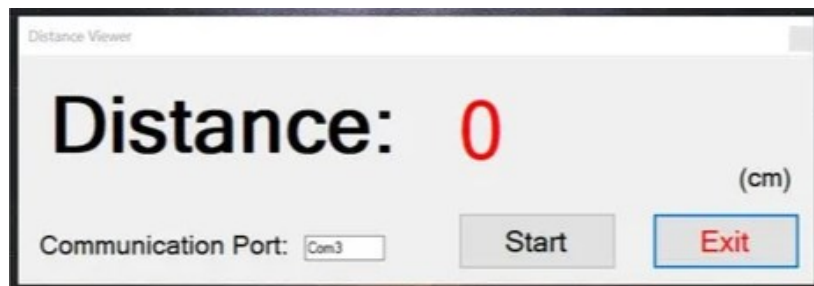


FIGURE 4-64 CCR DISTANCE VIEWER SOFTWARE

## **4.7 Summary**

In this chapter, the development strategy of the CCR has been given. The objectives of the project have been outlined. The detailed designs on the chasis of CCR, drivetrain, control and electronics have been given. Both indoor and outdoor tests on the robot will be given in Chapter 6.

# CHAPTER 5 SIMULATION AND EXPERIMENT TESTS OF TWIP

A TWIP robot is built with four main parts: controller and sensors, gear DC motors, battery, and structure. Arduino Uno is the controller of the TWIP and allows the driver shield to drive gear DC motors. The gear DC motors of the robot could robustly keep the robot stable. The driver shield is L298, which is a dual full-bridge driver. It can transform the real-time data from the Arduino board to the DC motors. To record the angular position like pitch, yaw, and wheel angles, Arduino is connected to two different sensors. (i.e., MPU 6050 which has accelerometer sensors, gyroscope). As it contains 16-bits analog to digital conversion hardware for each channel, it can be more precise.

Besides, using the XBee shield can wirelessly provide data transmission to the computer. The gear DC motors are made by Faulhaber with a maximum resolution of 350 rpm. Moreover, the power is supplied by Li-Po battery/4000 mA. The diameter of the wheels is 108 mm. The center mass of the robot is located in the middle of the wheels' axis (Figure 5-1).

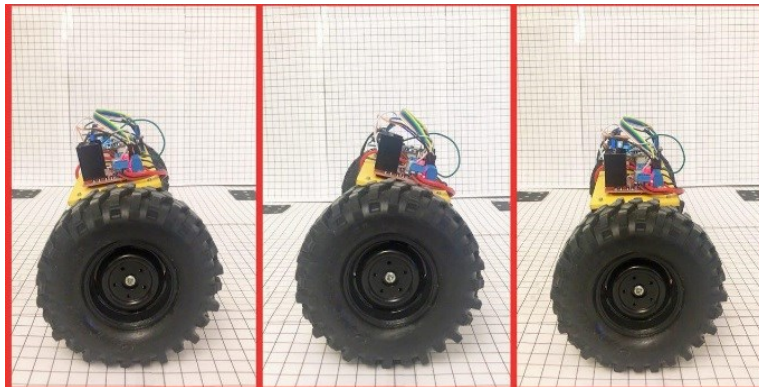


FIGURE 5-1 TWIP ROBOT WITH DIFFERENT PITCH ANGLE

## 5.1 Simulation results

The simulation is carried out in Matlab/Simulink. The comparison between the proposed SMC, PID, SFC controllers is made.



The simulation of the closed-loop PID controller is done in SIMULINK using the ode 45 methods with a variable time step. As shown in Figure 5-2, two different initial pinch angles are provided to evaluate the performance of PID controllers.

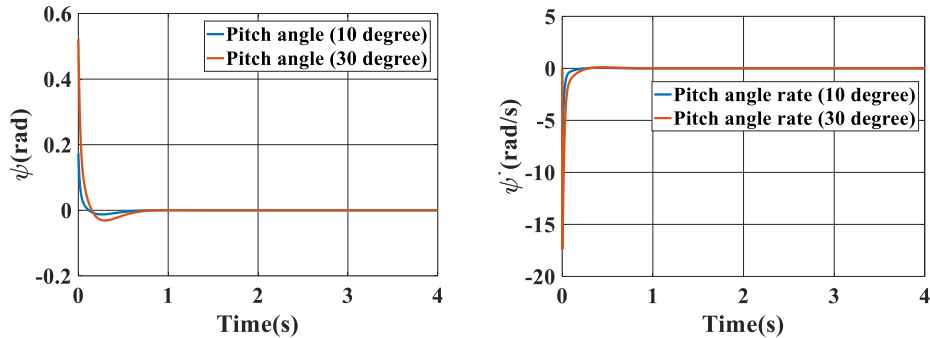


FIGURE 5-2 THE PITCH ANGLE AND ITS RATE OF PID CONTROLLER IN SIMULATION

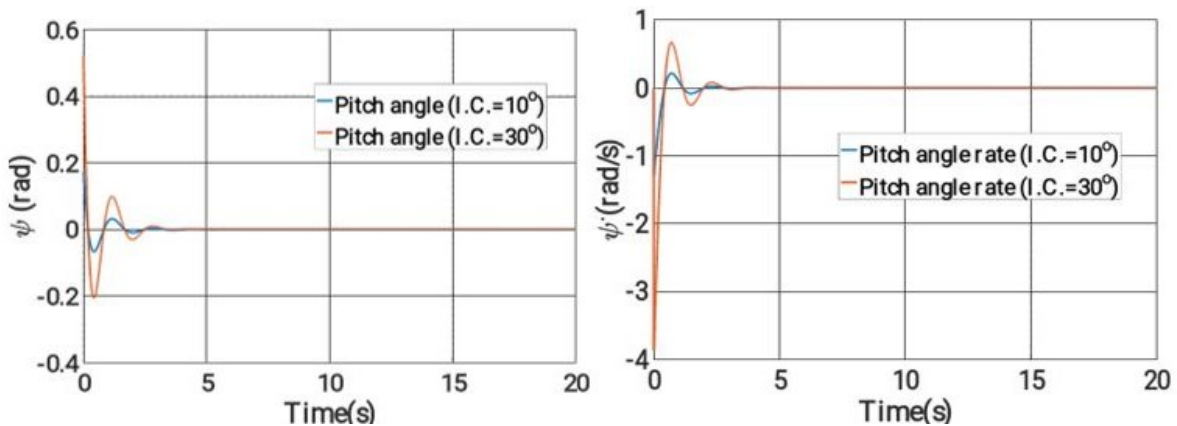


FIGURE 5-3 THE PITCH ANGLE AND ITS RATE OF SFC IN SIMULATION

The simulation of the closed-loop SFC is done in SIMULINK using the ode 45 method with a variable time step. As shown in Figure 5-3, two different initial pinch angles are provided to evaluate the performance of SFC.

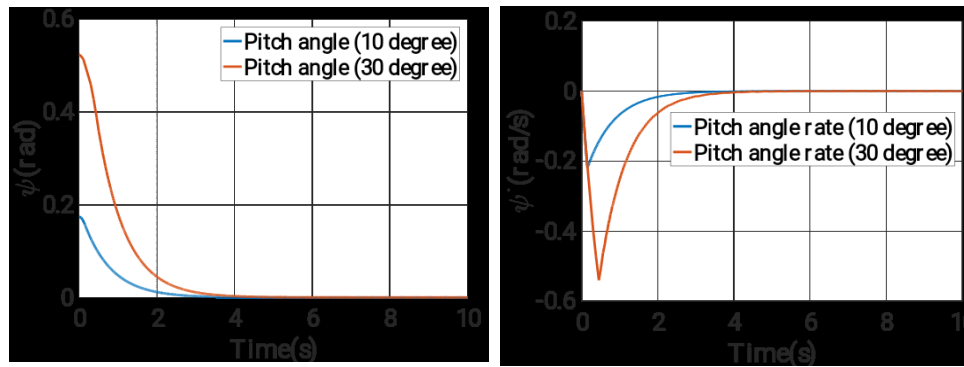


FIGURE 5-4 THE PITCH ANGLE AND ITS RATE OF SMC IN SIMULATION

The simulation results are summarized in Figure 5-4. From this table, one can see that the SMC is better transient performance than SFC does in terms of settling time and percent of overshoot.

TABLE 5-1 TRANSIENT PERFORMANCE OF SFC WITH LQR, AND SMC IN SIMULATION

Initial condition	SFC		SMC	
	10°	30°	10°	30°
Rise time (s)	0.181	0.166	3.144	4.374
Settling time (s)	2.25	3.04	1.638	2.581
Percentage of overshoot (%)	36.12	38.36	0	0

## 5.2 Experimental results

The developed SMC controller is a fully tested inbuilt TWIP robot. Extensive tests are done to compare with PID and SFC controllers. The experiment results of pitch angle and its rate of PIC and SFC controller are shown in Figure 5-5 and Figure 5-6.

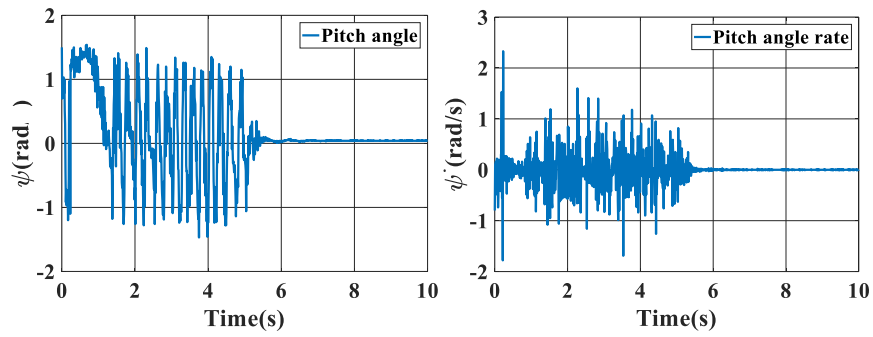


FIGURE 5-5 THE EXPERIMENT RESULTS OF PITCH ANGLE AND ITS RATE OF PID CONTROLLER

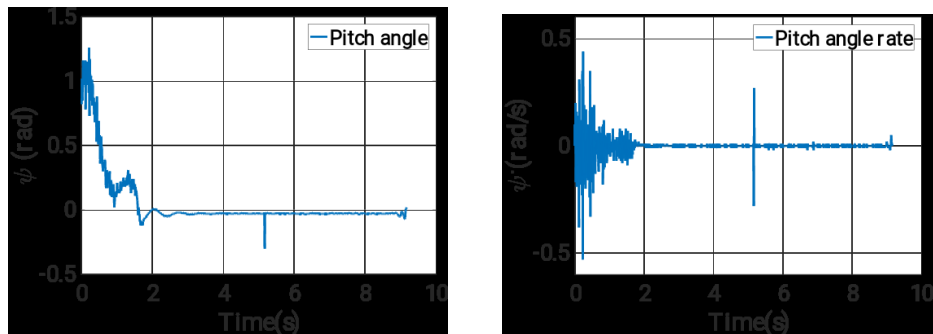


FIGURE 5-6 THE EXPERIMENT RESULTS OF PITCH ANGLE AND ITS RATE OF SFC

In the next, to evaluate the performance of the sliding mode control, the pitch angle and its rate are illustrated in Figure 5-7.

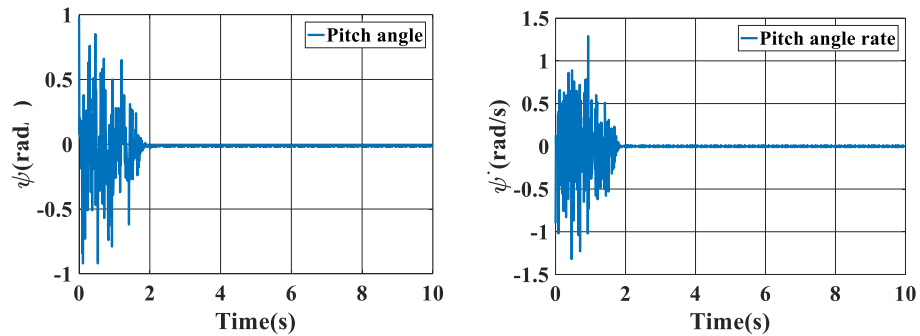


FIGURE 5-7 THE EXPERIMENT RESULTS OF PITCH ANGLE AND ITS RATE OF SMC

In the experimental tests, a big push is applied to the TWIP robot around one second to test the disturbance rejection ability of both controllers. From Figure 5-5 to Figure 5-7, one can see that PID, SFC, and SMC can recover from the push and achieve self-balancing. However, it only takes SMC less than two seconds to settle in the zero angles position while SFC takes more than two seconds, and the PID controller takes six seconds to reach the self-balancing state. The video of the experiments is uploaded on Youtube <https://youtu.be/EKycX3Wqg9k/> and <https://youtu.be/a6w5zxU8IBU>. The experimental tests demonstrate that the SMC controller outperforms the PID controller and SFC tuned by LQR.

Table 5-2 shows the performance comparison among the presented methods, PID, SFC controller, and SMC controller designed based on the 2-DoF model. As the comparison depicts, the overall performance of the presented SMC is better than those of the other methods. The settling time of the presented SMC illustrates that the robot can react faster compared to the SMC methods due to the consideration of 3 degree of freedoms (DoFs) for the dynamical modeling instead of 2 DoF (yaw angle). Although the overshoot of the proposed SMC controller is bigger than the one in [31], the important point which needs to be considered is the initial condition.

TABLE 5-2 SUMMARY OF PERFORMANCE CHARACTERISTICS IN THE LITERATURE AND CURRENT STUDY

	<b>SMC</b>	<b>SMC [current study]</b>	<b>LQR [current study]</b>	<b>PID [current study]</b>
<b>Settling Time (s)</b>	<4	2	3.1	6
<b>Overshoot (rad)</b>	~0.3 (small initial angels)	1.5 (big initial angles)	1.2 (big initial angles)	0.8 (big initial angles)
<b>Robustness test</b>	No	Very good	Good	Not good

The initial robot angles are remarkably bigger than those set in the SMC controller in Xu's work [31] to examine the robustness of the controllers. The system can respond faster than other methods do with bigger initial conditions because the controller is designed based on 3 DoF nonlinear dynamical models.

### **5.3 Summary**

In this chapter, an SMC with easy implementation was designed for balancing and stabilizing the robot based on the built nonlinear model in Chapter 3. Simulation tests were carried out to compare the proposed SMC with a PID controller and a state feedback controller (SFC) tuned by LQR. The experimental results demonstrated the superiority of the SMC controller to the other controllers, including PID, SFC, and SMC in [14] in terms of transient performance and disturbance rejection capability.

# CHAPTER 6 EXPERIMENTS AND RESULTS CCR

## 6.1 Chassis CCR

Stress analysis is performed on two critical components with significant forces acting on them, the double U profile aluminum mounting hexagon and drive pillow mounting shaft [36].

### 6.1.1 Adhesion mechanism Finite Element Analysis (FEA)

Due to the concurrent nature of the design process, the assumptions stated in Table 6-1 are used. FEA is conducted using parameters specified in

Table 6-2.

TABLE 6-1 ASSUMPTION USED IN CHASSIS STRESS ANALYSIS

Parameter	Value	Justification
Mass (kg)	4.0	Maximum adhesion system mass as identified in the specification (Section 4.4.2)
Payload (kg)	2.5	Mass of cameras and video data transmitters
Gravity (ms <sup>-2</sup> )	10	Simplified for ease of calculations

TABLE 6-2 KEY FACTORS FOR THE STRESS ANALYSIS OF THE ADHESION UNIT

Component	Adhesion unite mounting
Material	Aluminum 6082-T6
Yield strength (MPa)	250
Load	The moment generated 24 Nm
Constraint	Constrained at bolt interface

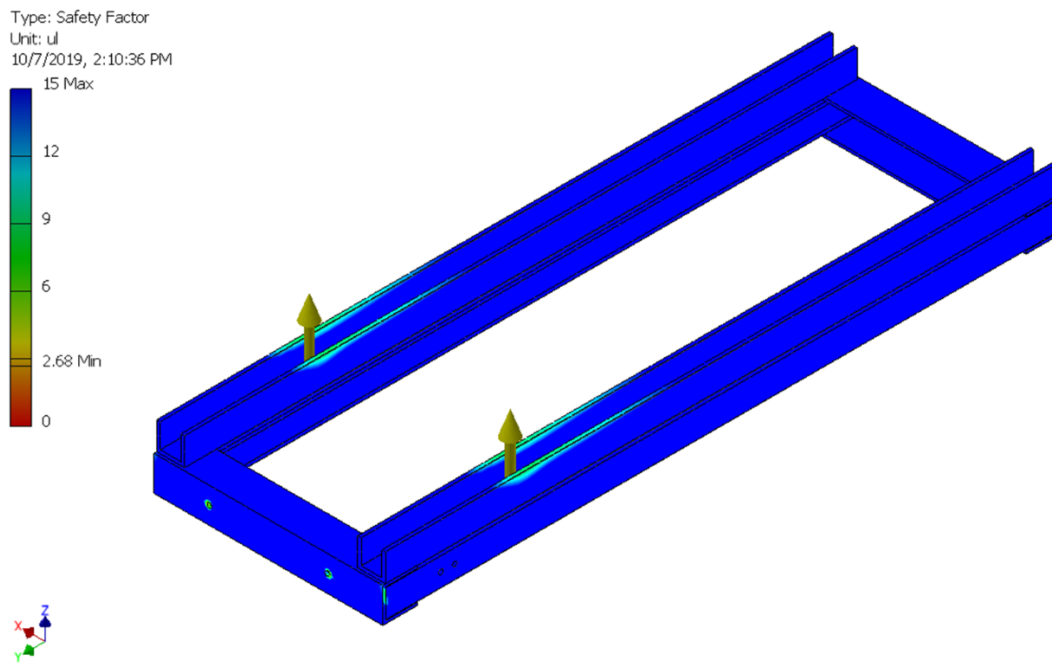


FIGURE 6-1 SAFETY FACTOR FOR ADHESION UNIT MOUNTING WITH 24 NM MOMENT

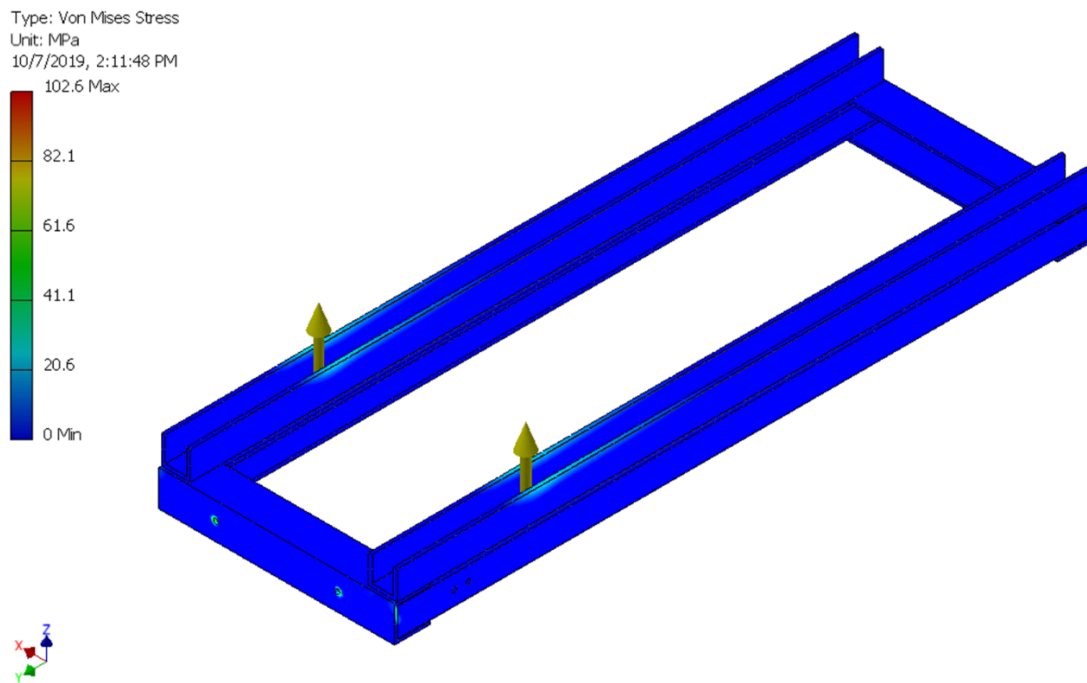


FIGURE 6-2 VON MISES STRESS FOR ADHESION UNIT MOUNTING WITH 24 NM MOMENT

Figure 6-1 shows that one side adhesion mechanism beam negatively deflects, whereas the rear positively deflects due to the moment being created. This does not have a noticeable effect on the system. Results are shown in Table 6-3 [37].

TABLE 6-3 RESULTS OF STRESS ANALYSIS OF THE ADHESION UNIT MOUNTING

<b>Parameter</b>	<b>Value</b>
Maximum von mises stress (MPa)	39.52
Percentage of yield stress (%)	0.12
Maximum displacement (mm)	0.06

### 6.1.2 Motor mounting FEA pillow mounting shaft

Table 6-4 shows the key analysis factors for the motor mounting plate.

TABLE 6-4 KEY FACTORS FOR THE STRESS ANALYSIS OF THE MOTOR MOUNTING

<b>Component</b>	<b>Motor mounting</b>
Material	Aluminum 6061 (closest to required material on software)
Yield strength (MPa)	250
Load	Force of 622 N is generated by the motor acting at the center of the motor mounting holes on the side of the plate. The forced used is half that of the calculated force since the total force will be shared across the two plates.
Constraints	Constrained at the base where the plate is bolted to the aluminum extrusions.

Figure 6-3 shows that the maximum stress is concentrated around the outside two bolt holes.



Type: Safety Factor  
Unit: ul  
10/7/2019, 2:04:33 PM

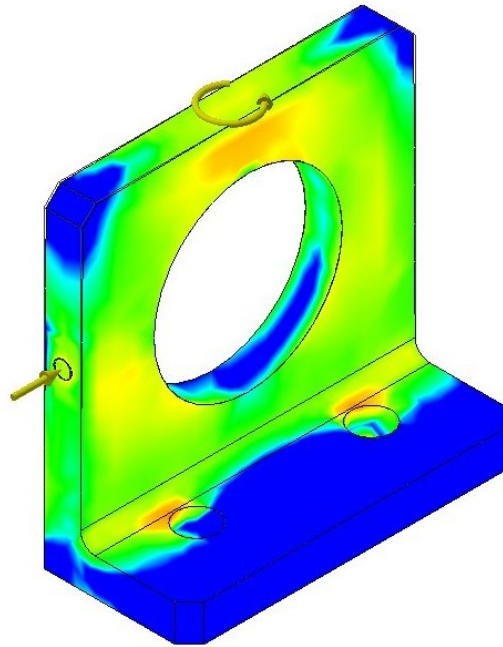
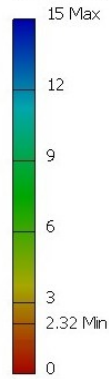


FIGURE 6-3 SAFTY FACTOR OF MOTOR MOUNTING WITH 622 N FORCE

Type: Displacement  
Unit: mm  
10/7/2019, 2:06:11 PM

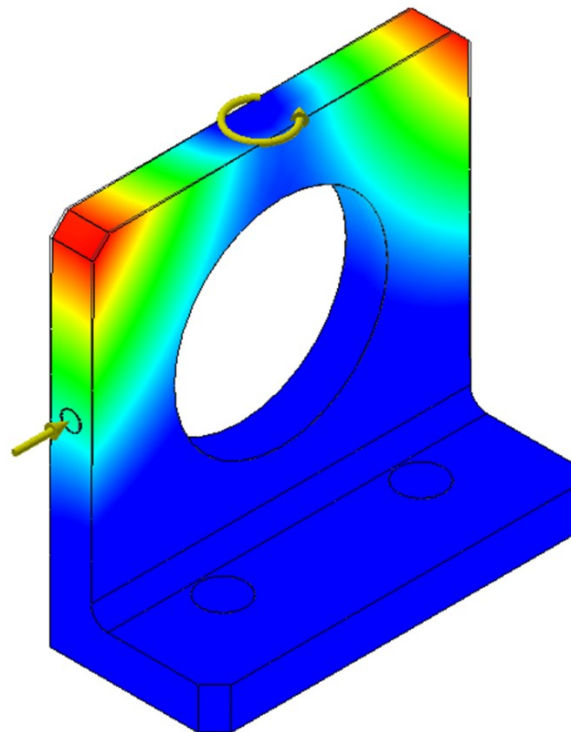
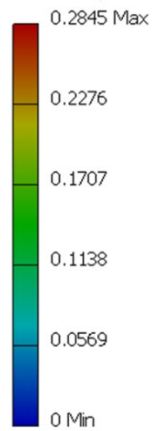


FIGURE 6-4 DISPLACEMENT OF MOTOR MOUNTING WITH 622 N FORCE

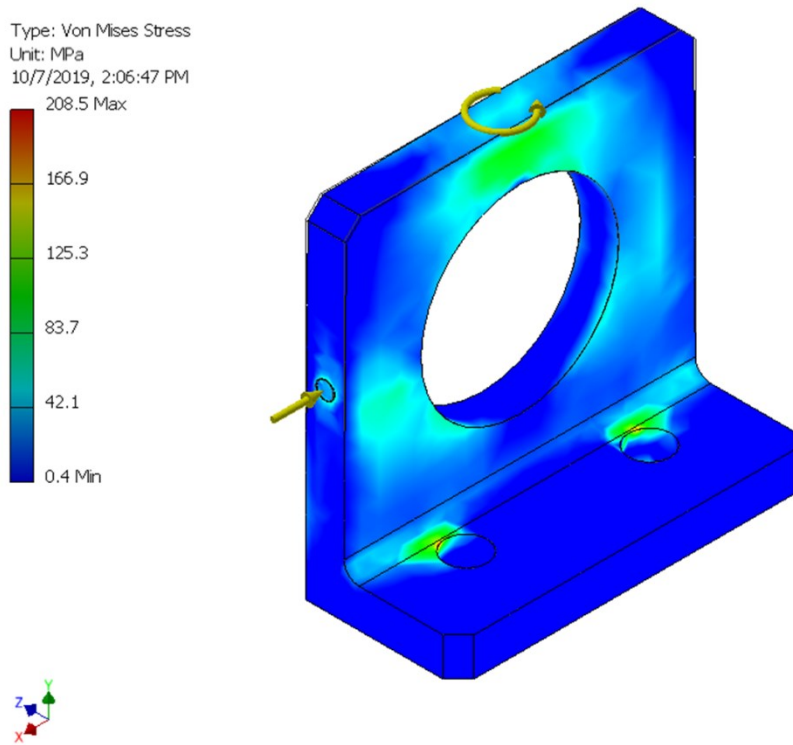


FIGURE 6-5 VON MISES STRESS OF MOTOR MOUNTING WITH 622 N FORCE

TABLE 6-5 RESULTS OF STRESS ANALYSIS OF THE MOTOR MOUNTING

Parameter	Value
Maximum von mises stress (MPa)	20.93
Percentage of yield stress (%)	0.02
Maximum displacement (mm)	0.02

### 6.1.3 Chassis CCR performance validation

The design, manufacture, and assembly of the chassis are completed within the timeframe (Figure 6-6, Figure 6-7) and taken to simulate at Concordia Robotic Control Lab (Figure 6-8).

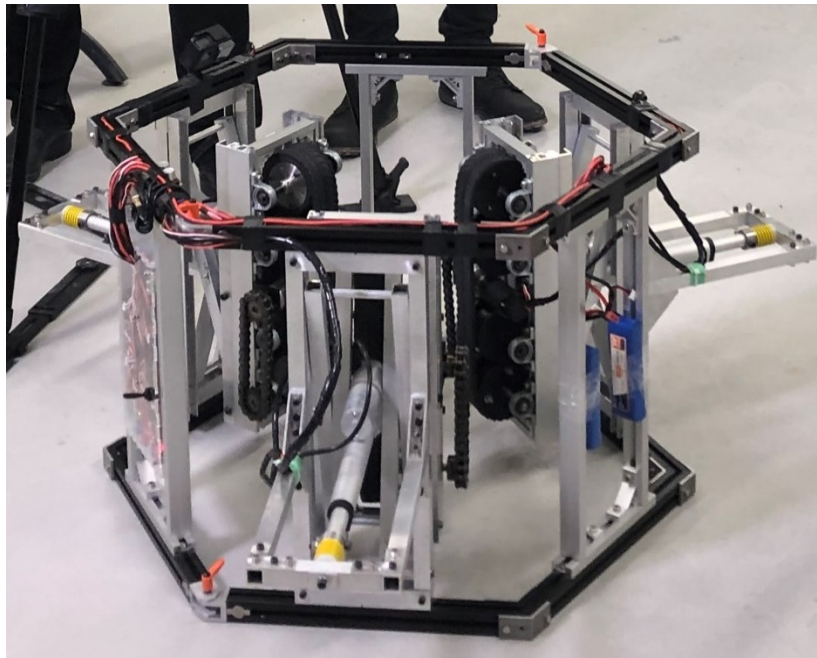


FIGURE 6-6 FINAL CHASSIS ASSEMBLY CLOSED HEXAGON



FIGURE 6-7 FINAL CHASSIS ASSEMBLY OPEN HEXAGON



FIGURE 6-8 FINAL CHASSIS ASSEMBLY AT THE CONCORDIA ROBOTIC CONTROL LAB

Table 6-6 shows the majority of the requirements outlined in the specification are fully met.

TABLE 6-6 CHASSIS RESULTS AGAINST SPECIFICATION

<b>ID</b>	<b>Constraint</b>	<b>Met</b>	<b>Explanation</b>
1	Modular architecture	Successfully	Misumi's aluminum extrusions is an excellent material for prototyping and modification.
2	Repair and maintenance	Unsuccessfully	Feedback from Guangdong Chengxin highway company reveals that it would not be easy to repair it on the field.
3	Durability	Alsmot successfully	Time does not allow the full system to be tested. Debris entry into chassis is minimal but not zero.
4	Lightweight	Successfully	The total mass is 34.5 kg, which is evenly distributed in the chassis, and the heaviest components are located closest to the ground level.
5	Size	Successfully	Fits within the turning circle and triangle constraints.
6	Systems integration	Successfully	Systems are fully integrated.
7	Load resistance	Alsmot successfully	Since the robot is not fully manufactured, this is not tested fully. Virtual stress analysis was performed on critical components successfully.
8	Ease of manufacture and assembly	Successfully	The chassis is fully manufactured and assembled within the time.
9	Material availability	Successfully	All materials selected are readily available. Sponsors donated many, and the rest is sourced inexpensively from university suppliers, Misumi and Faulhaber.

Direct feedback from Guangdong Chengxin highway company suggests that the chassis may get beached on some terrain and recommended that the optimum chassis shape should resemble Figure 6-9 [38].

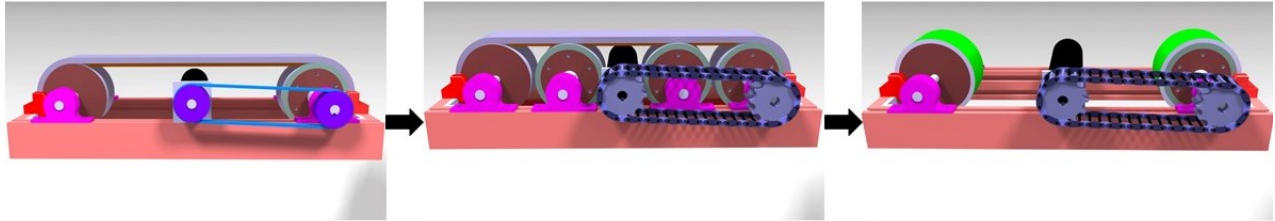


FIGURE 6-9 OPTIMUM ADHESION SYSTEM CHASSIS SHAPE

A robotics test expert from Concordia University (A. Faroughnasiraie, 2019) comment that if damage occurs in a real-life situation, it would take too long to repair; however, the rubber track would allow good stability and high friction. Despite the rubber track being selected for its high ease, friction, in practice inside of the track is not match with sprockets under high pressure. Furthermore, using two rollers and four extra pillows fewer 3.5 kg decreases the weight of the robot [39].

Urethane wheels are chosen for fast movement on stay cables with improving friction and reducing cable surface damage during inspection Figure 6-9. The wheel assembly consists of the wheels attached to springs and spacers inside the outer frame for adaptation to various cable gauges [40].

## 6.1.4 Drivetrain -testing of cable climbing robot

### 6.1.4.1 Virtual testing

Virtual impact shock testing is conducted to ensure that the robot could withstand large falls within its environment, Table 6-7 details these calculations.

TABLE 6-7 IMPACT SHOCK CALCULATIONS

Parameter	Value	Unit	Symbol	Formula
Mass	35	kg	m	n/a
Height of fall	0.10	m	s	n/a
Gravity	9.81	ms <sup>-2</sup>	a	n/a
Time to fall	1	S	t	$S=u+0.5at^2$
Falling velocity	35	ms <sup>-1</sup>	v	$v=mv^2$
Momentum	35	kgms <sup>-1</sup>	M	$M=mv^2$
Time to stop	0.8	s	t*	n/a
Force	50	N	F	$F=ma=M/t$
Weight	35-37	M	Kg	n/a

Two variables affect the force on the robot, the fall height, and the stopping time. The higher the fall or shorter the stopping time, the larger the force. The robot should not encounter a situation with a drop greater than 0.1m at the inspection. The stopping is an estimate based upon experiments carried out at the sample of cable with the existing robot at Concordia University robotic lab. Using the values calculated in Table 6-7, the force on the robot is over 780N. As this value is based on estimates, 1000 N is used for FEA for the worst-case loading scenarios where the entire force is through a single component.

Figure 6-10 shows the drivetrain unit under the loading.

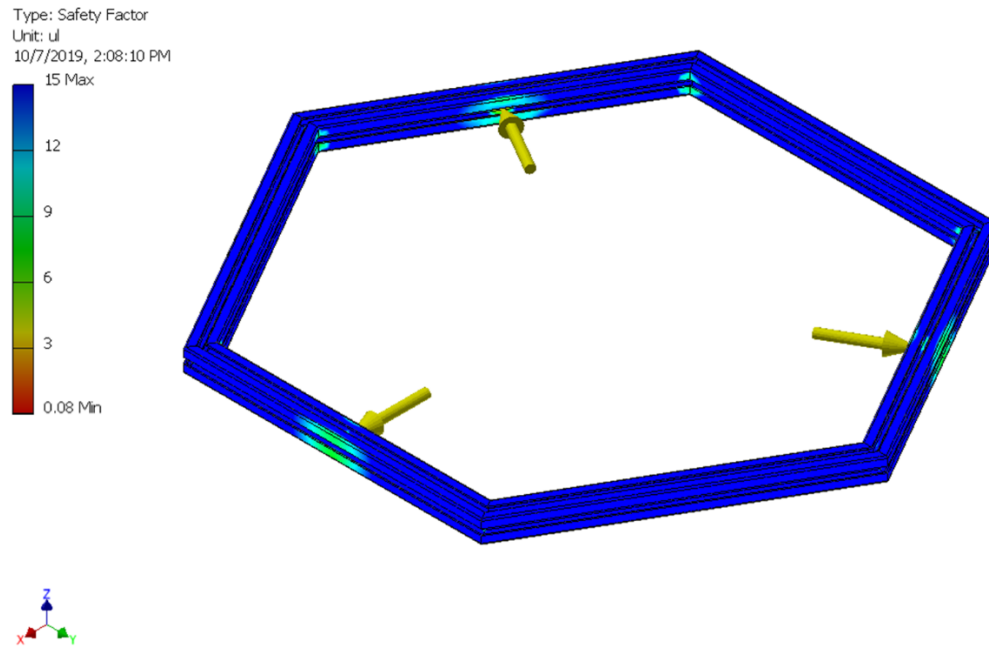


FIGURE 6-10 SAFTY FACTOR FEA MODELLING OF THE DRIVETRAIN UNIT

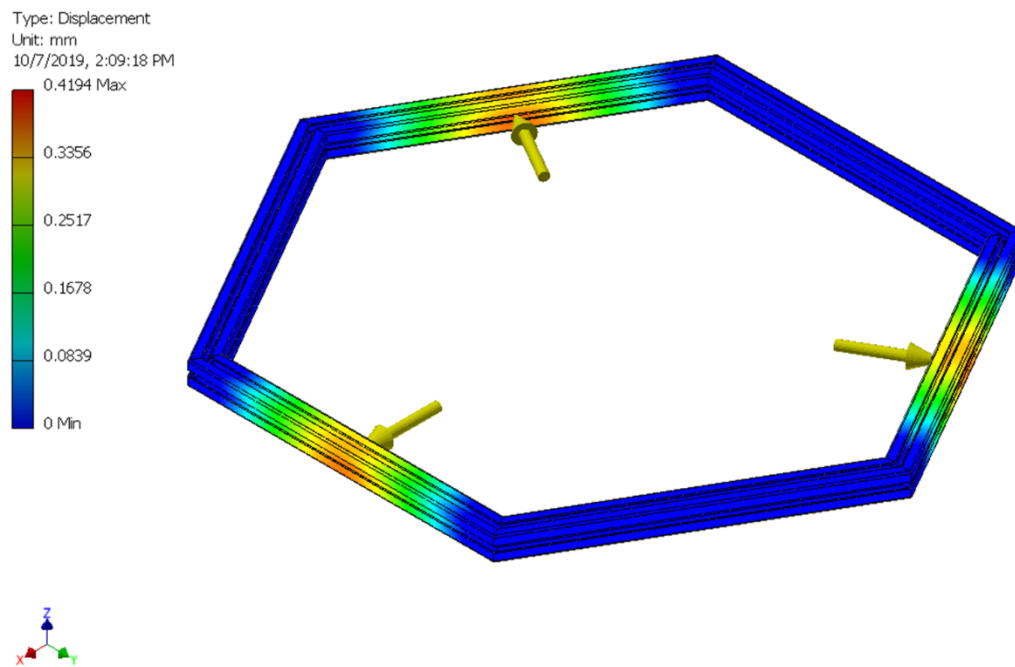


FIGURE 6-11 DISPLACEMENT FEA MODELLING OF THE DRIVETRAIN UNIT



The lowest safety factor of 2.08 (Figure 6-10) means a force of 2080 N could be withstood before the material yields, and plastic deformation occurs. It is standard practice in the industry to aim for a safety factor of between 1.5 and 2.5 (Engineering Toolbox, 2014). The rest of the drivetrain's load-bearing components were analyzed similarly [47].

### 6.1.4.2 Physical testing

In order to build a practical cable climbing robot, the robot should be developed with a clear understanding of the real environmental conditions. The climbing and self-landing mechanism are originally designed to use Misumi chain and U-Shaped aluminum channels on both sides of scissor sections (Figure 6-12). Loading testing is performed to determine the strength of the Araldite bond between two U-shaped aluminum channels. The results show the bond's linear strength could withstand  $>500\text{N}$ ; also, at high torsional force, the bond does not break easily. Therefore, it is decided to attach them with three pairs of 4mm bolts and nuts [48].

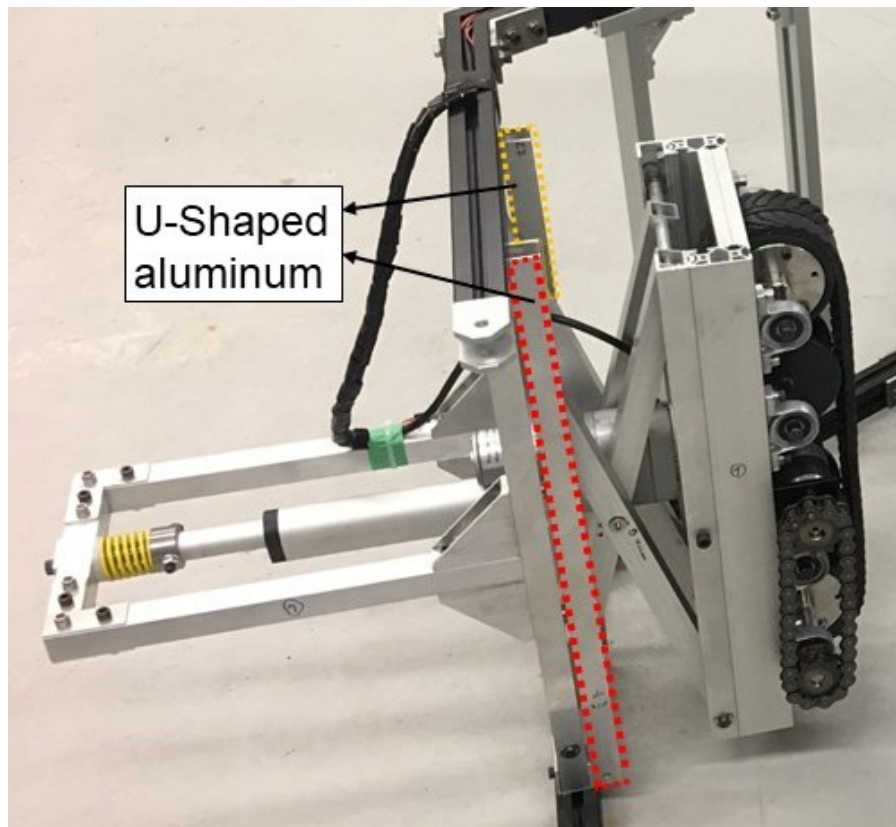


FIGURE 6-12 DOUBLE U-SHAPED ALUMINUM CHANNELS

## 6.1.5 Performance validation of drivetrain

All parts were manufactured to a level where the drivetrain could be assembled, to see if it would go together as planned. However, it is not at a stage where it could be operational. Due to manufacturing delays, the tracks are not constructed with time to test physically before the deadline. Future work recommendations can be found in Chapter 5

Table 6-8 details how well the final design met the specification.

TABLE 6-8 COMPARISON AGAINST SPECIFICATION

ID	Constraint	Met	Explanation
1	Cost	Successfully	The robot was built within the company's budget
2	Weight	Almost successfully	Robot is very heavy at 50kg. Although the whole robot is under the 47kg limit set
3	Modular	Successfully	The linear actuators units house their motors and control boards
4	Size	Successfully	The robot's overall dimensions fit within limits originally set
5	Adaptability	Successfully	Each adhesion unit can be easily removed and replaced
6	Repair/ maintenance	Successfully	The simple and easily accessible design allows for repair & maintenance
7	Complexity	Successfully	Each adhesion unit is identical reducing complexity
8	Durability	Almost successfully	The robot has been designed to be durable
9	Reliability	Almost successfully	The robot has been designed to be reliable
10	Torque	Successfully	The motor and gear combinations have the required torque
11	Traction	Almost successfully	The robot has been designed to have the required traction. However, this has not been tested
12	Obstacle crossing	Almost successfully	The design should be able to handle cable obstacles; however, this has not been tested

TABLE 6-9 COMPARISON AGAINST SPECIFICATION (CONTINUED)

13	Clearance	Successfully	The clearance on the robot is greater than originally specified
14	Mobility	Almost successfully	The robot has been designed to be mobile. However, this has not been tested
15	Power source	Almost successfully	The motors are suited to the power source; however, this has not been tested
16	Control	Almost successfully	The robot has been designed to be easily controllable. However, this has not been tested
17	Wiring	Unsuccessfully	The wiring between the chassis and adhesion units are alternatives should be investigated to allow continuous 180 degrees rotation
18	Environment	Almost successfully	The design should handle the required environments

### 6.1.6 Performance validation of control, electronics, and software

Table 6-10 compares the final design against the original electronic and software specification.

TABLE 6-10 ELECTRONIC AND SOFTWARE RESULTS AGAINST SPECIFICATION

ID	Constraint	Met	Explanation
1	Size	Successfully	The components chosen were small and final power board designs were 140x280 mm and main power boards, respectively
2	Mass	Successfully	Small, lightweight components were used when available
3	Modular	Successfully	The entire electronic, software and power system is modular, as demonstrated by the system architecture (Section 4.6.5)
4	Cost	Successfully	Electronic components were one of the most expensive parts of the full robot design; however, costs were kept to a minimum and are in line with previous CCR designs

TABLE 6-11 ELECTRONIC AND SOFTWARE RESULTS AGAINST SPECIFICATION (CONTINUED)

5	Reliability	Almost successfully	The new software and electronics tested on the old robot at the real condition performed reliably and did not experience any errors or dropouts. However, the full system has not been tested, so the reliability of the final system is not known
6	Communication	Successfully	Communication with the existing robot and new router did not experience any problems at the Concordia Robotics Lab
7	Data	Almost successfully	The robot was not constructed or wired up fully to test this functionality; however, subsystems were proven to work
8	Wiring	Almost successfully	The robot was not wired up; however, due to the final location of the boards within the chassis means that cable wiring may be inefficient
9	Emergency stop	Almost successfully	An emergency stop system was designed and simulated to specification; however, it was not tested physically
10	Fuse protection	Successfully	Fuse protection has been designed into the system
11	Protect battery	Successfully	The battery connectors were chosen only to allow a single polarity connection
12	Monitor battery	Unsuccessfully	Several batteries monitoring circuits were simulated however were not proven to work reliably, or to the accuracy, the level required so were therefore not manufactured or tested

A full modular electronic architecture is developed and sections tested. The ability to synchronized control of the three dc motors and linear actuators shows that this system is stable within the long cable for doing an inspection.

The size of the system and the requirement for wiring simplicity deviate slightly from the initial specification. The PCB shows the difficulty that small-scale custom PCB manufacturing brings,

mainly the inability to use very small surface mount components that cannot be soldered by hand. Although six dc driver motors are installed to allow controlling of each unit separately, space savings could be achieved within the chassis by designing one mainboard to power all systems.

An inspection provides valuable data from the status of the line, thus helps line engineers to plan for necessary repair or replacement works before any major damages, which may result in an outage.

The robotic system is currently evaluated in realistic field conditions for robot mobility, defect detectability, and field applicability. Mobility is an important design concern for fast cable inspection with irregular surface conditions with obstacles on bridge cables. Detectability of various types of inner and outer defects on bridge cables should be validated under realistic field conditions. The bridge inspection robot should apply to various field conditions.



*Figure 6-13 Test in Xili bridge, Guangzhou, P.R. China, March 2019*

# CHAPTER 7 CONCLUSION AND FUTURE WORKS ON TWIP AND CCR

## 7.1 Conclusion

In the first study, a customer-designed TWIP robot is presented, which is an inherently unstable and nonlinear system. An SMC for balancing and steering movement is designed based on the 3-DoF dynamic model derived by the Lagrangian function method. From the simulation results of the PID controller, SFC, and SMC for the TWIP system, it can be concluded that the SMC has the best transient performance in stabilizing the TWIP robot. To further evaluate the SMC, SFC and PID control performances, experimental tests are conducted to validate the effectiveness of the designed robot controllers. As it is presented in the tests as mentioned earlier results, the settling time of SMC is three times shorter than that of the PID controller. The performances of SMC are superior to those of SFC and SMC in [31] in terms of settling time and robustness. The future work includes the further improvement of control performances considering the actuation constraints.

A new cable climbing robot for suspension bridge inspection is designed and manufactured to meet the specifications of the industrial partner— GCH company. The design work includes both mechanical and electrical system design, robot controller design, and software programming and testing and considers the balance among size, mass, capabilities, and cost. The robots adopt a modular robotic architecture, allowing the platform to be adapted for specific tasks. These would connect using standardized interfaces, allowing quick robotic platform re-configuration.

The designed robot delivers the drivetrain with a high ratio of the mass at 71%, which allows the great mass reduction. The chassis is constructed of a lightweight aluminum beam, giving the strong structural strength and providing a platform to integrate the robot's systems and electronic components. The adhesion mechanisms are well designed and controlled by PID controllers. The linear actuators are synchronized and controlled accurately. The self-locking mechanisms and shock absorber mechanisms improve robot movement on the bridge cable surface. A modular electronic and software system are designed for the cable climbing robot, including innovation in the telemetry system and power-saving electronic (auto-landing).

The controller units, sensors, and drive units are designed to guarantee that the robot can climb up and land safely. The diameter of the cables that the robot can climb ranges from 100mm to

300mm and with the slant angle up to 0 degrees (i.e., vertical cable). Both indoor and outdoor tests show that the designed robot has met the designed specifications and can fulfill the inspection task (Figure 6-13).

## 7.2 Future works

The future works on TWIP will be focused on the further improvement of control performance considering the actuation constraints.

The modular architecture of CCR allows future engineers to easily adapt and improve this cable climbing robot. The analysis of CCR systems in section 2.2.2 combined with the experience and knowledge gained from designing the new robot highlight the following items for future work with regard to each subsystem:

- Chassis
  - Improve the design to increase the climbing speed from current 8m/s to higher speed and increase the payload from current 10kg to 15kg including vision and another non-destructive testing instrument; Investigate different shapes to remove the possibility of crashing since the current protruding design using the linear actuators makes the robot dimension pretty big.
  - Develop sliding cover panels to allow easier access to internal components and batteries.
- Drivetrain
  - Complete mechanical tasks on current design (add armor for sprockets, chains, and dc motors).
  - Use FEA to identify areas of mass saving in the adhesion mechanisms.
  - Wire the motors, controllers, and test physically.
- Electronics and Software
  - Produce a single power board capable of powering all modular systems.
  - Design complete software to drive fully autonomously the robot and test on.
  - Develop a battery monitoring system.
  - Develop the CCR software for image processing and neural network.
  - Develop the network connection for image processing.

## Reference

- [1] A. N. K. Nasir, M. A. Ahmad and R. M. T. R. Ismail, "The Control of a Highly Nonlinear Two-wheels Balancing Robot: A Comparative Assessment between LQR and PID-PID Control Schemes," *International Journal of Mechanical and Mechatronics Engineering*, vol. 4, no. 10, pp. 942-947, 2010.
- [2] H. Marzi, "Fuzzy Control of an Inverted Pendulum using AC Induction Motor Actuator," in *CIMSA 2006 - IEEE International Conference on Computational Intelligence for Measurement Systems and Applications*, Spain, pp. 109-114, 2006.
- [3] C.-C. Tsai, S.-Y. Ju and S.-M. Hsieh, "Trajectory Tracking of a Self-Balancing Two-Wheeled Robot Using," in *The 2010 IEEE/RSJ International Conference on*, Taipei, pp. 3943-3948, 2010.
- [4] A. Unluturk and O. Aydogdu, "Adaptive control of two-wheeled mobile balance robot capable to adapt different surfaces using a novel artificial neural network-based real-time switching dynamic controller," *International Journal of Advanced Robotic Systems*, vol. 14, no. 2, pp. 1-9, 2017.
- [5] J. Villacres, M. Viscaino, M. Herrera and O. Camacho, "Cotrollers comparison to stabilize a two-wheeled inverted pendulum: PID, LQR and sliding mode control," *International Journal of Control Systems and Robotics*, vol. 1, pp. 29-36, 2016.
- [6] N. R. Gans and S. Hutchinson, "Visual Servo Velocity and Pose Control of a Wheeled Inverted Pendulum through Partial-Feedback Linearization," in *2006 IEEE/RSJ International Conference on Intelligent Robots and Systems, IROS*, Beijing, pp. 3823-3828, 2006.
- [7] M. u. Hasan, K. M. Hasan, M. U. Asad, U. Farooq and J. Gu, "Design and experimental evaluation of a state feedback controller for two wheeled balancing robot," in *17th IEEE International Multi Topic Conference*, pp 366-371, 2014.
- [8] M.-L. Chen, "Analysis and Design of Robust Feedback Control Systems for a Nonlinear Two-Wheel Inverted Pendulum System," in *2012 International Symposium on Computer, Consumer and Control*, Taichung, pp. 949-953, 2012.
- [9] T. Nomura, Y. Kitsuka, H. Suemitsu and T. Matsuo, "Adaptive backstepping control for a two-wheeled autonomous robot," in *ICROS-SICE International Joint Conference*, Fukuoka, pp. 4687-4692, 2009.
- [10] K. Pathak, J. Franch and S. Agrawal, "Velocity control of a wheeled inverted pendulum by partial feedback linearization," in *43rd IEEE Conference on Decision and Control (CDC) (IEEE Cat. No.04CH37601)*, Nassau, vol. 4, pp. 3962-3967, 2004.



- [11] K. Pathak, J. Franch and S. Agrawal, "Velocity and position control of a wheeled inverted pendulum by partial feedback linearization," *IEEE Transactions on Robotics*, vol. 21, no. 3, pp. 505 - 513, 2005.
- [12] J. Huang, Z.-H. Guan, T. Matsuno, T. Fukuda and K. Sekiyama, "Sliding-Mode Velocity Control of Mobile-Wheeled Inverted-Pendulum Systems," *IEEE Transactions on Robotics*, vol. 26, no. 4, pp. 750 - 758, 2010.
- [13] M. Yue, X. Sun, N. Li and C. An, "Dynamic Motion Planning and Adaptive Tracking Control for a Class of Two-Wheeled Autonomous Vehicle With an Underactuated Pendular Suspension," *Journal of Dynamic Systems, Measurement, and Control*, vol. 137, no. 10, pp. 101006-1 - 101007-11, 2015.
- [14] Z. Zhang, I. Wang and L. Li, "Design and implementation of two-wheeled mobile robot by variable structure Sliding Mode Control," in *35th Chinese Control Conference (CCC)*, Chengdu, pp. 5869-5873, 2016.
- [15] N. Esmaili, A. Alfi and H. Khosravi, "Balancing and Trajectory Tracking of Two-Wheeled Mobile Robot Using Backstepping Sliding Mode Control: Design and Experiments," *Journal of Intelligent & Robotic Systems*, vol. 87, no. 3-4, pp. 601-613, 2017.
- [16] W. Lv, Y. Kang and P. Zhao, "Speed and orientation control of a two-coaxial-wheeled inverted pendulum," in *Proceedings of the 32nd Chinese Control Conference*, Xi'an, pp. 334-337, 2013.
- [17] A. B. Mehrabi, C. A. Ligozio, A. T. Ciolko and a. S. T. Wyatt, "Evaluation, Rehabilitation Planning, and Stay-Cable Replacement Design for the Hale Boggs Bridge in Luling, Louisiana," *Journal of Bridge Engineering*, vol. 15, no. 4, pp. 364-372, 2010.
- [18] D. Schmidt and K. Berns, "Climbing robots for maintenance and inspections of vertical structures—A survey of design aspects and technologies," *Robotics and Autonomous Systems*, vol. 61, no. 12, pp. 1288-1305, 2013.
- [19] F.-Y. Xu, X.-S. Wang and L. Wang, "Climbing model and obstacle-climbing performance of a cable inspection robot for a cable-stayed bridge," *Transactions- Canadian Society for Mechanical Engineering*, vol. 35, no. 2, pp. 269-289, 2011.
- [20] M. Higuchi, Y. Maeda and S. Hagihara, "Development of a Mobile Inspection Robot for Power Transmission Lines," *Journal of the Robotics Society of Japan*, vol. 9, no. 4, pp. 457-463, 1991.
- [21] J. Sawada, K. Kusumoto, Y. Maikawa, T. Munakata and Y. Ishikawa, "A mobile robot for inspection of power transmission lines," *IEEE Transactions on Power Delivery*, vol. 6, no. 1, pp. 309 - 315, 1991.
- [22] H. S. Han, J. J. Yu, C. G. Park and J. G. Lee, "Development of inspection gauge system for gas pipeline," *KSME International Journal*, vol. 18, no. 3, pp. 370-378, 2004.

- [23] M. Browne, N. Mayer and T. Cutmore, "A multiscale polynomial filter for adaptive smoothing," *Digital Signal Processing*, vol. 17, no. 1, pp. 69-75, 2007.
- [24] J. Luo, S. Xie and Z. Gong, "Cable maintenance robot and its dynamic response moving on the horizontal cable," in *ICAR '05. Proceedings., 12th International Conference on Advanced Robotics*, Seattle, WA, USA, pp. 514-517, 2005.
- [25] H.-B. Yun, S.-H. Kim, L. Wu and J.-J. Lee, "Development of Inspection Robots for Bridge Cables," *The Scientific World Journal*, vol. 2013, 2013.
- [26] K. H. Cho, Y. H. Jin, H. M. Kim, H. Moon, J. C. Koo and H. R. Choi, "Caterpillar-based cable climbing robot for inspection of suspension bridge hanger rope," in *IEEE International Conference on Automation Science and Engineering (CASE)*, Madison, WI, USA, pp. 1059-1062, 2013.
- [27] K. H. Cho, Y. H. Jin, H. M. Kim, H. Moon, J. C. Koo and H. R. Choi, "Multifunctional Robotic Crawler for Inspection of Suspension Bridge Hanger Cables: Mechanism Design and Performance Validation," *IEEE/ASME Transactions on Mechatronics*, vol. 22, no. 1, pp. 236 - 246, 2017.
- [28] Z. Zheng and N. Ding, "Design and Implementation of CCRobot-II: a Palm-based Cable Climbing Robot for Cable-stayed Bridge Inspection," in *International Conference on Robotics and Automation (ICRA)*, Montreal, QC, Canada, pp. 9747-9753, 2019.
- [29] F. Dai, X. Gao, S. Jiang, W. Guo and Y. Liu, "A two-wheeled inverted pendulum robot with friction compensation," *Mechatronics*, vol. 30, pp. 116-125, 2015.
- [30] J. Luo, S. Xie, Z. Gong and T. Lu, "Development of cable maintenance robot for cable-stayed bridges," *Industrial Robot: An International Journal*, vol. 34, no. 4, pp. 303-309, 2007.
- [31] F. Xu and X. Wang, "Design and experiments on a new wheel-based cable climbing robot," in *IEEE/ASME International Conference on Advanced Intelligent Mechatronics*, Xian, China, pp. 418-423, 2008.
- [32] F. Xu and Q. Jiang, "Dynamic obstacle-surmounting analysis of a bilateral-wheeled cable-climbing robot for cable-stayed bridges," *Industrial Robot*, vol. 46, no. 3, pp. 431-443, 2019.
- [33] H. Jordan and C. Christiand, "The development of climbing mechanism for cable inspection robot," *cylinder*, vol. 5, no. 1, 2019.
- [34] X. Li, C. Gao, Y. Guo, F. He and Y. Shao, "Cable surface damage detection in cable-stayed bridges using optical techniques and image mosaicking," *Optics & Laser Technology*, vol. 110, pp. 36-43, 2019.

- [35] J. Zhu, Z. Sun, W. Huang and Q. Chen, "Design of a Master-Slave Composite Wall Climbing Robot System for Penstock Assembly Welding," in *ICIRA 2019: Intelligent Robotics and Applications*, Switzerland, vol. 11741, pp. 123-134, 2019.
- [36] R. Plaut, "Snap loads and torsional oscillations of the original Tacoma Narrows Bridge," *Journal of Sound and Vibration*, vol. 309, no. 3-5, pp. 613-636, 2008.
- [37] M. R. Jahanshahi, S. F. Masri, C. W. Padgett and G. S. Sukhatme, "An innovative methodology for detection and quantification of cracks through incorporation of depth perception," *Machine Vision and Applications*, vol. 24, no. 2, pp. 227-241, 2013.
- [38] X. Fengyu, S. Jingjin and J. GuoPing, "Kinematic and Dynamic Analysis of a Cable-Climbing Robot," *International Journal of Advanced Robotic Systems*, vol. 12, no. 7, 2015.
- [39] C. Balaguer, A. Gimenez and A. Jardon, "Climbing Robots' Mobility for Inspection and Maintenance of 3D Complex Environments," *Autonomous Robots*, vol. 18, no. 2, pp. 157-169, 2005.
- [40] Y. Guan, L. Jiang, X. Zhang and H. Zhang, "Climbing gaits of a modular biped climbing robot," in *IEEE/ASME International Conference on Advanced Intelligent Mechatronics*, Singapore, pp. 532-537, 2009.
- [41] K. H. Cho, Y. H. Jin, H. M. Kim and H. R. Choi, "Development of novel multifunctional robotic crawler for inspection of hanger cables in suspension bridges," in *IEEE International Conference on Robotics and Automation (ICRA)*, Hong Kong, China, pp. 2673-2678, 2014.
- [42] M. J. Spenko, G. C. Haynes, J. A. Saunders, M. R. Cutkosky, A. A. Rizzi, R. J. Full and D. E. Koditschek, "Biologically Inspired Climbing with a Hexapedal," *Journal of Field Robotics*, vol. 25, no. 4-5, pp. 223-242, 2008.
- [43] H. M. Kim, K. H. Cho, F. Liu and H. Choi, "Development of Cable Climbing Robotic System for Inspection of Suspension Bridge," in *Proceedings of the 28th ISARC*, Seoul, Korea, 2011.
- [44] M. Zheng, Y. Li, J. Li and K. Yuan, "Structure Design and Kinematical Analysis of a New Type Cable Climbing Robot," in *Second International Conference on Intelligent Human-Machine Systems and Cybernetics*, Nanjing, Jiangsu, China, pp. 284-287, 2010.
- [45] F. Xu, X. Wang and L. Wang, "Cable inspection robot for cable-stayed bridges: Design, analysis, and application," *Journal of Field Robotics*, vol. 28, no. 3, pp. 441-459, 2011.
- [46] X. Wang and F. Xu, "Design and Experiments on Cable Inspection Robot," in *IECON 2007 - 33rd Annual Conference of the IEEE Industrial Electronics Society*, Taipei, Taiwan, pp. 2870-2875, 2007.

- [47] Z. Zheng, X. Yuan, H. Huang, X. W. Yu and N. Ding, "Mechanical Design of a Cable Climbing Robot for Inspection on a Cable-Stayed Bridge," in *Proceedings of the 2018 13th World Congress on Intelligent Control and Automation*, Changsha, China, pp. 1680-1684, 2018.
- [48] J. Yuan, X. Wu, Y. Kang and A. Ben, "Research on reconfigurable robot technology for cable maintenance of cable-stayed bridges in-service," in *International Conference on Mechanic Automation and Control Engineering*, Wuhan, China, pp. 1019-1022, 2010.
- [49] N. G. M. Thao, D. H. Nghia and N. H. Phuc, "A PID backstepping controller for two-wheeled self-balancing robot," in *International Forum on Strategic Technology 2010*, Ulsan, pp. 76-81, 2010.
- [50] M. Velazquez, D. Cruz, S. Garcia and M. Bandala, "Velocity and Motion Control of a Self-Balancing Vehicle Based on a Cascade Control Strategy," *International Journal of Advanced Robotic Systems*, vol. 13, no. 3, 2016.
- [51] H. B. Xu, B. Xu and J. Ding, "Study of Control System for Climbing Robot based on Multi-sensor," *Journal of Physics: Conference Series*, vol. 1288, no. 1, 2019.
- [52] A. Baghani, M. Ahmadabadi and A. Harati, "Kinematics Modeling of a Wheel-Based Pole Climbing Robot (UT-PCR)," in *Proceedings of the 2005 IEEE International Conference on Robotics and Automation*, Barcelona, Spain, Spain, pp. 2099-2104, 2005.
- [53] P. Wilson, *The Circuit Designer's Companion*, Elsevier Ltd., 4th Edition, 2018.
- [54] IPC, *Generic Standard on Printed Board Design*, IPC Association Connecting Electronics Industries, 2003, webpage: <http://www.ipc.org/pdfs/pubscat.pdf>.
- [55] D. L. Jones, *PCB Design Tutorial*, David L. Jones, June, 2004, website: <http://www.alternatezone.com/>.
- [56] J. F. Whitfield, *The Electrician's Guide to the 17th Edition of the IEE Wiring Regulations BS 7671:2008 and Part P of the Building Regulations*, Saffron Walden, United Kingdom: EPA PRESS, 2010.
- [57] OptiFuse, "Fuse Selection Guide," OPTIFUSE, 2010, webpage: <https://www.optifuse.com/>
- [58] H. Kawasaki, S. Murakami, H. Kachi and S. Ueki, "Novel climbing method of pruning robot," in *SICE Annual Conference*, Tokyo, Japan, pp. 160-163, 2008.
- [59] P. Li, X. Duan, G. Sun, X. Li, Y. Zhou and Y. Liu, "Design and control of a climbing robot for inspection of high mast lighting," *Assembly Automation*, vol. 39, no. 1, pp. 77-85, 2019.
- [60] C. Ye, J. Li, S. Yu and G. Ding, "Movement Analysis of Rotating-Finger Cable Inspection Robot," in *ICIRA 2019: Intelligent Robotics and Applications*, Switzerland, vol. 11744, pp. 326-337, 2019.

